

**FINAL REPORT**

***Load Response Comparison Between Fiber and Steel  
Reinforced Concrete Pipe-Phase Two***

***Contract Number BD-530***

David Bloomquist, P.E.

Yu Chen

Melissa Crosby

Department of Civil and Coastal Engineering  
University of Florida, Gainesville



**Developed for the**



Rick Renna, P.E., Program Manager  
February 2009

## **DISCLAIMER**

The opinions, findings, and conclusions expressed in this publication are those of the author and not necessarily those of the State of Florida Department of Transportation.”

**SI (MODERN METRIC) CONVERSION FACTORS (from FHWA)**

**APPROXIMATE CONVERSIONS TO SI UNITS**

SYMBOL	WHEN YOU KNOW	MULTIPLY BY	TO FIND	SYMBOL
<b>LENGTH</b>				
in	inches	25.4	millimeters	mm
ft	feet	0.305	meters	m
yd	yards	0.914	meters	m
mi	miles	1.61	kilometers	km

SYMBOL	WHEN YOU KNOW	MULTIPLY BY	TO FIND	SYMBOL
<b>AREA</b>				
in <sup>2</sup>	squareinches	645.2	square millimeters	mm <sup>2</sup>
ft <sup>2</sup>	squarefeet	0.093	square meters	m <sup>2</sup>
yd <sup>2</sup>	square yard	0.836	square meters	m <sup>2</sup>
ac	acres	0.405	hectares	ha
mi <sup>2</sup>	square miles	2.59	square kilometers	km <sup>2</sup>

SYMBOL	WHEN YOU KNOW	MULTIPLY BY	TO FIND	SYMBOL
<b>VOLUME</b>				
fl oz	fluid ounces	29.57	milliliters	mL
gal	gallons	3.785	liters	L
ft <sup>3</sup>	cubic feet	0.028	cubic meters	m <sup>3</sup>
yd <sup>3</sup>	cubic yards	0.765	cubic meters	m <sup>3</sup>

NOTE: volumes greater than 1000 L shall be shown in m<sup>3</sup>

SYMBOL	WHEN YOU KNOW	MULTIPLY BY	TO FIND	SYMBOL
<b>MASS</b>				
oz	ounces	28.35	grams	g
lb	pounds	0.454	kilograms	kg
T	short tons (2000 lb)	0.907	megagrams (or "metric ton")	Mg (or "t")

SYMBOL	WHEN YOU KNOW	MULTIPLY BY	TO FIND	SYMBOL
<b>TEMPERATURE (exact degrees)</b>				
°F	Fahrenheit	5 (F-32)/9 or (F-32)/1.8	Celsius	°C

SYMBOL	WHEN YOU KNOW	MULTIPLY BY	TO FIND	SYMBOL
<b>ILLUMINATION</b>				
fc	foot-candles	10.76	lux	lx
fl	foot-Lamberts	3.426	candela/m <sup>2</sup>	cd/m <sup>2</sup>

SYMBOL	WHEN YOU KNOW	MULTIPLY BY	TO FIND	SYMBOL
<b>FORCE and PRESSURE or STRESS</b>				
lbf	poundforce	4.45	newtons	N
lbf/in <sup>2</sup>	poundforce per square inch	6.89	kilopascals	kPa

**APPROXIMATE CONVERSIONS TO SI UNITS**

SYMBOL	WHEN YOU KNOW	MULTIPLY BY	TO FIND	SYMBOL
<b>LENGTH</b>				
mm	millimeters	0.039	inches	in
m	meters	3.28	feet	ft
m	meters	1.09	yards	yd
km	kilometers	0.621	miles	mi

SYMBOL	WHEN YOU KNOW	MULTIPLY BY	TO FIND	SYMBOL
<b>AREA</b>				
mm <sup>2</sup>	square millimeters	0.0016	square inches	in <sup>2</sup>
m <sup>2</sup>	square meters	10.764	square feet	ft <sup>2</sup>
m <sup>2</sup>	square meters	1.195	square yards	yd <sup>2</sup>
ha	hectares	2.47	acres	ac
km <sup>2</sup>	square kilometers	0.386	square miles	mi <sup>2</sup>

SYMBOL	WHEN YOU KNOW	MULTIPLY BY	TO FIND	SYMBOL
<b>VOLUME</b>				
mL	milliliters	0.034	fluid ounces	fl oz
L	liters	0.264	gallons	gal
m <sup>3</sup>	cubic meters	35.314	cubic feet	ft <sup>3</sup>
m <sup>3</sup>	cubic meters	1.307	cubic yards	yd <sup>3</sup>

SYMBOL	WHEN YOU KNOW	MULTIPLY BY	TO FIND	SYMBOL
<b>MASS</b>				
g	grams	0.035	ounces	oz
kg	kilograms	2.202	pounds	lb
Mg (or "t")	megagrams (or "metric ton")	1.103	short tons (2000 lb)	T

SYMBOL	WHEN YOU KNOW	MULTIPLY BY	TO FIND	SYMBOL
<b>TEMPERATURE (exact degrees)</b>				
°C	Celsius	1.8C+32	Fahrenheit	°F

SYMBOL	WHEN YOU KNOW	MULTIPLY BY	TO FIND	SYMBOL
<b>ILLUMINATION</b>				
lx	lux	0.0929	foot-candles	fc
cd/m <sup>2</sup>	candela/m <sup>2</sup>	0.2919	foot-Lamberts	fl

SYMBOL	WHEN YOU KNOW	MULTIPLY BY	TO FIND	SYMBOL
<b>FORCE and PRESSURE or STRESS</b>				
N	newtons	0.225	poundforce	lbf
kPa	kilopascals	0.145	poundforce per square inch	lbf/in <sup>2</sup>

\*SI is the symbol for International System of Units. Appropriate rounding should be made to comply with Section 4 of ASTM E380.  
(Revised March 2003)

Technical Report Documentation Page

1. Report No.	2. Government Accession No.	3. Recipient's Catalog No.	
4. Title and Subtitle  <i>Load Response Comparison Between Fiber and Steel Reinforced Concrete Pipe-Phase Two</i>		5. Report Date December 2008	
		6. Performing Organization Code	
7. Author(s) David Bloomquist , Andrew Boyd, Yu Chen, Melissa Crosby		8. Performing Organization Report No.	
9. Performing Organization Name and Address Department of Civil and Coastal Engineering 365 Weil Hall University of Florida Gainesville, Florida 32611		10. Work Unit No. (TR AIS)	
		11. Contract or Grant No. BD-530	
12. Sponsoring Agency Name and Address Florida Department of Transportation 605 Suwannee Street, MS 30 Tallahassee, FL 32399		13. Type of Report and Period Covered Final Report 6/2005 - 12/2008	
		14. Sponsoring Agency Code	
15. Supplementary Notes			
16. Abstract A novel geotechnical enclosure has been designed and constructed for testing prototype materials under a variety of loading conditions. While the large 20'x10'x8' was designed to test buried pipes, it is capable of providing a wide range of geotechnical conditions. Kevlar lifting bags will provide up to 118 feet of geostatic surcharge and the extremely rigid walls prevent active soil conditions from developing.			
17. Key Word soil box, geostatic testing chamber, buried pipe		18. Distribution Statement No restrictions.	
19. Security Classif. (of this report) Unclassified.	20. Security Classif. (of this page) Unclassified.	21. No. of Pages 187	22. Price

## EXECUTIVE SUMMARY

The following is a compilation of several documents related to the design and construction of a large geotechnical testing enclosure or chamber – often referred to as a “soil box”. Due to the interest in testing full-scale buried pipes, FDOT issued an RFP in Fall 2003, to which UF responded. The submitted proposal that was subsequently approved consisted of two phases. The first was to design and construct a vessel sufficiently large to test reinforced concrete and fiber reinforced pipes under various loading conditions. The objective of Phase 2 was to perform the actual testing.

Originally, the plan was to simply purchase a dumpster type container and modify it to accept the pipes and loading system. However, it became apparent that no “off-the-shelf” unit would meet the research requirements. Hence, through exhaustive Finite Element Modeling the University of Florida designed a unique engineered structure. This design was submitted to FDOT engineers as well as two experts on soil box testing, Drs. Ian Moore and Tim McGrath. They opined that the design would be too flexible, thereby affecting (adversely or otherwise) the pipes’ responses to loading. Specifically that active earth pressures would ensue from the outward movement of the walls, thereby altering the stress distribution throughout the soil mass and by extension the pipes themselves.

Based on the consultants’ (as well a FDOT structural engineer) comments, the design was re-analyzed and substantially stiffened. This new design was re-submitted to the above individuals for review and were subsequently incorporated into the final design.

After a bidding process, a local fabricator, ArcRite in Palatka Florida, was selected and proceeded to manufacture the complex chamber.

In July of 2008, the soil box sections were delivered to the University’s Coastal Laboratory in Gainesville, and assembled. Unfortunately, during this time frame, Hardie Pipe, the fiber reinforced pipe firm whose pipes were to be evaluated, decided to withdraw from Florida and hence negated the proposed testing. However, with the soil box now complete, various projects have been identified and the anticipation is that significant usage will follow via this one of a kind enclosure.

# TABLE OF CONTENTS

	<u>Page</u>
EXECUTIVE SUMMARY .....	v
LIST OF TABLES .....	vii
LIST OF FIGURES .....	viii
CHAPTER	
1 BACKGROUND.....	1
Introduction.....	1
Project Time-line .....	2
Original Design Concept.....	5
2 PLAXIS ANALYSIS .....	7
Input Parameters – Finite Element Analysis.....	7
3 STRUCTURAL ANALYSIS AND ALTERATIONS TO THE ORIGINAL DESIGN .....	20
Simplification, Assumptions and Model of the Original Design.....	20
Evaluation and Revised Design .....	21
Front Panel .....	21
Top Panel.....	25
End Panels .....	26
4 DESIGN CONCLUSIONS .....	35
Tie Rod Addition .....	38
Miscellaneous Soil Box Details.....	40
5 SOIL BOX CONSTRUCTION.....	44
APPENDIX A – SUPPLEMENT TO DRAFT FINAL REPORT.....	A-1
APPENDIX B – PRELIMINARY ACOUSTIC EMISSION TESTING .....	B-1

## LIST OF TABLES

<u>Table</u>	<u>Page</u>
1	Typical Roll-off Container Dimensions (internal walls are smooth).....3
2	Material Properties for the Soil (Loose & Dense) .....8
3	Material Properties for the 18”-diameter Concrete Pipes (FRCP & SRCP).....8
4	Material Properties for the 24”-diameter Concrete Pipes (FRCP & SRCP).....8
5	Material Properties for the 48”-diameter Concrete Pipes (FRCP & SRCP).....9
6	Effect of Using Different I-beams on End Panel Deflection .....30
7	Parts List for the Original Box Design .....39
8	Additional Parts Required for Revised Container .....39



## LIST OF FIGURES

<u>Figure</u>	<u>Page</u>
1	“Off the shelf” container originally considered .....3
2	Original idea for the “soil box” .....3
3	Soil Displacement (in feet) for 24” FRCP .....9
4	Soil Displacement (in feet) for 24” SRCP .....10
5	Generated FEM mesh .....11
6	Stress distribution for tandem pipes.....12
7	Original twin portal design - 1’ soil support.....13
8	Single portal design concept - 1’ soil support.....14
9	FEM mesh generation for single portal .....15
10	Resulting stress distribution for single portal - 1.5’ soil support.....16
11	Resulting stress distribution for single portal - 2.0’ soil support.....17
12	Single portal - 2’ soil support.....18
13	Boundary effects for offset portal .....19
14	Assumed maximum applied pressures.....20
15	Front panel displacement plot of the original design.....22
16	Wall thickness versus wall displacement.....23
17	External stiffeners added.....23
18	Proposed brace structure and vertical I-beams on front and rear panels .....24
19	Brace structure for front and rear panels.....24
20	Original top deflection plot with plate thickness = 0.5 <i>in</i> .....25
21	Top panel deflection versus wall plate thickness.....26
22	The revised braces.....27
23	Extension of I-beams at the end panels.....28
24	The top panel deflection of the revised design .....29
25	Deflection of end panels utilizing a W16×57 section. ....31
26	Deflection of end panels - W16×77 .....31
27	Deflection of end panels - W16×89 .....32
28	End panel deflection using W18×65 .....32

29	Deflection of end panels using W18×71 .....	33
30	End panel displacement contours using W18×97 I-beams .....	33
31	Deflection of end panels by using W18×106 .....	34
32	Deflection of end panels using W18×119 I-beams .....	34
33	Original end panel deflection with pane thickness = 0.5 in.....	36
34	Plot of Wall Thickness versus End Panel Deflection .....	36
35	End panels strengthened by adding vertical I-beams.....	37
36	Added tie rods .....	38
37	Spacers primed and painted .....	45
38	Bolts and nuts being cleaned and painted.....	46
39	Trees removed for crane maneuvering space.....	47
40	Side panel showing pipe access port.....	48
41	End panels in foreground and bottom panel in background .....	49
42	Soil box – Various views: a) Inside view .....	50
	b) Front view .....	51
	c) Side view .....	52
	d) End view .....	53
	e) Pipe hole and cover .....	54
	f) Close up of fastened nuts and bolts .....	54

## CHAPTER 1. BACKGROUND

### Introduction

The FDOT's structures research center recently conducted a large-scale research project to evaluate the response of buried pipes to repetitive surface loads. Eighteen flexible pipes were installed at FDOT's structural field-testing facility in Tallahassee with the following specifics:

- Six types of pipes, four plastic, one aluminum and one steel
- Pipes were three feet in diameter except for one plastic pipe that was 4 feet in diameter
- Each type was installed at 0.5 D, 1.0 D and 2.0 D below the surface (overburden depth, where D is pipe diameter)
- Multiple strain gages and soil stress cells were installed at various locations on the pipes and in the surrounding soil

Three installation depths and six pipe types equated to eighteen test samples. The objective of this field test was to attempt to evaluate the response of the pipes to repeated vertical loading. Such parameters as: pipe deflection, stress/strain generation and development of soil stresses adjacent to the pipe were recorded. Pipe material and overburden depth were two of the variable parameters scrutinized.

While the above project provided interesting data, of particular interest was the contribution of the confining backfill soil to the pipes' load resistance. The type and quality of soil (i.e., degree of compaction) in contact with and surrounding the pipe has a major influence on pipe response (deformation), and hence its load resistance capacity. While the aforementioned project did tacitly attempt to control the compactive effort, it was felt that consistency in the as-compacted soil properties dramatically affected the results in a manner that could not be quantitatively determined. That is to say, without precise knowledge of the density of the soil throughout the strata, attempts to correlate soil properties with pipe deformation characteristics were not possible. Finally, the moisture content of the soil influences its' resistance, and this condition (e.g., worst case scenario, a saturated soil) could not be easily duplicated in the field setup. Thus, the idea was instigated to design and build a device capable of testing pipes, (et. al.), under controlled, insitu, conditions.

## **Project Time-line**

Concurrently with the above project, the use of fiber reinforced concrete pipe (FRCP) or fiber cement pipe (FCP) has recently been the subject of FDOT interest. Several manufacturers have requested that the Agency adopt specifications to allow its use as an alternate to reinforced (steel) concrete pipe (RCP). While the load/deformation properties of the pipe alone are well documented (via the 3-edge bearing test), the soil-structure interaction is (or was) not. Hence, tests funded by a pipe manufacturer were conducted both in Australia and the U.S. in various soil “boxes”. In order to create the desired far-field effects that the walls would have on the soil resistance, box walls contained springs to simulate or provide pseudo soil displacement during loading. Unfortunately, unless the spring stiffness is similar to the soil modulus, large differences in lateral resistance could and would occur. Therefore, FDOT became interested in acquiring a large soil-testing chamber that would ameliorate the spring-type box limitations by reducing the influence of the container walls. Another desirable feature would allow longer and larger sections of pipe to be tested under saturated soil conditions.

Hence, a contract was awarded (Fall 2003) to UF to develop a geotechnical container capable of testing the above mentioned pipes. Originally, it was assumed that a traditional manufactured container would provide the necessary rigidity if pipe loading was solely applied co-linear to its footprint (see Figure 1). However due the limitations of such a setup and after consultation with FDOT officials, another idea arose to utilize Kevlar air bags on the soil surface, thereby providing a wider range of loading conditions. This in turn necessitated the abandonment of the “off the shelf” concept and required the design and construction of a much more heavily reinforced container.

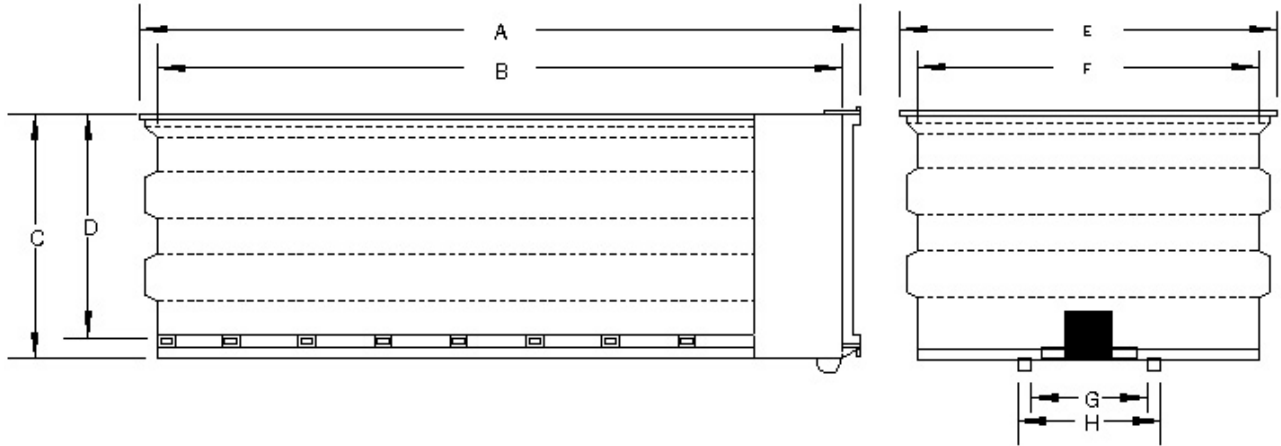


Figure 1. “Off the shelf” container originally considered.

Table 1. Typical Roll-off Container Dimensions (internal walls are smooth)

Size	A	B	C	D	E	F	G	H
20 YD	18'-8"	18'	4'-10"	4'	8'-2"	7'-6"	35.5"	38.5"
30 YD	18'-8"	18'	6'-10"	6'	8'-2"	7'-6"	35.5"	38.5"
<b>40 YD</b>	<b>20'- 8"</b>	<b>20'</b>	<b>8'</b>	<b>7'</b>	<b>8'-2"</b>	<b>7'-6"</b>	<b>35.5"</b>	<b>38.5"</b>



Figure 2. Original idea for the “soil box”.

The first in-house design consisted of steel plates bolted together to form a 20' x 10' x 8' high container. I-beams were added to produce the required strength (note: deflections of the walls under load were tacitly assumed not to be deleterious to the pipe testing, since each pipe type would be subjected to the same boundary conditions. A UF structural engineer oversaw the design, verifying its structural reliability. However, it is important to note that while he did design a safe box, he did not design a rigid one, since deflections resulting from his design did not compromise its integrity.

Based on the above, a Master's student (Melissa Crosby) proceeded to analyze the various pipe loading scenarios using the geotechnical engineering software, PLAXIS 3-D. While this program is excellent for evaluating soil-structure interaction conditions, an assumption on box deformations had to be made, since the program cannot compute these internally. Thus several wall deflections had to be inputted and the resulting geostatic stresses imparted on the pipes assessed. In hindsight, this was not the most efficacious methodology, since we were never sure what the actual deflections would be. We decided to assume rigid boundaries (the most desirable condition) with the thought that we could stiffen the box sufficiently to approach this condition.

During this phase, a major change in the box design added two additional portals, whereby two pipes could be tested simultaneously – negating the soil variability aspect that would no doubt arise if tested sequentially. A thorough stress analysis confirmed that because of the large box size, there would be minimal cross-over stress interactions between the pipes themselves and the wall surfaces. This signified that the tandem testing program was indeed viable – once again pointing out that rigid boundary conditions would be met.

Throughout the above effort, progress reports were prepared and delivered to the various pipe manufactures representatives as well as FDOT engineers for comment. In addition, UF and FDOT personnel visited UCF where a small soil box was being used for pipe testing.

Valuable comments received by the various parties and changes made to incorporate them into the design. (For example, the use of Visqueen or Teflon sheets coated with lithium grease along the sides of the container to reduce soil/structure friction). In addition, FDOT suggested that two

experienced soil box researchers be added to the consultant team to review UF's proposal. Hence Drs. Ian D. Moore and Timothy McGrath also reviewed the proposal and submitted substantive comments for discussion.

In July 2004, a meeting was held at UF to discuss the proposal. In attendance were: Drs. Moore and McGrath, Rick Renna, Dr. David Horhota, Marc Ansley, and Larry Jones, from FDOT, and Andrew Boyd, David Bloomquist and Melissa Crosby from UF. During the meeting, the written comments from the consultants were discussed and responded to by the PIs. All of the suggestions were incorporated into the final design and construction.

### **Original Design Concept**

In order to construct a container that is sufficiently large to minimize wall influences, as well as keep costs as reasonable as possible, the concept was to purchase a vessel akin to a roll-off container (used in construction debris removal). For example, a 40 CY container would allow for an eight-foot long section of pipe be tested if placed perpendicular to the long axis of the container. This would also provide 8.5 feet of clear distance from the pipe to the wall (20 feet minus 3 foot diameter divided by 2 for each side). Several manufacturers of these containers signified that they could construct a wider version (10 feet) to provide additional testing length. Based on soil stresses generated from surface loads, 8.5 feet of clear space would greatly reduce any wall effects on the pipe performance.

However, to verify this design concept, PLAXIS (soil/structure interaction FEM program) was employed to model the geometry of the enclosure to insure compliance with predicted boundary effects. Multiple runs were performed using standard soil type, density and pipe properties as input variables. For each simulation, the lateral stresses developed at the container boundaries and pipes were determined.

Based on responses from both industry (RCP and FRCP manufacturers) and FDOT, additional enhancements were suggested incorporated into the final container design. Specifically:

- A. All walls of the container will be lined with Teflon sheets (two layers) with a lithium grease interface that will reduce the friction developed between the walls and the soil. Note, this has been discussed previously.
  
- B. Loading of the overburden soil/pipes will be applied via steel plates on the soil surface. Tentatively, 36" x 36" plates will be used. However, in order to model deep burial conditions, a series of lifting bags will be added that, when inflated, can simulate up to 100 feet of overburden geostatic stress. This will greatly expand the testing capabilities of the system since pipe deformation, as a function of overburden depth will then be possible. Also, since the entire surface of the soil will be covered with individual steel plates overlain by these 36" x 36" Kevlar bags, they will provide a constant contact stress as the bags deform. One possible testing scenario would be to inflate all bags to some uniform pressure and then continue inflating the one (or ones) directly over the pipe to simulate a static point or line load. These bags could also reduce or eliminate the need for a hydraulic actuator. Furthermore, by using a fluid to inflate the bags, rather than air provides much better control on stresses and displacements.



## CHAPTER 2. PLAXIS ANALYSIS

An FEM analysis of the proposed container (using PLAXIS) was completed to ensure that boundary conditions do not adversely impact the soil-structure interaction of the pipe(s). Special attention was taken to model the pipe material properties (modulus), since this attribute affects the lateral pressures generated in the soil. Both flexible and rigid (RCP) pipes were analyzed using the program. Once the mesh was created, a parametric study was performed on the effect of loading level versus soil pressure generation as a function of density/type. Various overburden heights were investigated using both dry and saturated conditions. All of the contemplated full-scale tests will be modeled again, once the finalized container design is approved.

The major drawback to the PLAXIS analysis was the fact that it is a for geotechnical analysis – as opposed to a structural engineering software program. That is to say, it was assumed that the box would remain rigid during testing. This assumption was quickly exposed once the structural engineer finished a structural analysis of the container. However, since the student performing the geotechnical analysis was not trained in this area, she continued her investigation, realizing that ultimately the box would have to be significantly stiffened prior to testing.

### **Input Parameters-Finite Element Analysis**

Two different manufactured concrete pipes are to be tested inside the soil box, fiber reinforced and standard reinforced concrete pipes. The proposed pipe diameters to be used for testing are 18” and 24” with a possibility of a 48” diameter pipe. In order to ensure proper bedding, a depth of at least one diameter below the pipe inside the soil box will be used in the analysis and research. For example, the 24” diameter pipe will require two feet of soil beneath resulting in an approximate height of four feet above the crown of the pipe to the top of the box. An overburden soil depth of six feet will allow the distribution of stresses simulating in-situ conditions. The maximum load applied on the soil is assumed to be 16,000 lbs/ft<sup>2</sup>. Loose and dense compacted soil defines the two types of backfill used in the analysis. The loose compacted soil has a Young’s Modulus value of 216,000 lbs/ft<sup>2</sup> and the dense compacted soil 489,600 lbs/ft<sup>2</sup>. Input parameters for the SRCP and FRCP different size diameter pipes are displayed below. Young’s

Modulus for the FRCP and SRCP were determined using referenced literature. The SRCP modulus value was calculated using the American Concrete Institute (ACI 318). Compressive strength for concrete pipe normally ranges from 4000 lbs/in<sup>2</sup> to 6000 lbs/in<sup>2</sup> (Rinker Materials, 2003). Elastic modulus for the SRCP was calculated using equation 6.1 with a compressive strength ( $f'_c$ ) of 4000 lbs/in<sup>2</sup>. Elastic modulus for the FRCP to determine normal stiffness and flexural rigidity of the concrete pipe used was  $3.62 \times 10^6$  lbs/in<sup>2</sup>.

$$E_c = 57,000 * \sqrt{f'_c}$$

Table 2. Material Properties for the Soil (Loose & Dense)

Parameter	Name	Loose	Dense	Unit
Material Model	Model	Mohr-Coulomb	Mohr-Coulomb	-
Type of material behavior	Type	Drained	Drained	-
Soil weight above phr. level	$\gamma_{unsat}$	120	120	lbs/ft <sup>3</sup>
Soil weight below phr. level	$\gamma_{sat}$	120	120	lbs/ft <sup>3</sup>
Young's modulus	$E_{ref}$	216,000	489,600	lbs/ft <sup>2</sup>
Poisson's ratio	$\nu$	0.3	0.3	-
Cohesion	$c_{ref}$	0.00001	0.00001	lbs/ft <sup>2</sup>
Friction angle	$\phi$	35	35	DEG.
Dilatancy angle	$\psi$	5	5	DEG.

Table 3. Material Properties for the 18"-diameter Concrete Pipes (FRCP & SRCP)

Parameter	Name	FRCP	SRCP	Unit
Type of behavior	Material type	Elastic	Elastic	-
Normal stiffness	EA	147,372,845	280,303,765	lbs/ft
Flexural Rigidity	EI	38,138,787	66791264	lbs-ft <sup>2</sup> /ft
Weight	W	150	150	lbs/ft <sup>3</sup>
Poisson's ratio	$\nu$	0.15	0.15	-

Table 4. Material Properties for the 24"-diameter Concrete Pipes (FRCP & SRCP)

Parameter	Name	FRCP	SRCP	Unit
Type of behavior	Material type	Elastic	Elastic	-
Normal stiffness	EA	198,636,143	382,227,687	lbs/ft
Flexural Rigidity	EI	93,303,588	168,720,067	lbs-ft <sup>2</sup> /ft
Weight	W	150	150	lbs/ft <sup>3</sup>
Poisson's ratio	$\nu$	0.15	0.15	-

Table 5. Material Properties for the 48"-diameter Concrete Pipes (FRCP & SRCP)

Parameter	Name	FRCP	SRCP	Unit
Type of behavior	Material type	Elastic	Elastic	-
Normal stiffness	EA	665,723,216	1,228,267,715	lbs/ft
Flexural Rigidity	EI	1,263,829,838	2,322,073,435	lbs-ft <sup>2</sup> /ft
Weight	W	150	150	lbs/ft <sup>3</sup>
Poisson's ratio	$\nu$	0.15	0.15	-

The following two plots show the displacement values for the two types of pipes. Of particular interest is the effect of friction on the walls that reduces vertical displacements dramatically.

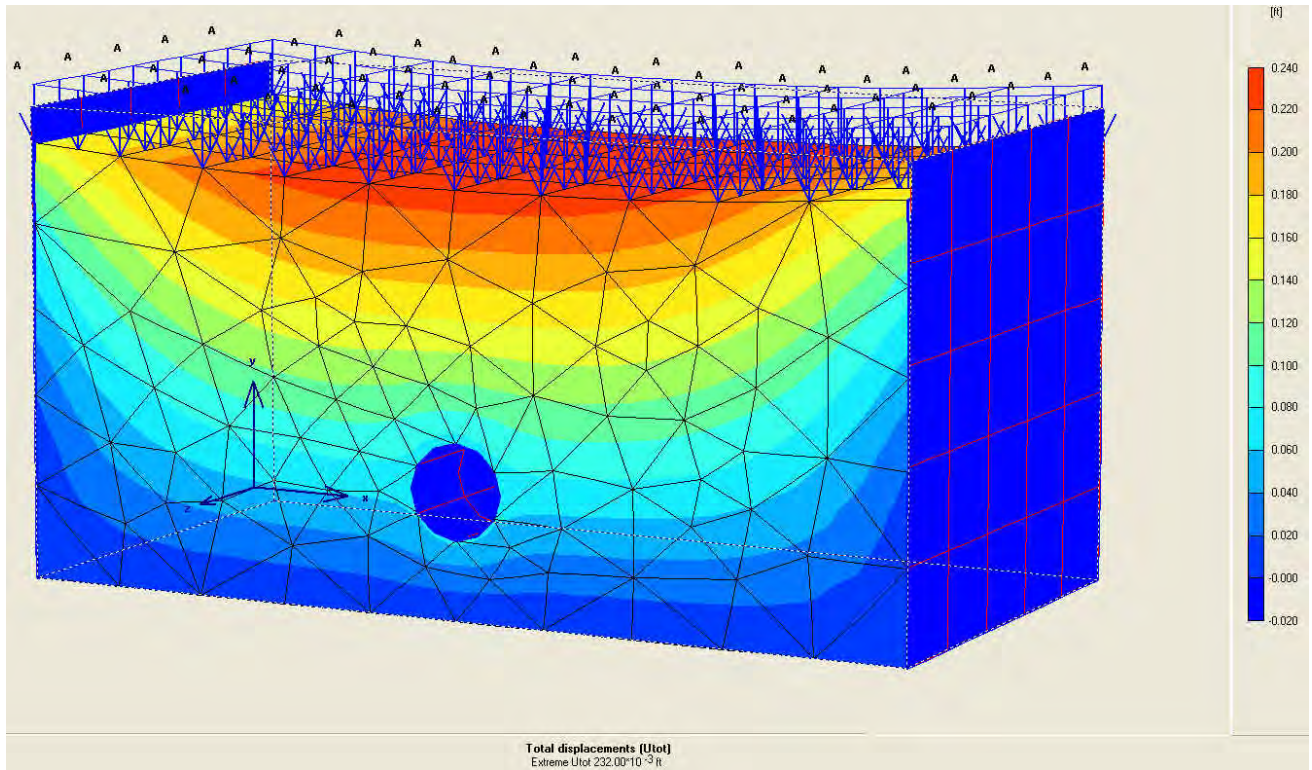


Figure 3. Soil Displacement (in feet) for 24" FRCP.

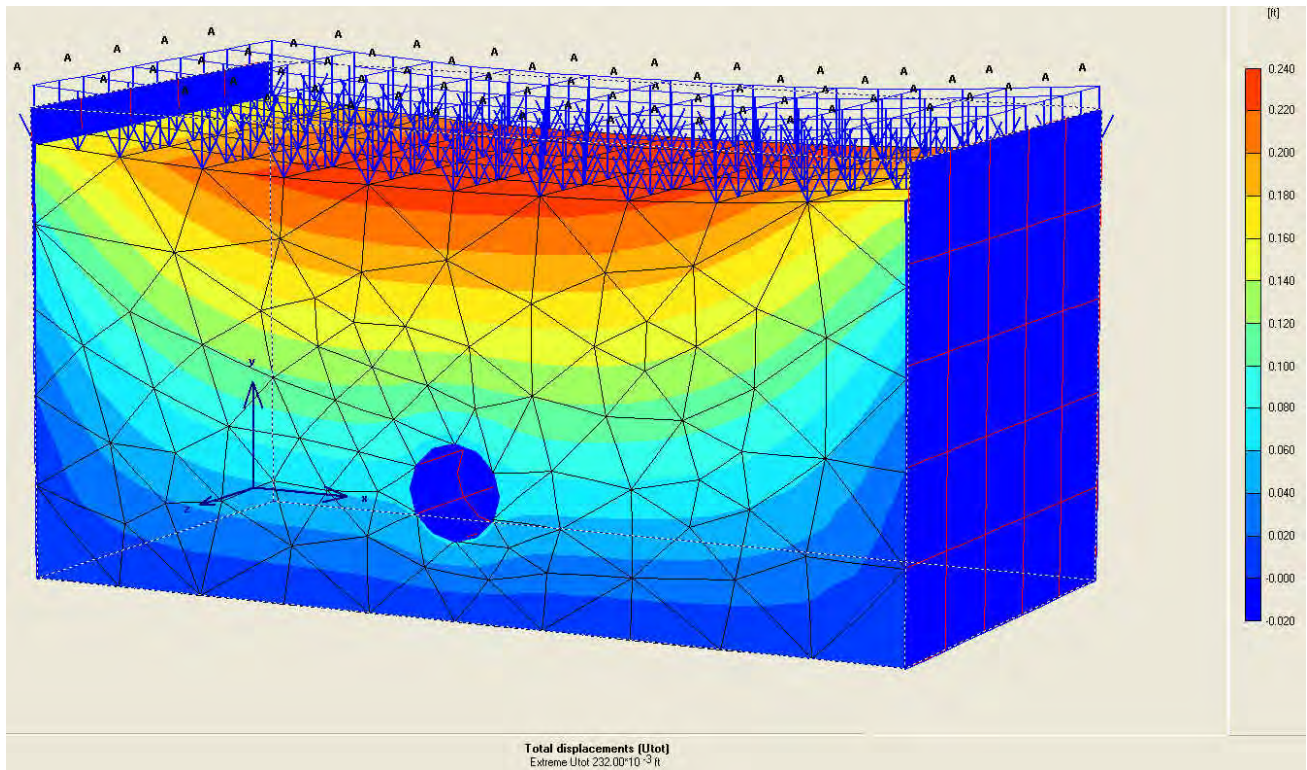


Figure 4. Soil Displacement (in feet) for 24" SRCP.

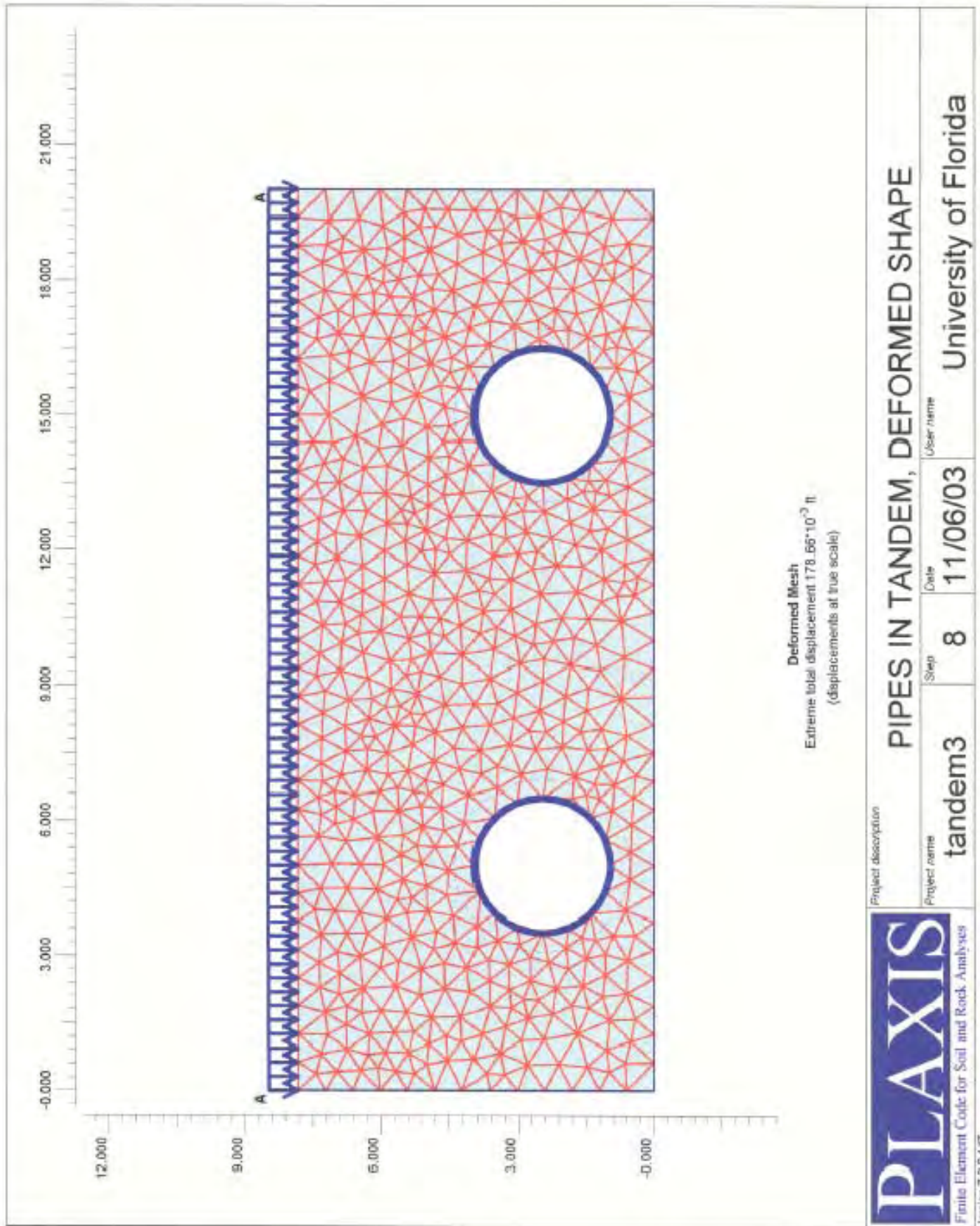
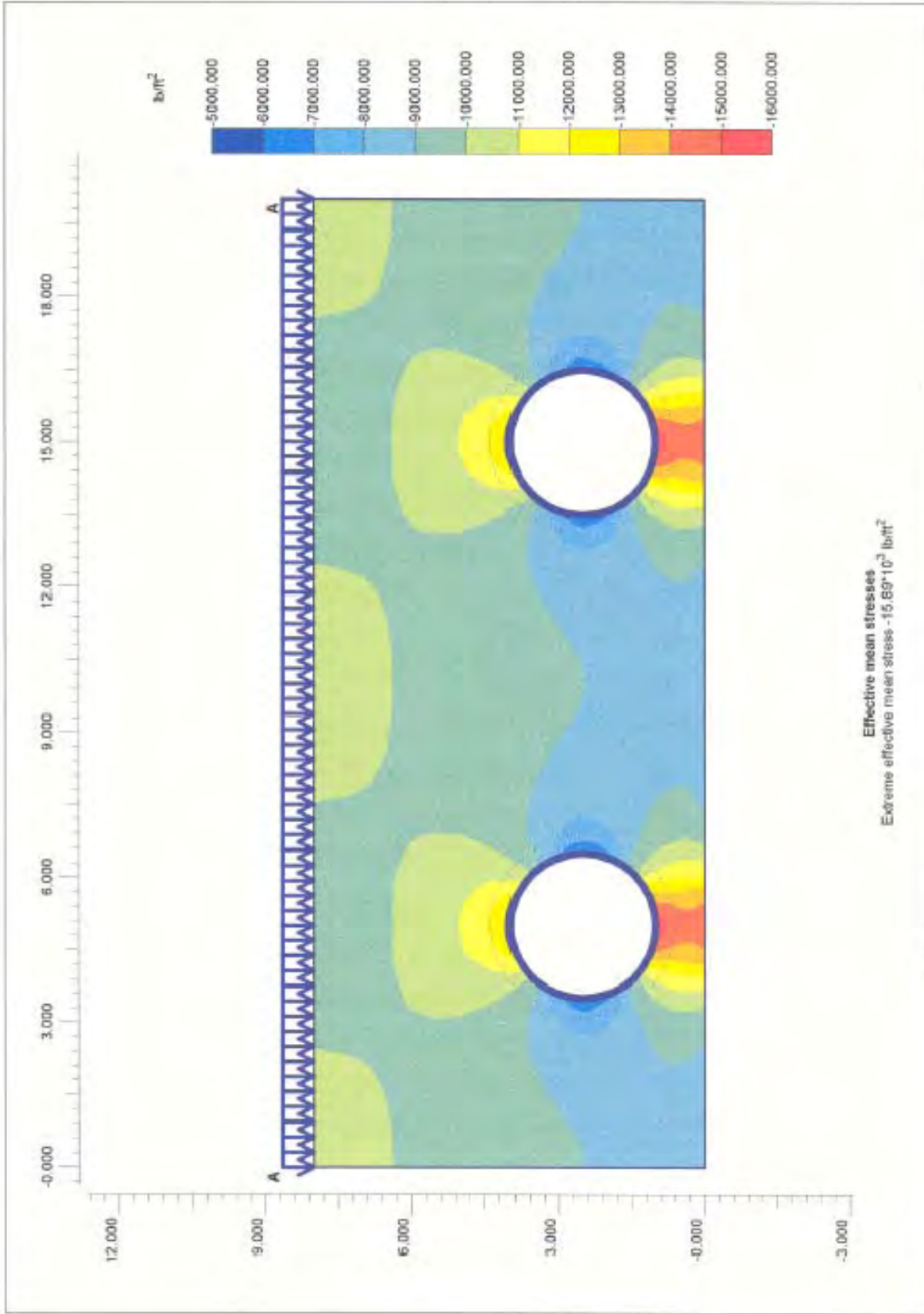


Figure 5. Generated FEM mesh




		Project description	
		PIPES IN TANDEM, STRESS DISTRIBUTION	
Project name	Sheet	Date	User name
tandem3	8	11/06/03	University of Florida

Figure 6. Stress distribution for tandem pipes

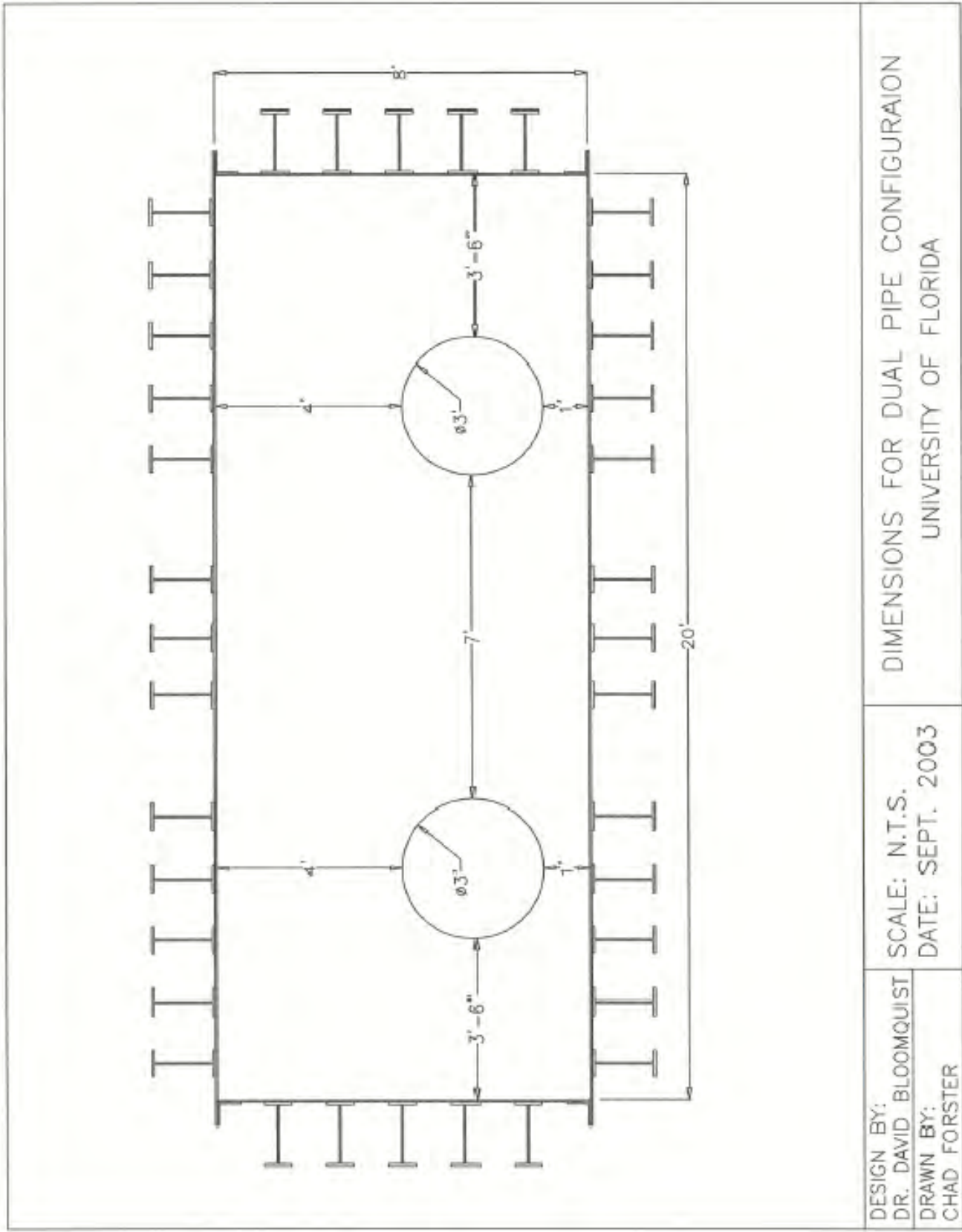
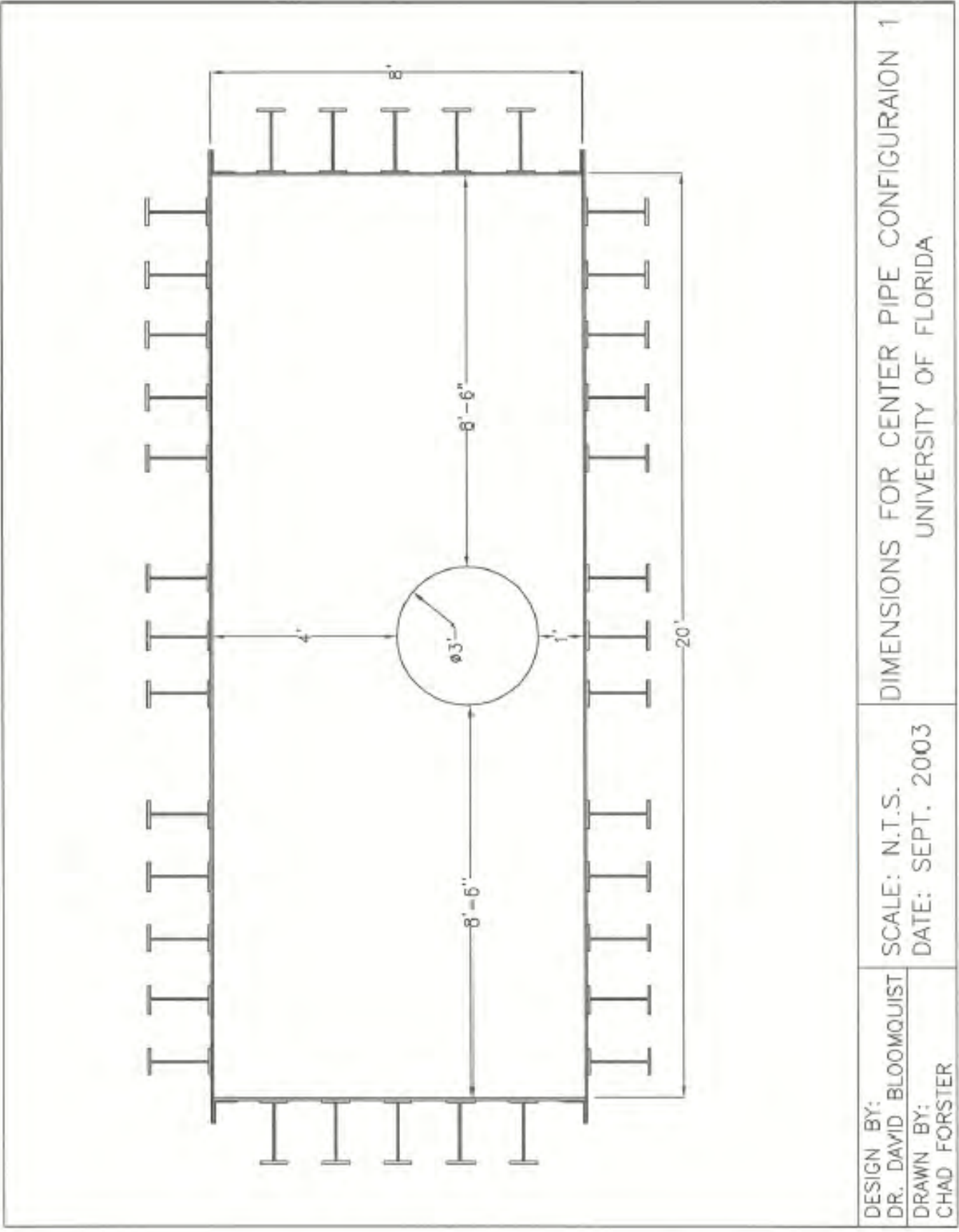


Figure 7. Original twin portal design - 1' soil support



DESIGN BY: DR. DAVID BLOOMQUIST	SCALE: N.T.S. DATE: SEPT. 2003	DIMENSIONS FOR CENTER PIPE CONFIGURATION 1 UNIVERSITY OF FLORIDA
DRAWN BY: CHAD FORSTER		

Figure 8. Single portal design concept - 1' soil support



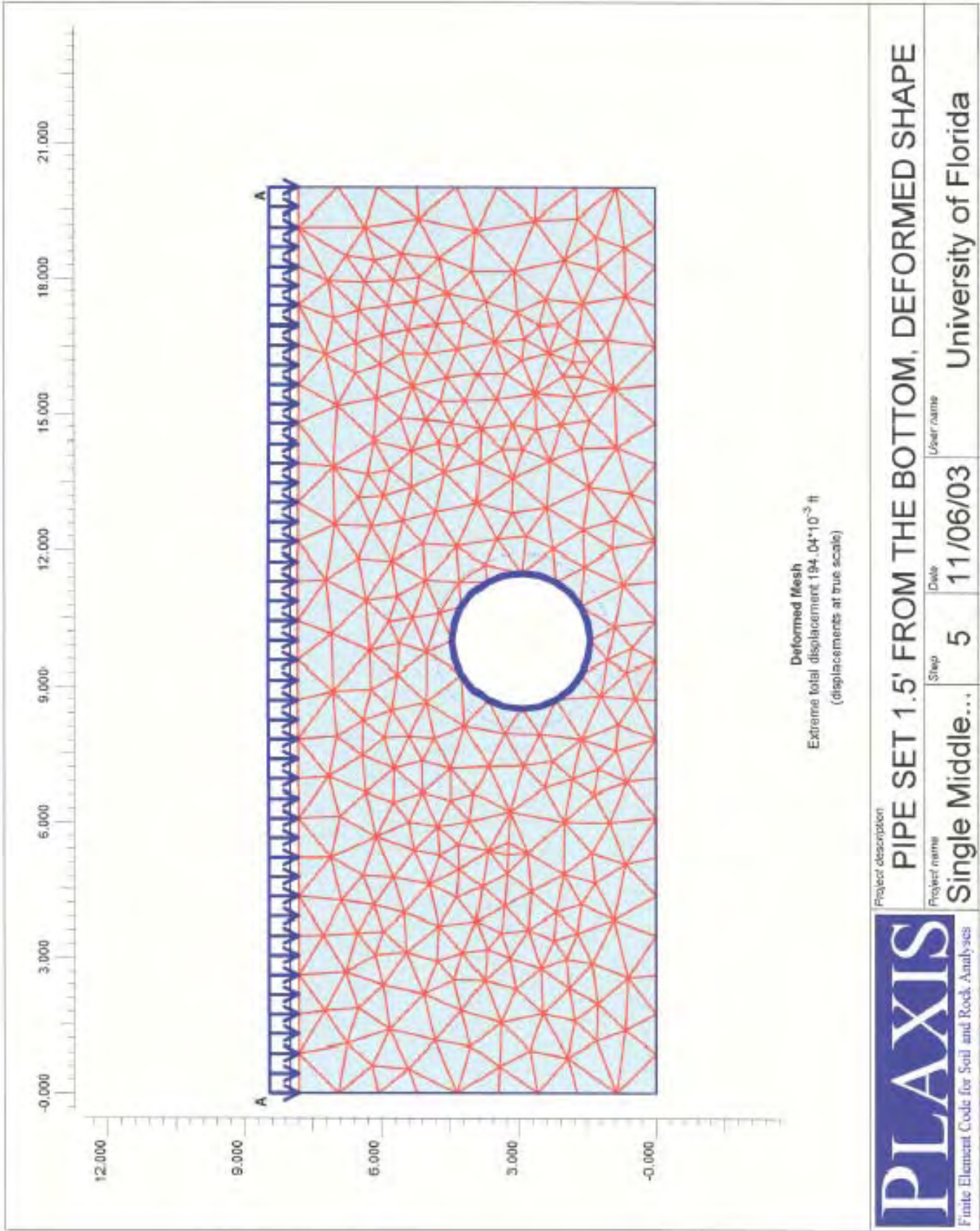


Figure 9. FEM mesh generation for single portal

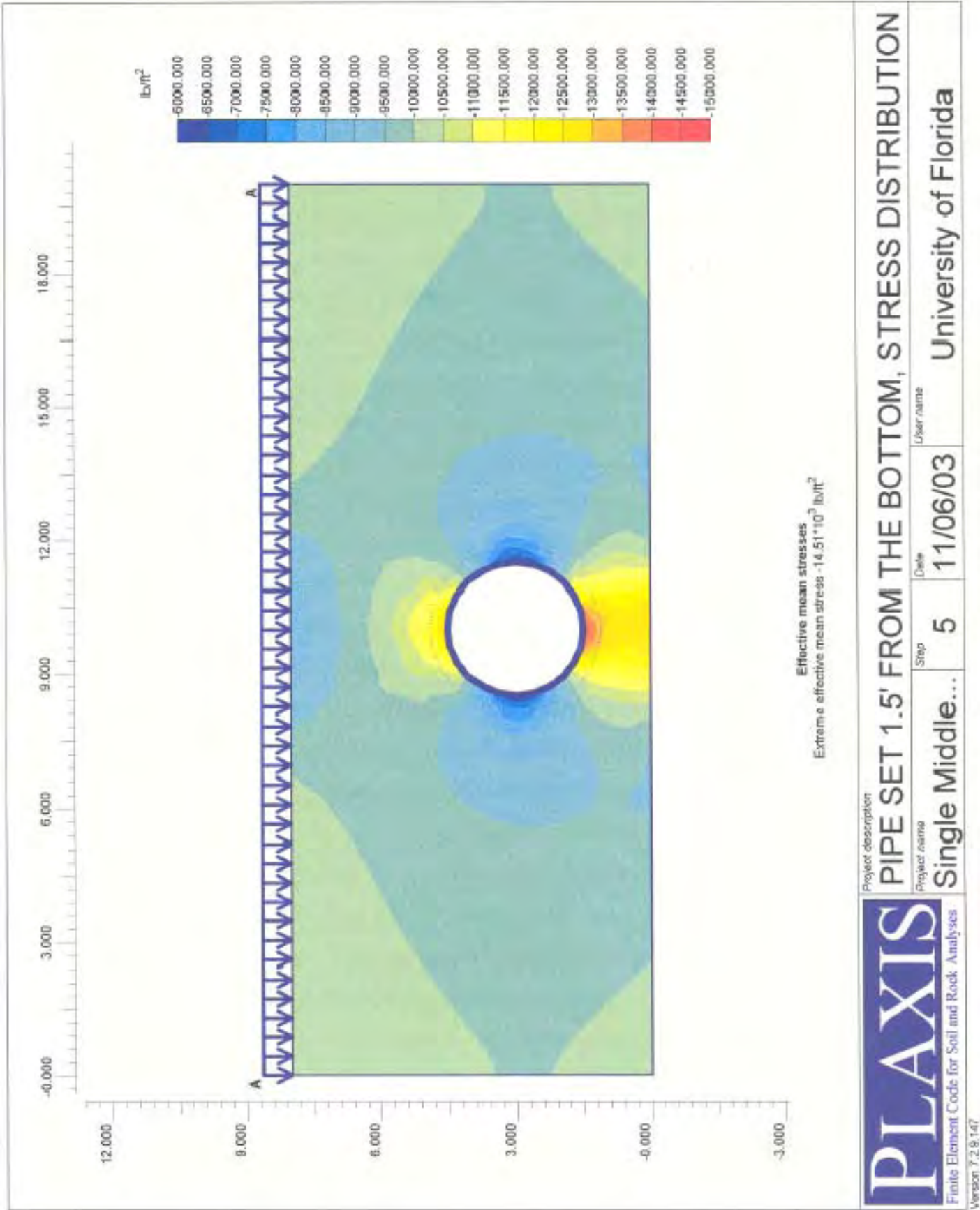


Figure 10. Resulting stress distribution for single portal - 1.5' soil support

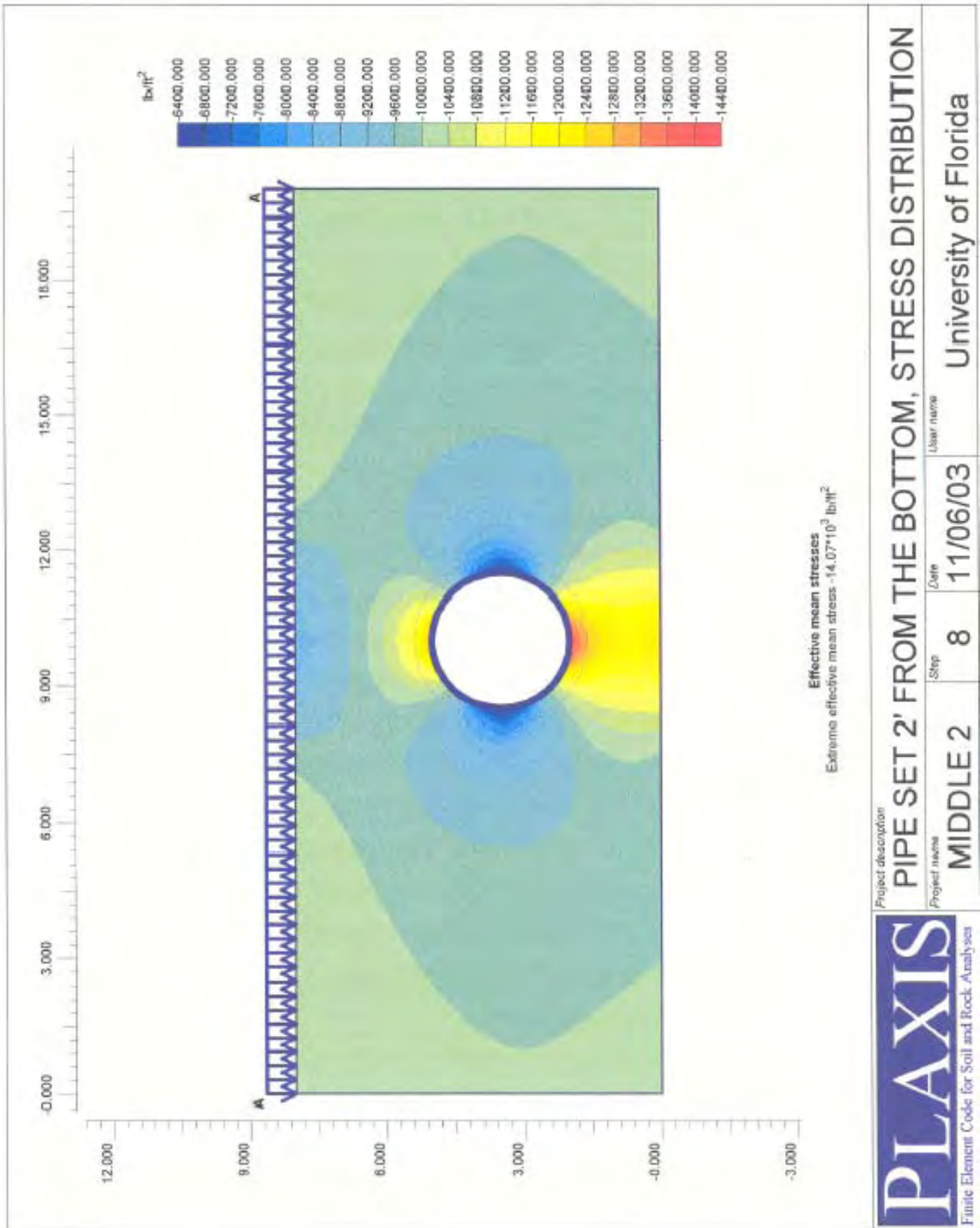


Figure 11. Resulting stress distribution for single portal - 2.0' soil support

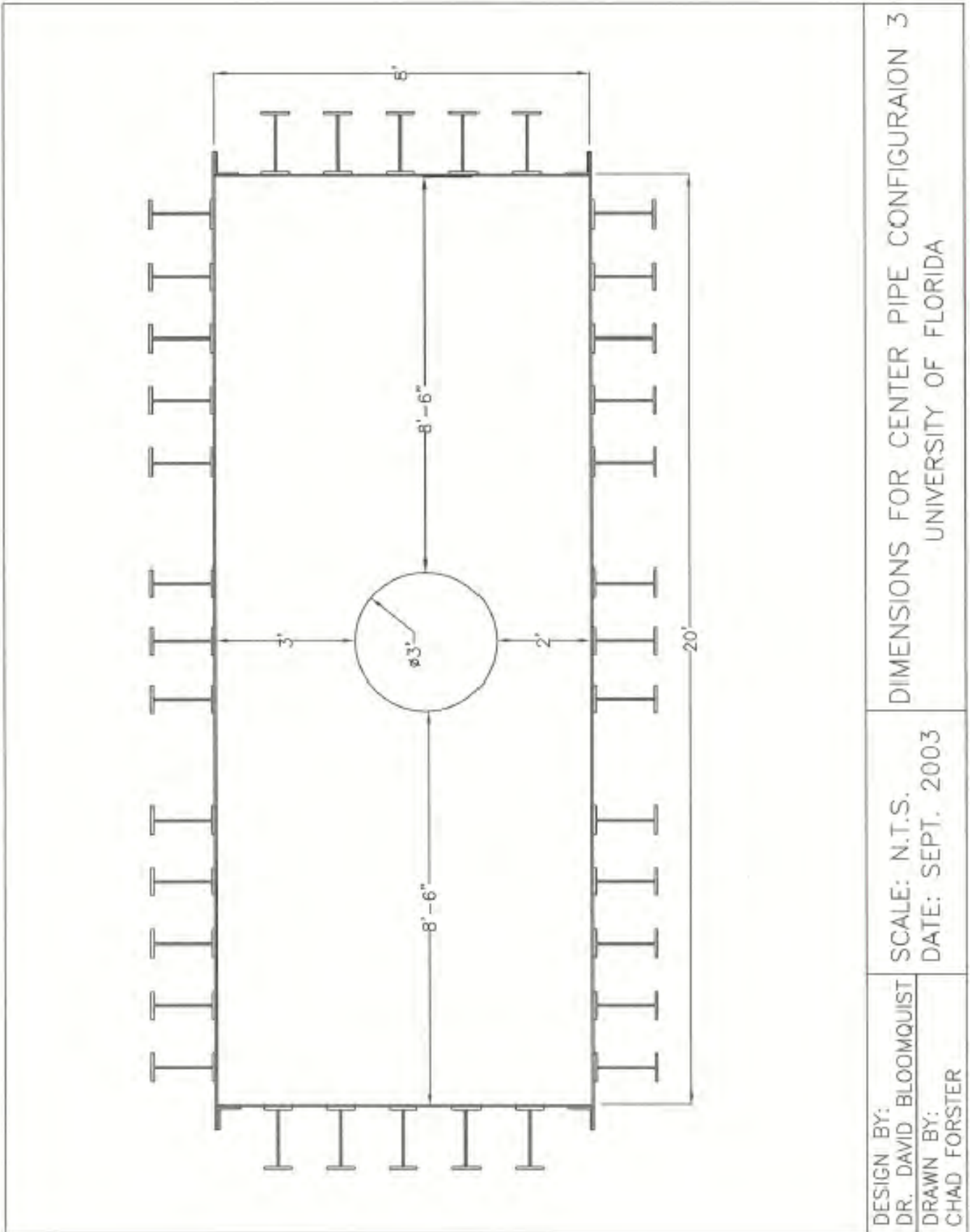


Figure 12. Single portal - 2' soil support

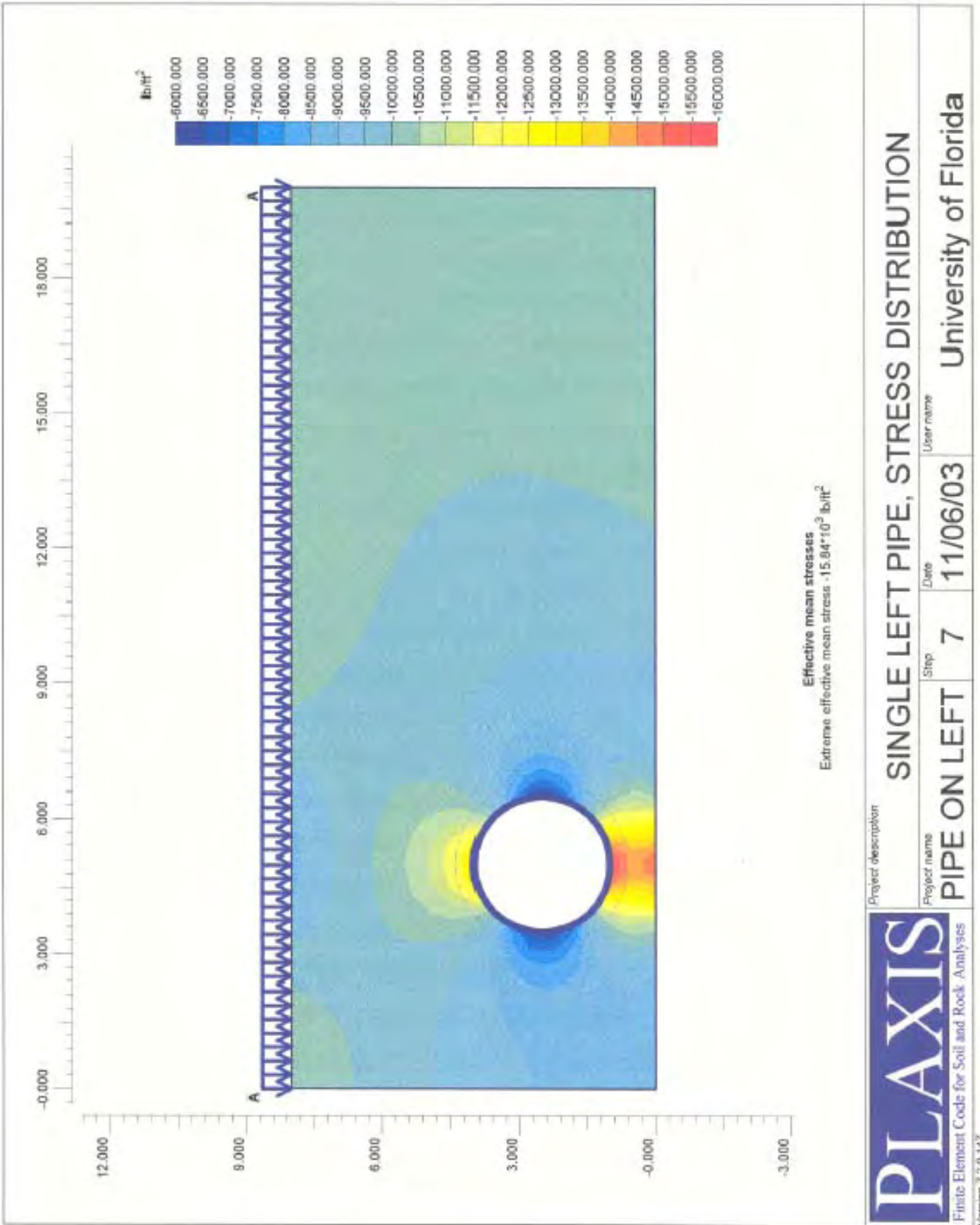


Figure 13. Boundary effects for offset portal

The previous plots are provided to illustrate the stress distributions generated from the surface loading. Based on the results from the Master’s student research, it is possible to test two pipes simultaneously without incurring a substantial (less than 8%) overlap of stresses.

### CHAPTER 3. Structural Analysis and Alterations to the Original Container Design

#### *Simplification, Assumptions and Model of the Original Design*

The container is subjected to both vertical and horizontal loading. The vertical loads are applied upward on the top panel and downward on the floor assuming a hydrostatic, 118 psi contact pressure. Hence, the horizontal loads applied on the four side panels were also assumed to be 118 psi, i.e., a very conservative assumption. This is shown in the figure below.

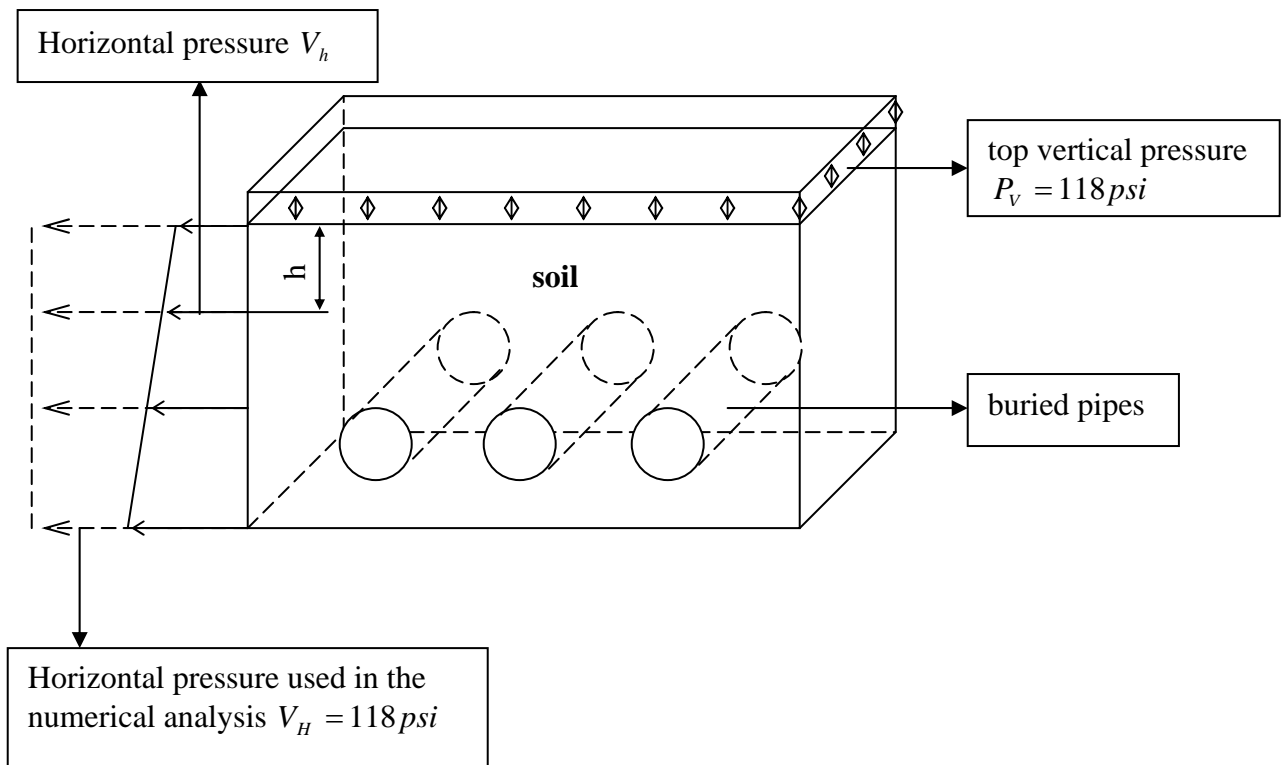


Figure 14. Assumed maximum applied pressures

The horizontal pressure  $V_h = K_0(\gamma_s h + P_v)$ , in which  $K_0 < 1$  and top vertical pressure is assumed to be  $P_v = 118 \text{ psi}$ . In order to analyze the worst conditions (i.e., assuming that the container is a hydrostatic vessel)  $K_0 = 1$  thereby producing a homogeneous, isotropic pressure throughout the entire container. It is also assumed that  $\gamma_s h = 0$  since  $\gamma_s h \ll P_v$  (i.e., no surcharge above the applied surface load) and that all steel panels will be subjected to an applied pressure of  $118 \text{ psi}$ .

In order to evaluate the structural rigidity, numerical analysis software ADINA 8.1 was employed to perform these calculations. It is important to note that we were provided expert advice on the use of the program from Dr. Hong, a visiting structural engineering professor from MIT. The steel panels were configured as shell elements while the entire structure is made up of a combination of 14 panels bolted together into a 3D structure. The main purpose of this analysis is to verify the structural rigidity of the original design by analyzing the displacements of the plates and members, and if needed refine the design to provide the required stiffness.

### ***Evaluation and Revised Design***

**Front Panel.** The results of the analysis show that the original design, while structurally sound, suffered from a lack of stiffness. This is evident in the ADINA displacement plots shown on the following pages. The maximum displacement occurs at the center of the front (and rear due to symmetry) panel as indicated by the arrows. The locations in red denote the “critical” or most flexible areas. The addition of vertical I-beams at each of those locations is a viable solution. However, locations 2 and 4 are at the junction where the panels connect to one another, hence it is not possible to attach a vertical beam in these locations. Alternative solutions are outlined below:

1. Increase the panel thickness. From the figure it is seen that if the wall thickness is doubled from  $0.5 \text{ in}$  to  $1.0 \text{ in}$ , the displacement reduces to less than  $0.2 \text{ in}$ .
2. Add vertical I-beams at positions 1, 3 and 5.
3. Install a small brace to reduce displacement at positions 2 and 4.

The alternative solutions were analyzed and a comparison amongst displacements for the original and revised designs are shown on the previous page. For a particular wall thickness, when solution #2 is employed, the displacement drops but not a substantial amount. For solution #3, the displacement drops for a 0.5 in. plate thickness then even increases for larger thicknesses. It is worth noting that the maximum displacement now occurs in the middle of the panel, which occurs at location 3.

After strengthening, the maximum displacement is reduced from 0.61 in. to 0.17 in. for the 0.5 in. wall thickness.

Hence, when solutions 2 and 3 are combined, the results are very conservative. While the displacement is dramatically reduced, solution #3 is the most cost effective (rationale provided in the Design Conclusions).

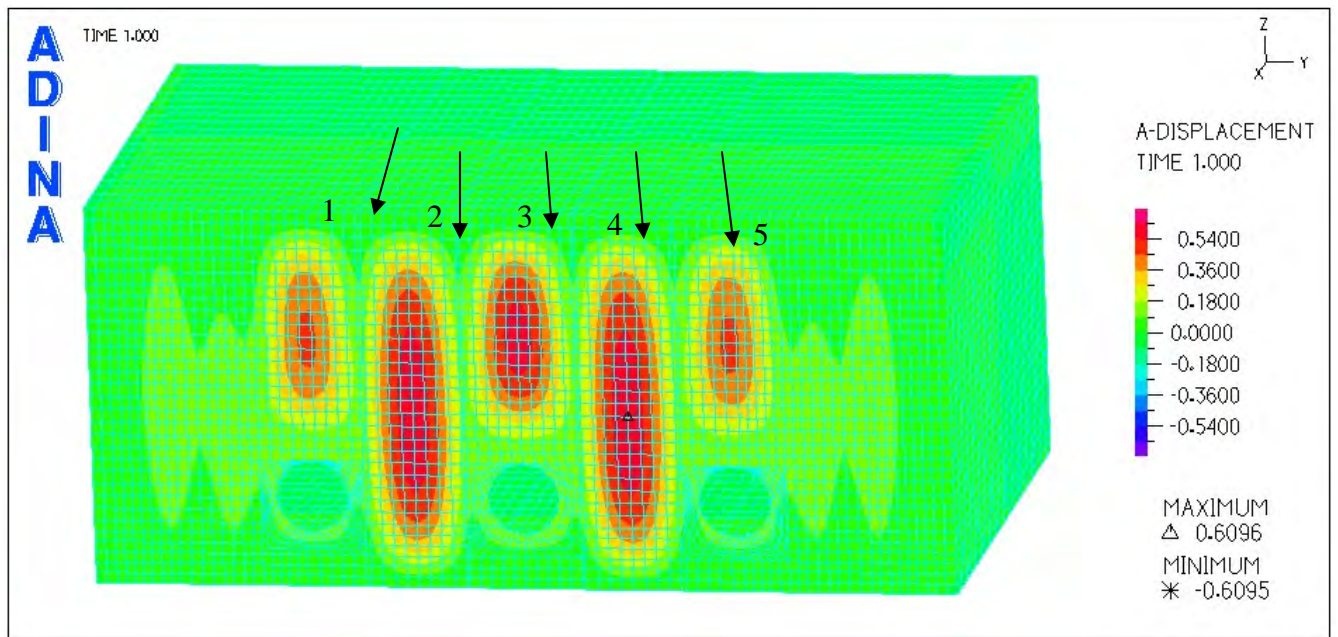


Figure 15. Front panel displacement plot of the original design (displacements in inches). (Locations 1-5 are the critical points requiring reinforcement).



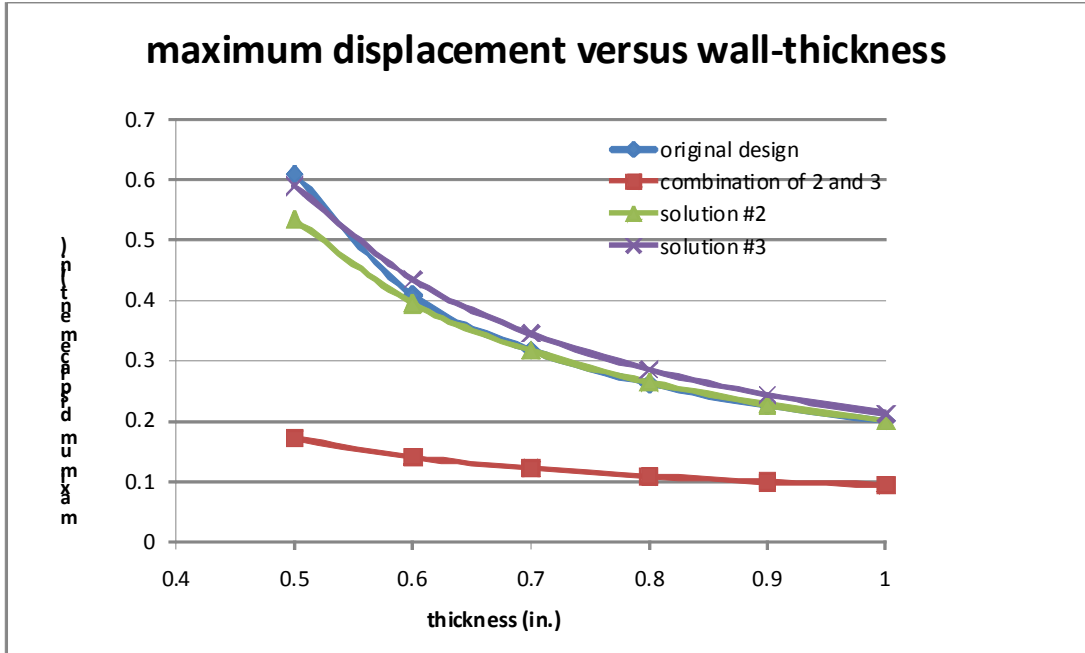


Figure 16. Wall thickness versus wall displacement

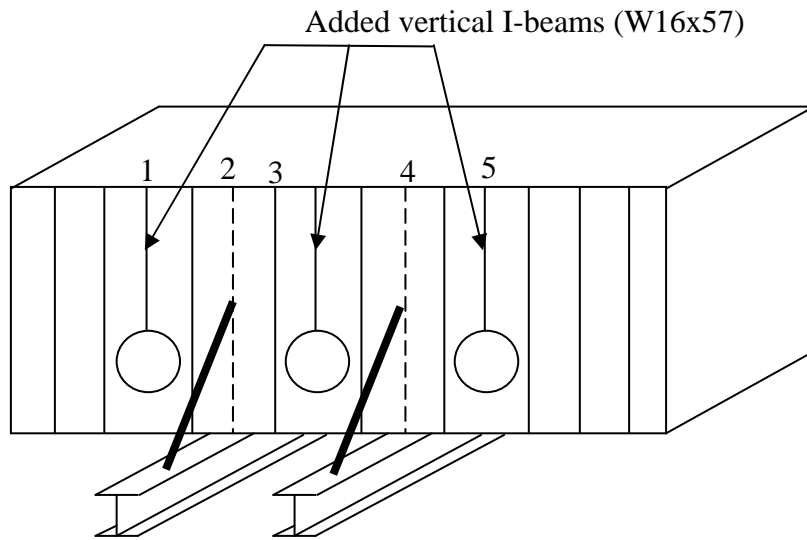


Figure 17. External stiffeners added

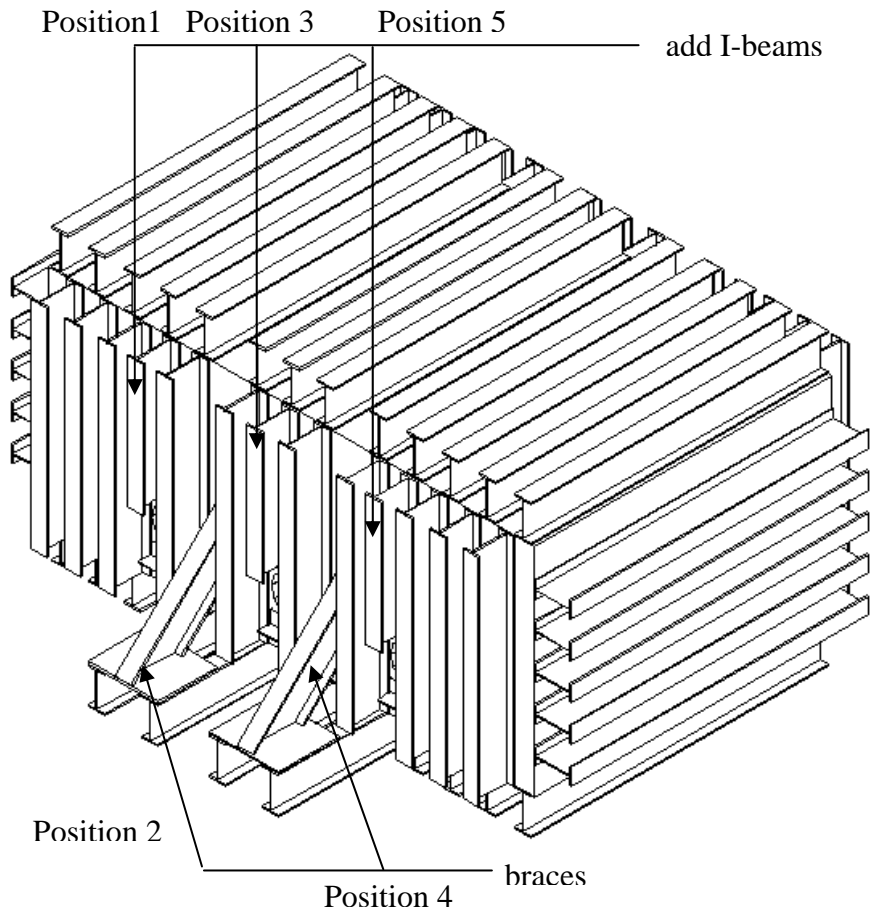


Figure 18. Proposed brace structure and vertical I-beams on front and rear panels.

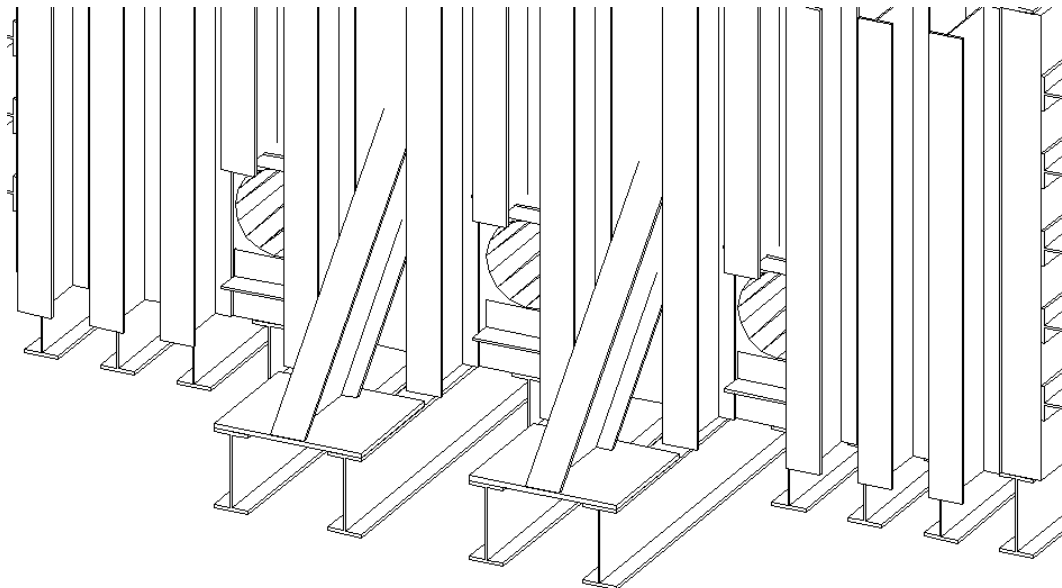


Figure 19. Brace structure for front and rear panels.

**Top panel.** The original design resulted in a maximum deflection of 0.8347 *in.* in the top panel as shown in the figure below. Therefore the top panel required strengthening. The solution was to add I-beams at locations designated as 6, 7, 8 and 9.

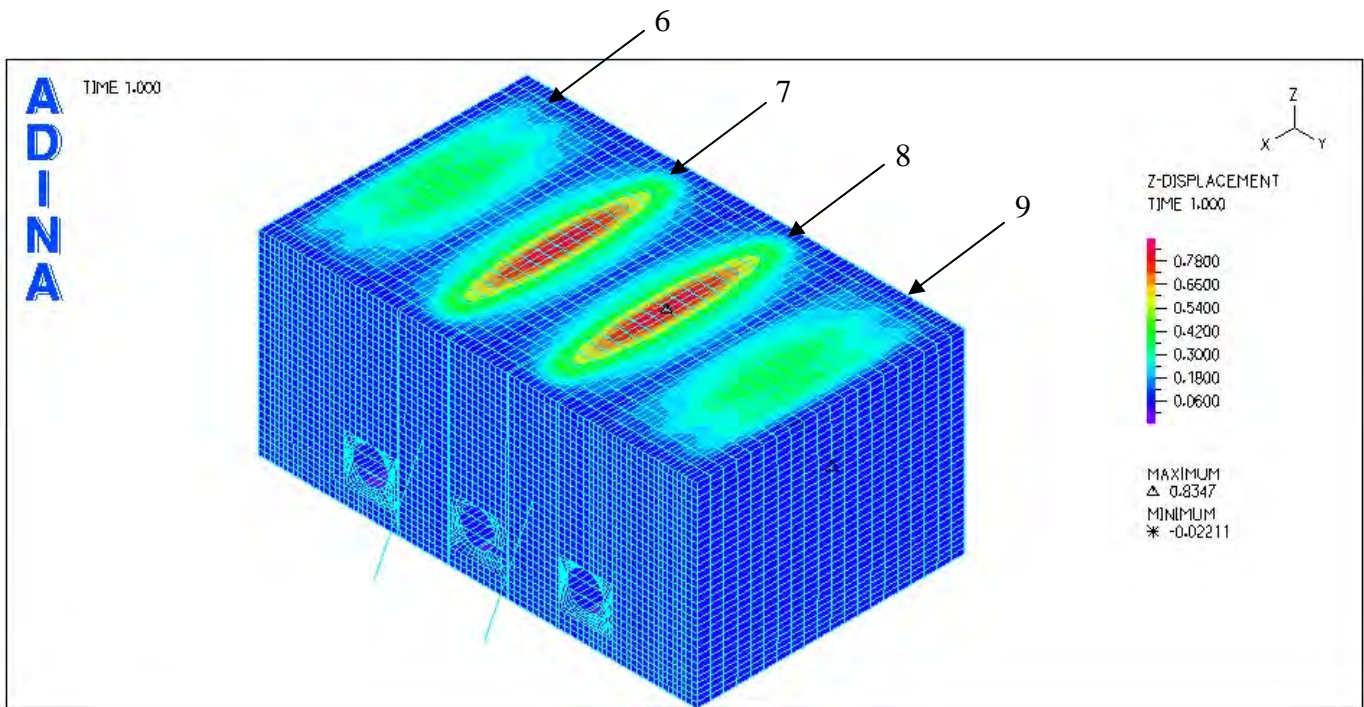


Figure 20. Original top deflection plot with plate thickness = 0.5 *in.*

The new maximum deflection at top panel is plotted in Figure 21. By adding the stiffeners, the plate thickness was maintained at 0.5 *in* to reduce the weight (for lifting). The maximum deflection was subsequently lowered to 0.3459 *in.* During the actual tests, the deflection of top panel is less critical to the test results because the vertical loads are transmitted through the soil and minor deflection of the top will be compensated for in the lift bags.

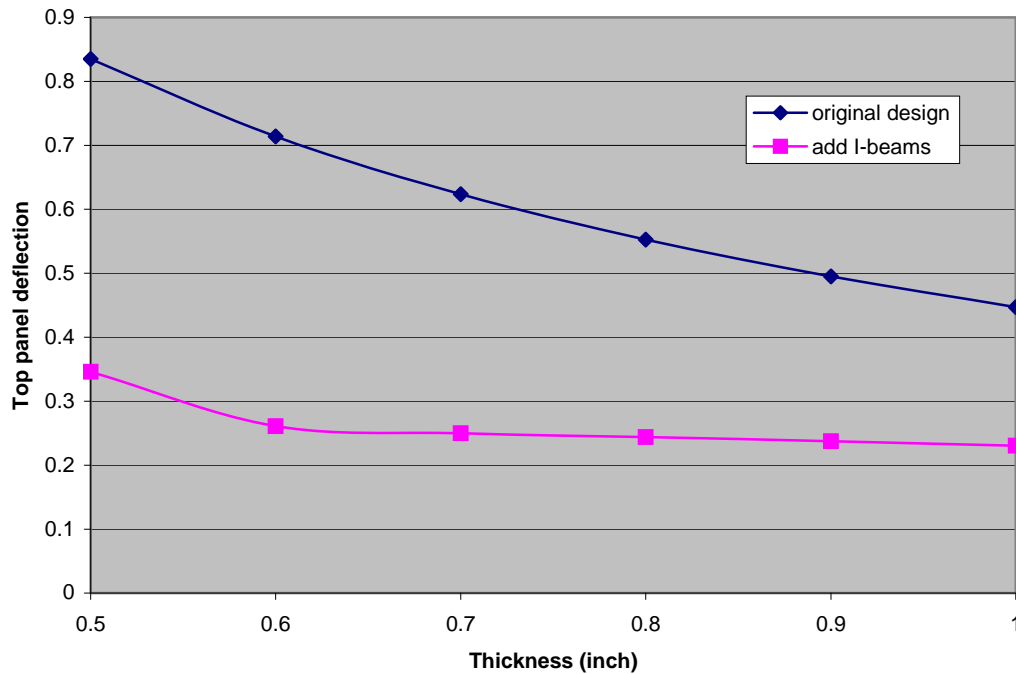


Figure 21. Top panel deflection versus wall plate thickness.

**End panels.** The original design produced a maximum deflection of 0.4247 *in.* at the end panels as shown in the ADINA plot. The maximum is located at node point 9809 (-66,216,70.4) as shown in red. Therefore the end panels also required strengthening. Several solutions were considered.

1. Change end panel I-beams from W16×57 to W16×67 or W16×77.
2. Increase wall thickness.
3. Add another series of horizontal I-beams to each end panel.
4. Add three vertical I-beams to each end panel.

i) Results for solutions #1 and #2. All units are in inches.

Thickness	0.5	0.6	0.7	0.8	0.9	1.0
W16×57	0.4247	0.3964	0.3777	0.3715	0.3667	0.3661
W16×67	0.3530	0.33	0.3156	0.3079	0.3065	0.3061
W16×77	0.2912	0.2873	0.2779	0.2689	0.2672	0.2666

ii) Results for solution # 1 and # 3

Thickness	0.5	0.6	0.7	0.8	0.9	1.0
W16×57	0.4247	0.3964	0.3777	0.3715	0.3667	0.3661
W16×67	0.3198	0.2797	0.2718	0.2645	0.2576	0.2521
W16×77	0.2811	0.2691	0.2577	0.2473	0.2403	0.2337

iii) Results for solution #4.

Thickness	0.5	0.6	0.7	0.8	0.9	1.0
W16×57	0.1970	0.1745	0.1619	0.1540	0.1492	0.1471

The structural analysis indicates that the bolted connection is strong enough to resist the tensile and shear stresses. However, to be even more conservative, tie rods are employed for additional strengthening, a fact that is not included in the analysis. The original span of the top I-beams did not completely span the panel and therefore the prying action at the ends of the top panel I-beams was considered in the analysis. However, a subsequent change to the design now extends the beams to the edges, thereby eliminating the prying action. The stiffness of the plates spanning the two I-beams and the two I-beams themselves are not included in the model. The purpose of these braces is to reduce the deflection at the end of the canted I-beams to zero, which is modeled in the analysis. Hence additional I-beams were added beneath the angled braces as shown in Figure 22. All of the external bracing allowed for a nominal 5/8 in. wall thickness for the sides and bottom to be used in order to save weight and reduce cost. The 0.5 in. top plate was maintained.

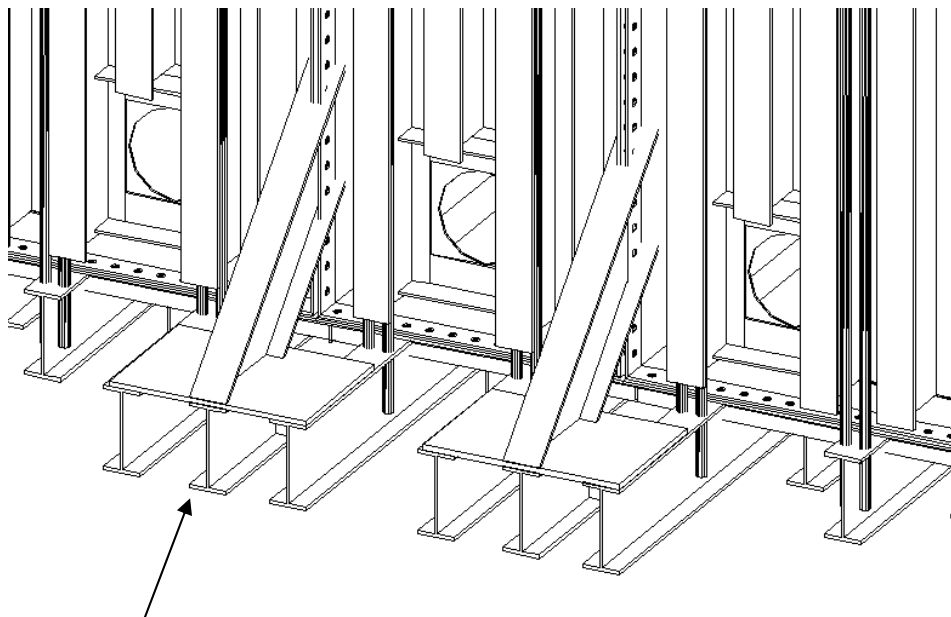


Figure 22 The revised braces.

The reason no short horizontal I-beams were added between the vertical I-beams is due to the existence of sub-panel connections, which make it difficult to install horizontal I-beams at those locations.

The bottom plate is the same as the top. However, the major difference between the top and bottom plates is that the bottom plate, supported by I-beams, is anchored to the structural floor slab. This reduces lateral and vertical movement of the bottom plate to zero. The analysis shows the maximum deflection at the bottom plate is less than 0.1 inch, due to the elastic deformation of the materials.

The steel top plates do not span in the short direction between the vertical I-beams. Only six beams are extended out beyond the panel to provide attachment for the tie rods. As mentioned previously, to reduce the prying action at the end of the I-beams the I-beams were extended out to the edge of the container. This is shown in Figure 23 below.

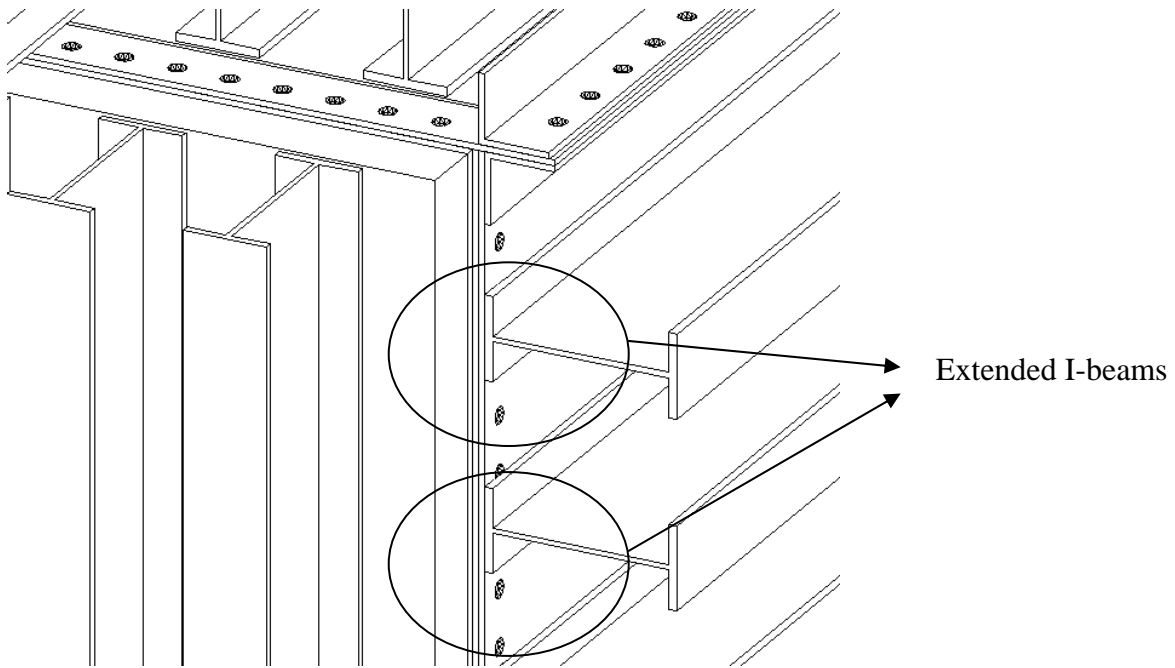


Figure 23. Extension of I-beams at the end panels.

The large deflections at positions 7 and 8 are due to the connections between subpanels that make up the top panel. The distances between I-beams at positions 7 and 8 is 25 inches, i.e., relatively larger than the other distances of approximately 17.5 in. This is the

reason for non-uniform lid deformation. However, after revising the design describe above, the top deflection is now more uniform, as can be seen in the Figure 24 below.

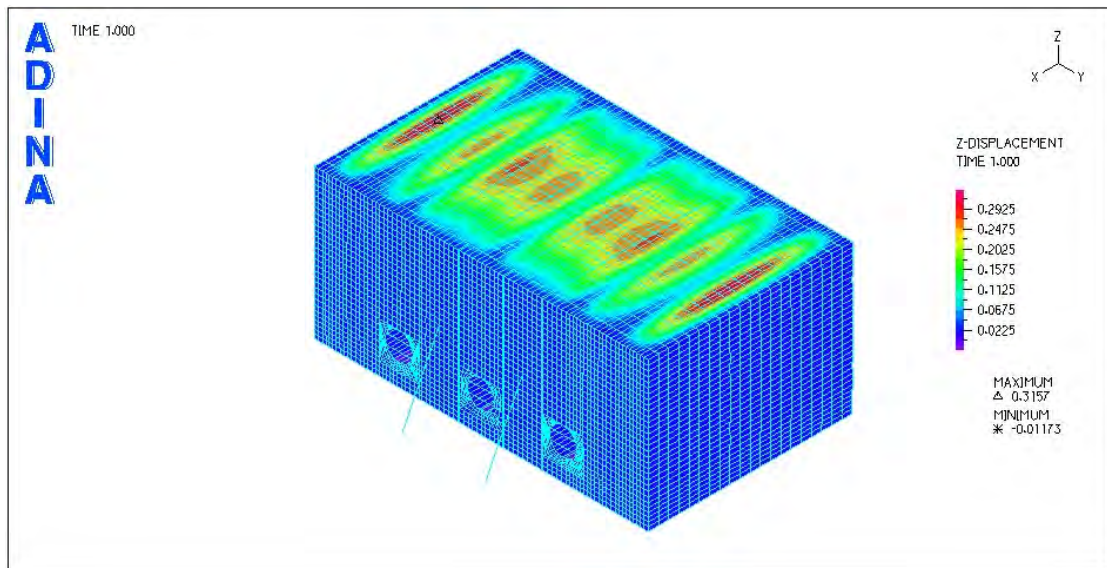
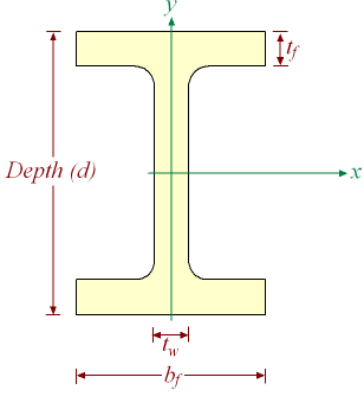


Figure 24. The top panel deflection of the revised design (units inches).

T

his is due to the use of a larger size I-beam ( $W18 \times 119$ ). The maximum deflection is thus reduced to 0.1908 in. The effect of different size I-beams is provided in Table 6. In addition, a general deflection plot for the different types of I-beams is plotted in Figures 25 through 32. Please note that the colors represent deflection patterns, but only for a particular plot. That is to say, pink on one plot is not an absolute displacement that can be compared to the pink on another. Regardless, it shows how the larger beams help distribute the stresses more uniformly.

Table 6. Effect of Using Different I-beams on End Panel Deflection

	I-beam type	d (in)	bf (in)	tf (in)	tw (in)	Maximum deflection (in)
	W16×57	16.430	7.120	0.715	0.430	0.4247
	W16×77	16.520	10.295	0.760	0.455	0.3130
	W16×89	16.750	10.365	0.875	0.525	0.2760
	W16×100	16.970	10.425	0.985	0.585	0.2488
	W18×65	18.350	7.590	0.750	0.450	0.3228
	W18×71	18.470	7.635	0.810	0.495	0.3005
	W18×97	18.590	11.145	0.870	0.535	0.2239
	W18×106	18.730	11.200	0.940	0.590	0.2097
	W18×119	18.970	11.265	1.060	0.655	0.1908

The following ADINA plots show the deflection contours for the end panels for the various I-beams. As can be seen, the final choice reduces the maximum deflection to a reasonable value. Again, the underlying assumption is a uniform hydrostatic pressure of 118 psi is being applied to the entire end panel surface. This will not occur during actual testing and thus is a very conservative assumption.



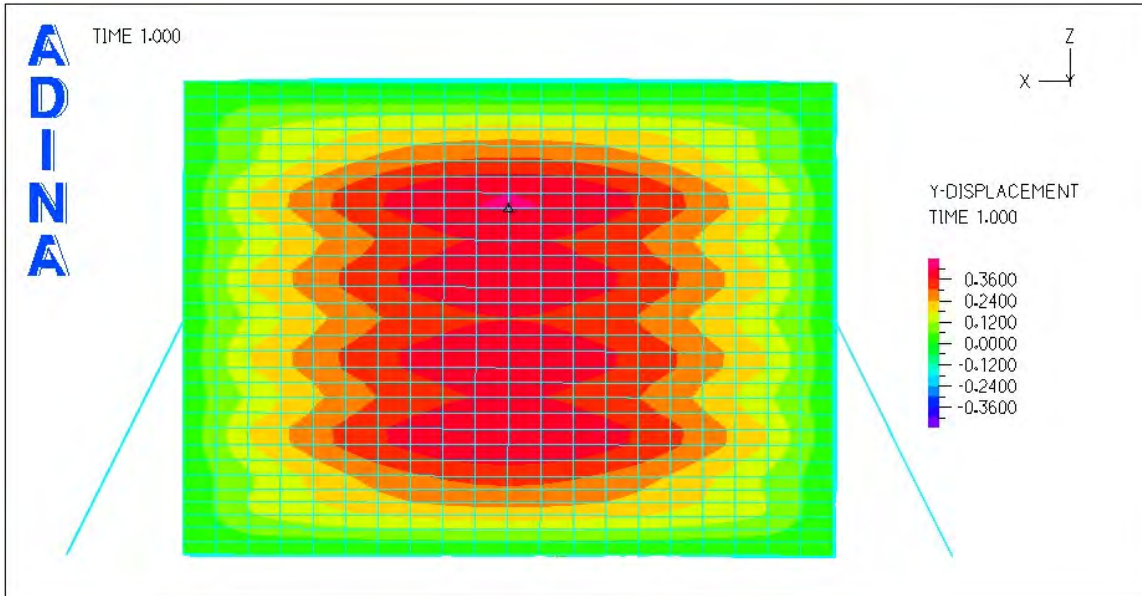


Figure 25. Deflection of end panels utilizing a W16×57 section (note units are inches). The triangle icon represents a max deflection point of 0.427 inches.

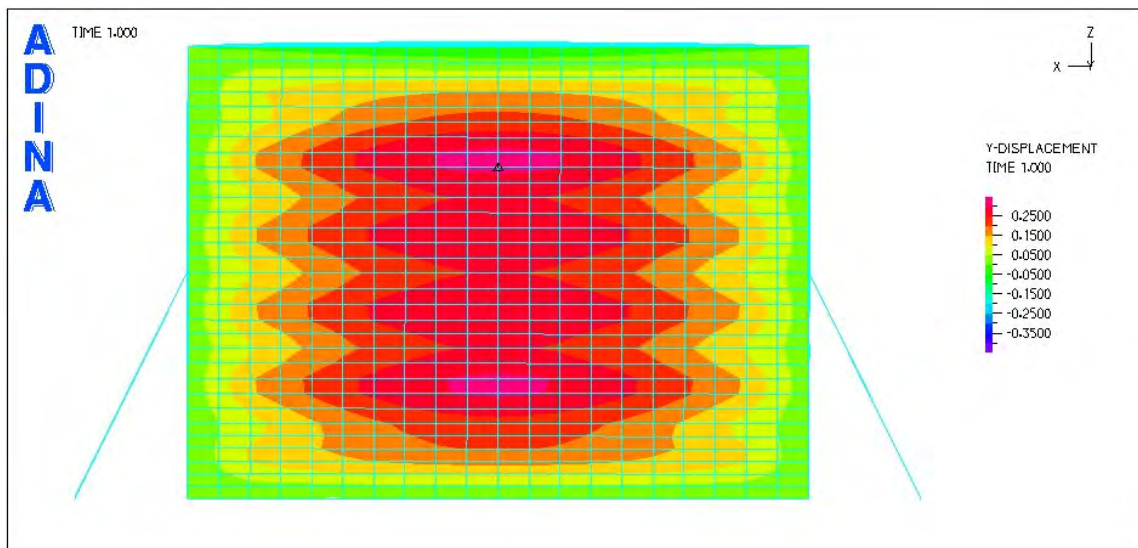


Figure 26. Deflection of end panels - W16×77 (units are inches). Two stress contours are created with a maximum displacement of 0.313 inches.

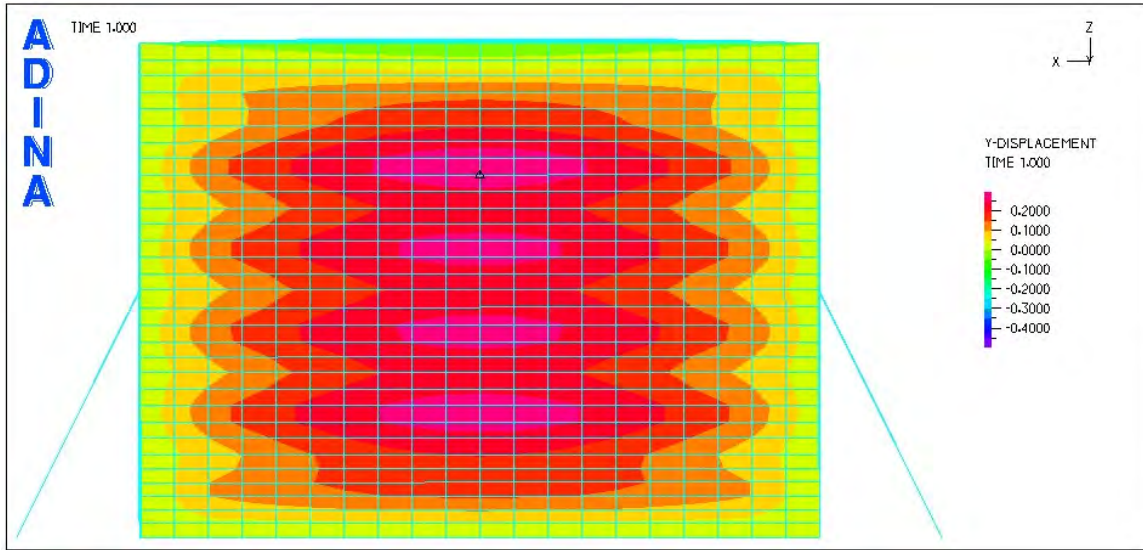


Figure 27. Deflection of end panels - W16×89 (units are inches).  
As the I-beams increase in depth, the stress contours continue to evolve vertically, but reduce in magnitude as well (0.276 inches).

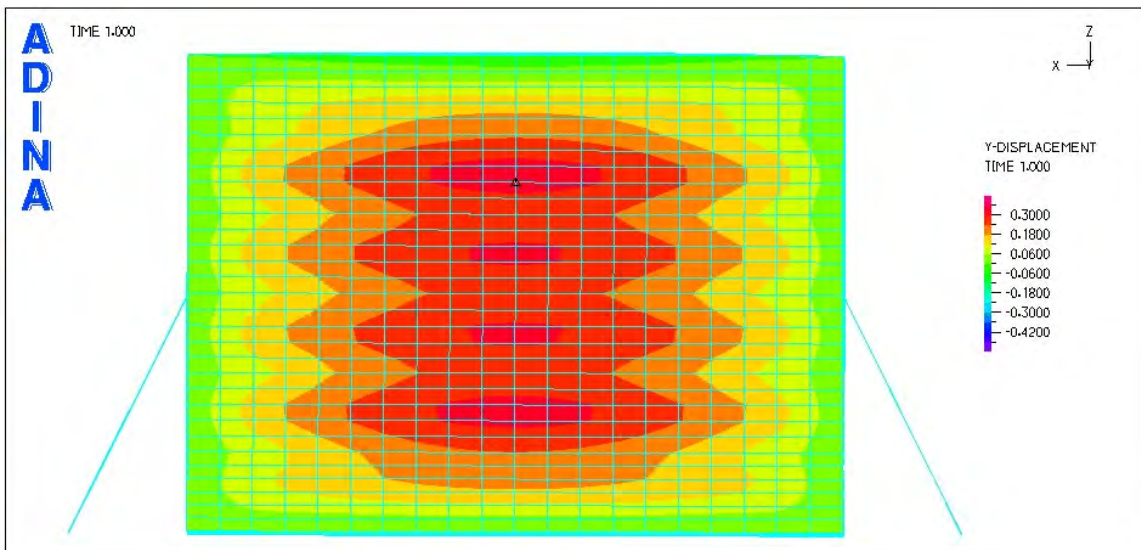


Figure 28. End panel deflection using W18×65 (inches).  
By increasing the width and reducing the depth of the I-beam produces a stress distribution similar to the W16×77 element.

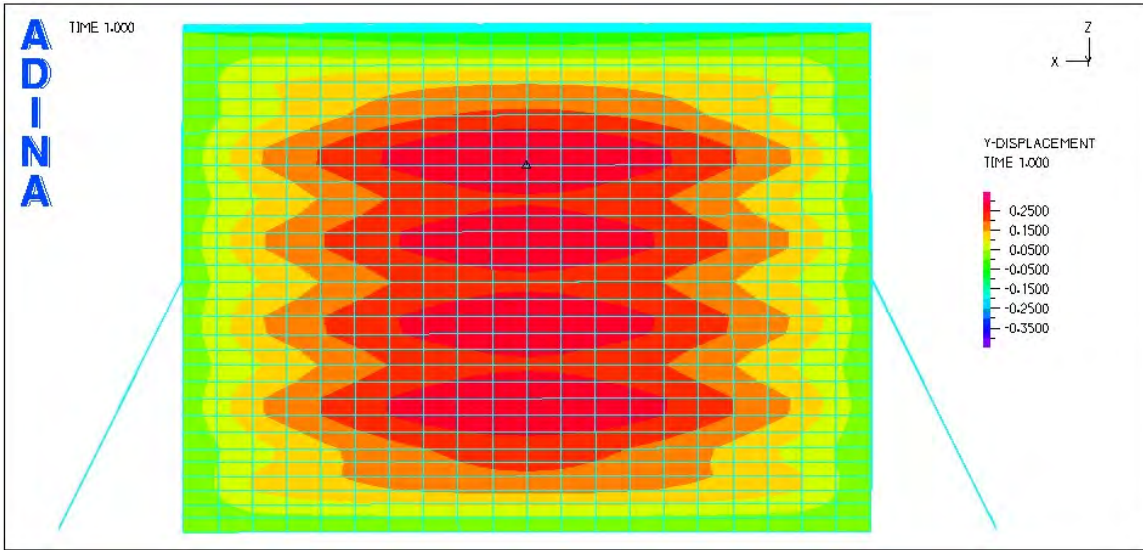


Figure 29. Deflection of end panels using W18×71 (inches).

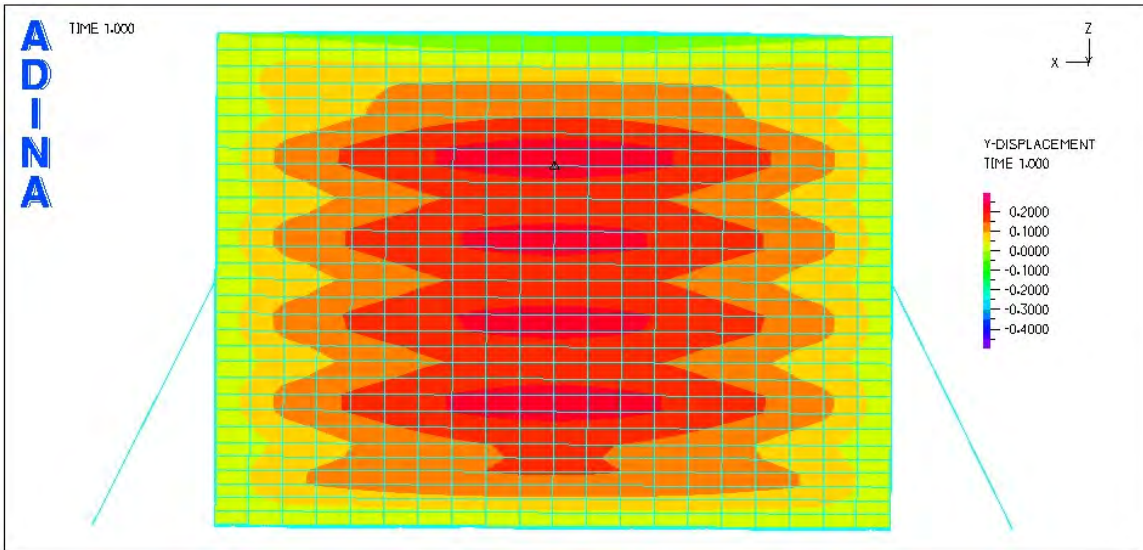


Figure 30. End panel displacement contours (inches) using W18×97 I-beams.

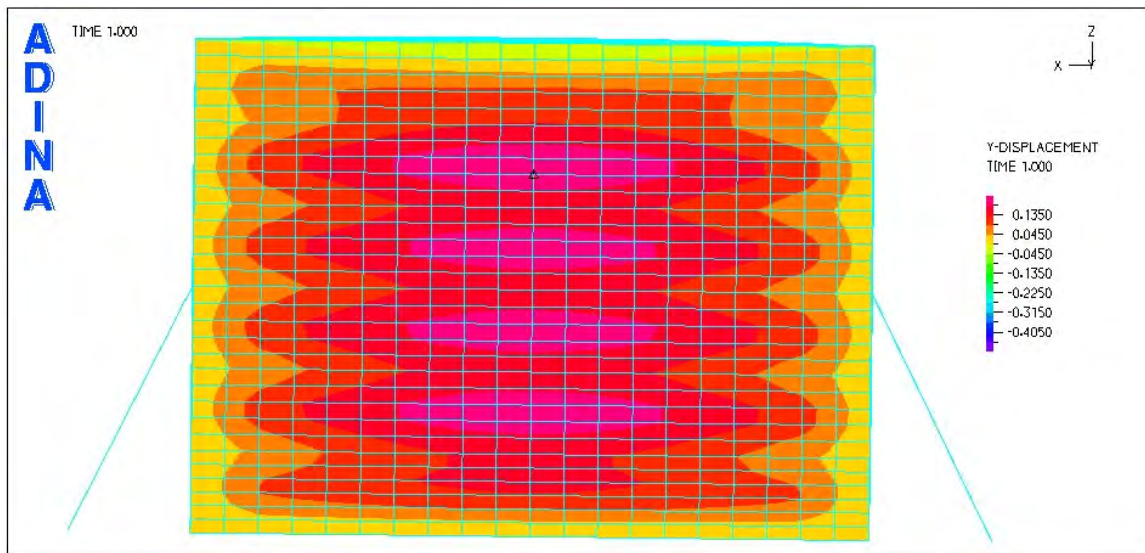


Figure 31. Deflection of end panels by using W18×106 (inches).

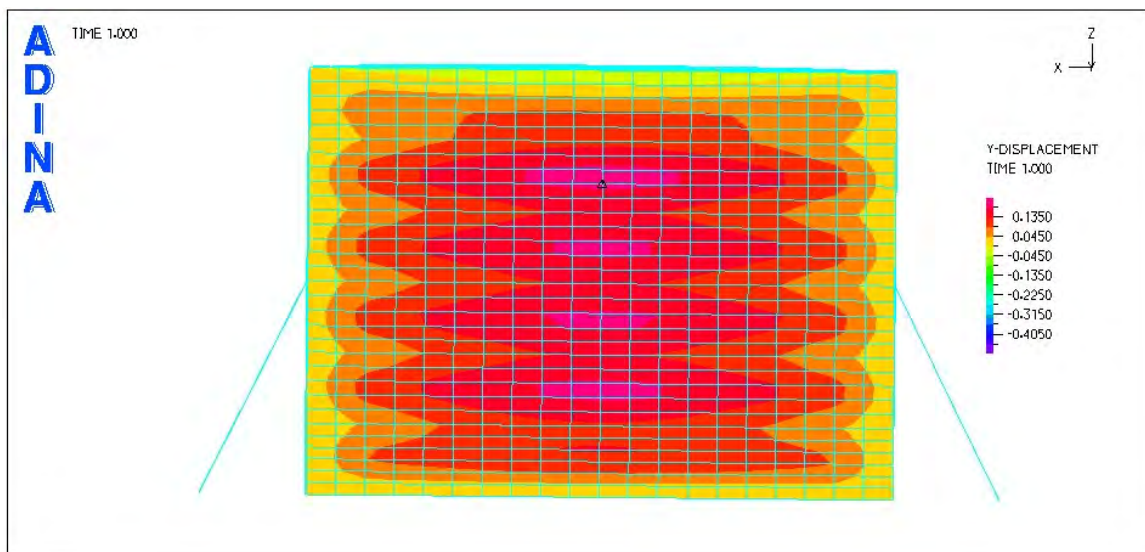


Figure 32. Deflection of end panels using W18×119 I-beams (inches).  
This is the minimum size structural element that meets the 0.2 inch maximum deflection objective.

## CHAPTER 4. DESIGN CONCLUSIONS

Based on the expert advice from the consultation team and FDOT personnel, the design of this new testing container has been dramatically improved, which in hindsight, was warranted. It bears mentioning that this improved design would not have been possible were it not for the valuable suggestions of an experienced review board. Even though the cost of this new design increased over the original one (\$82K versus \$32K), it will produce a much better test bed. Hopefully, the construction of this unique device will come to fruition in the near future thereby providing researchers an opportunity to simulate prototype events in a laboratory environment.

The remainder of this report provides summaries of the various aspects of the design and construction. The first section outlines the genesis of the box idea, while the second, provides examples from the PLAXIS analysis. Finally, the structural design analysis is included indicating the changes made to the original box as well as quantitative results vis-à-vis wall deflections. It is germane to point out once again, that this design assumes a hydrostatic loading (118 psi) throughout the container. Hence, it is a “worst-worst case” scenario in terms of deflections that still provides a substantial factor of safety – even more important when student researchers are involved.

The analysis shows that solution #3 is the most effective, easiest, and probably the most economical one. This is to install a small brace to reduce displacement along the wall openings. (at positions 2 and 4). These short (3 foot), inclined braces replace full length (i.e. 10 foot) I-beams, thereby reducing weight and cost while providing better access to the openings.

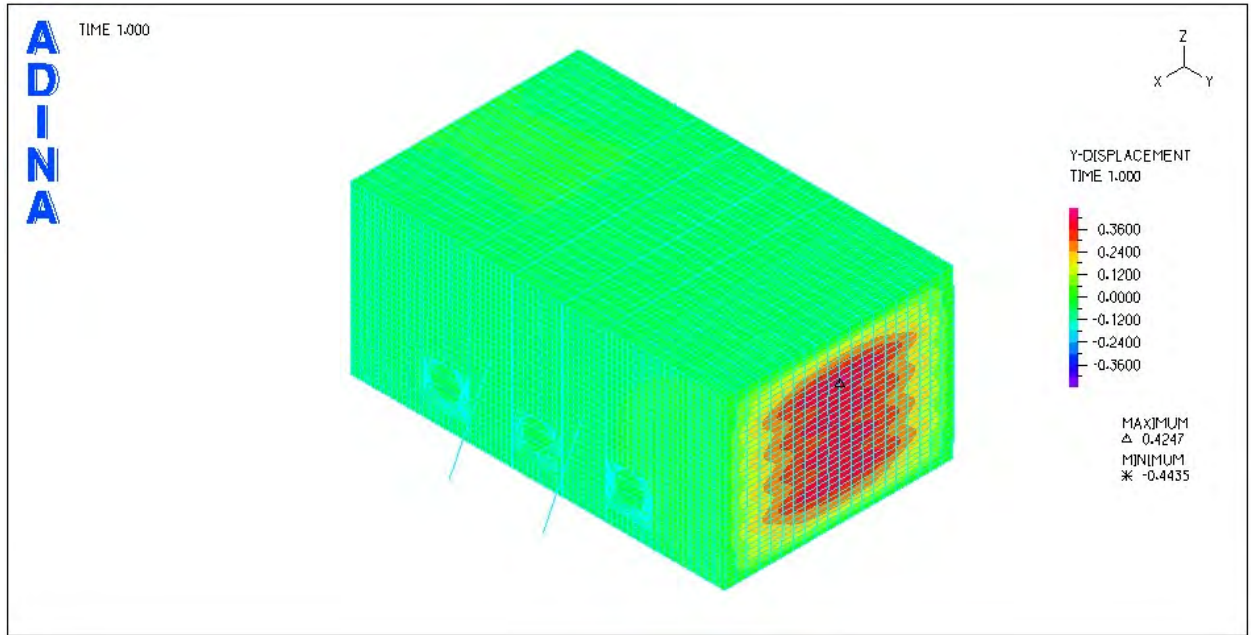


Figure 33. Original end panel deflection with panel thickness = 0.5 in.

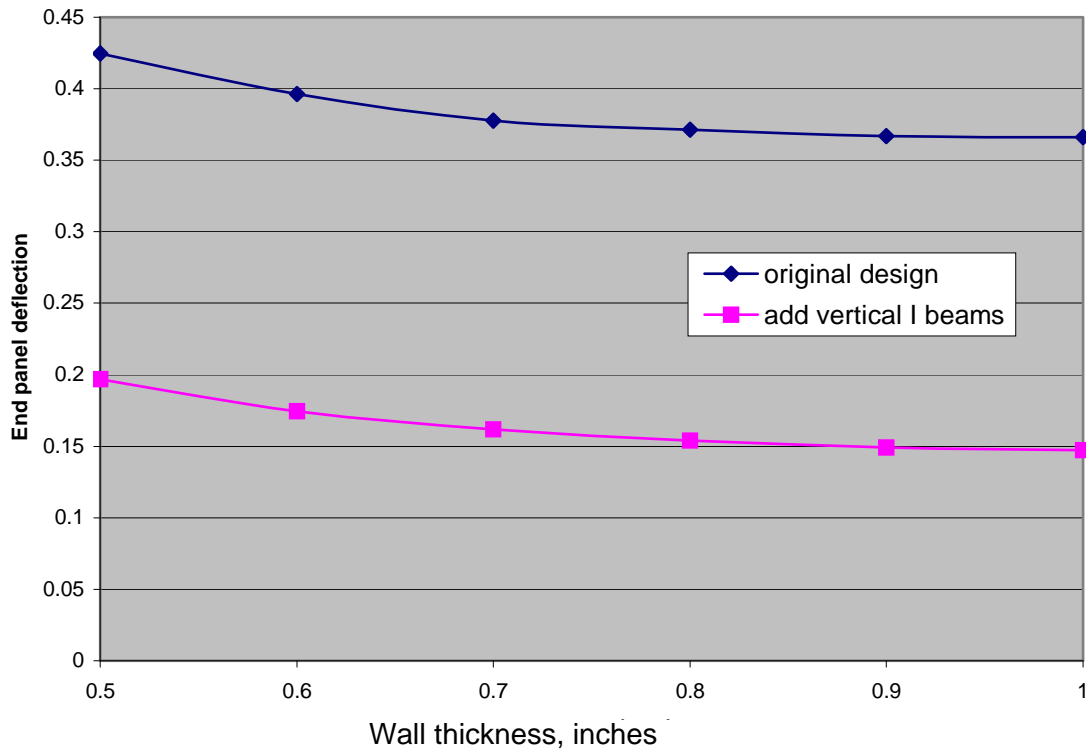


Figure 34. Plot of Wall Thickness versus End Panel Deflection

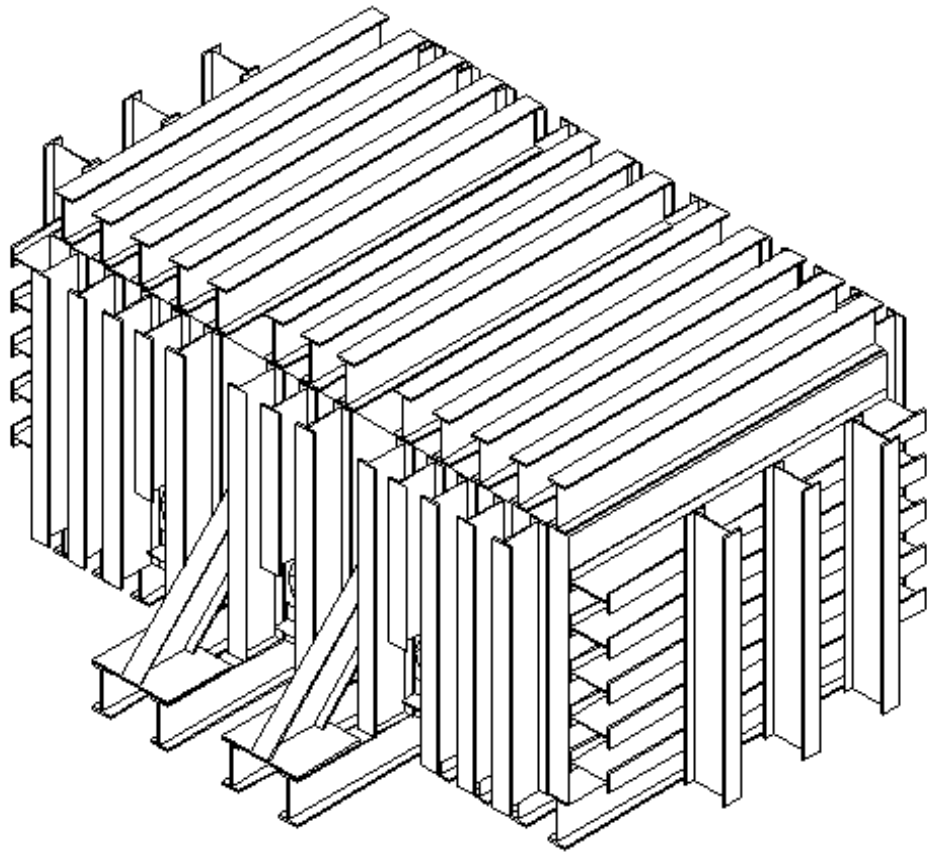


Figure 35. End panels strengthened by adding vertical I-beams.

## Tie Rod Addition

The aforementioned enhancements provide a very stiff structural vessel. However, as mentioned previously, there was a concern regarding the bolted connections for the panels. To further strengthen these areas, tie rods were added to “tie” the top and bottom sections together. These are shown in the figure below. In addition, six of the I-beams are extended out beyond the walls to provide the necessary attachment for the rods.

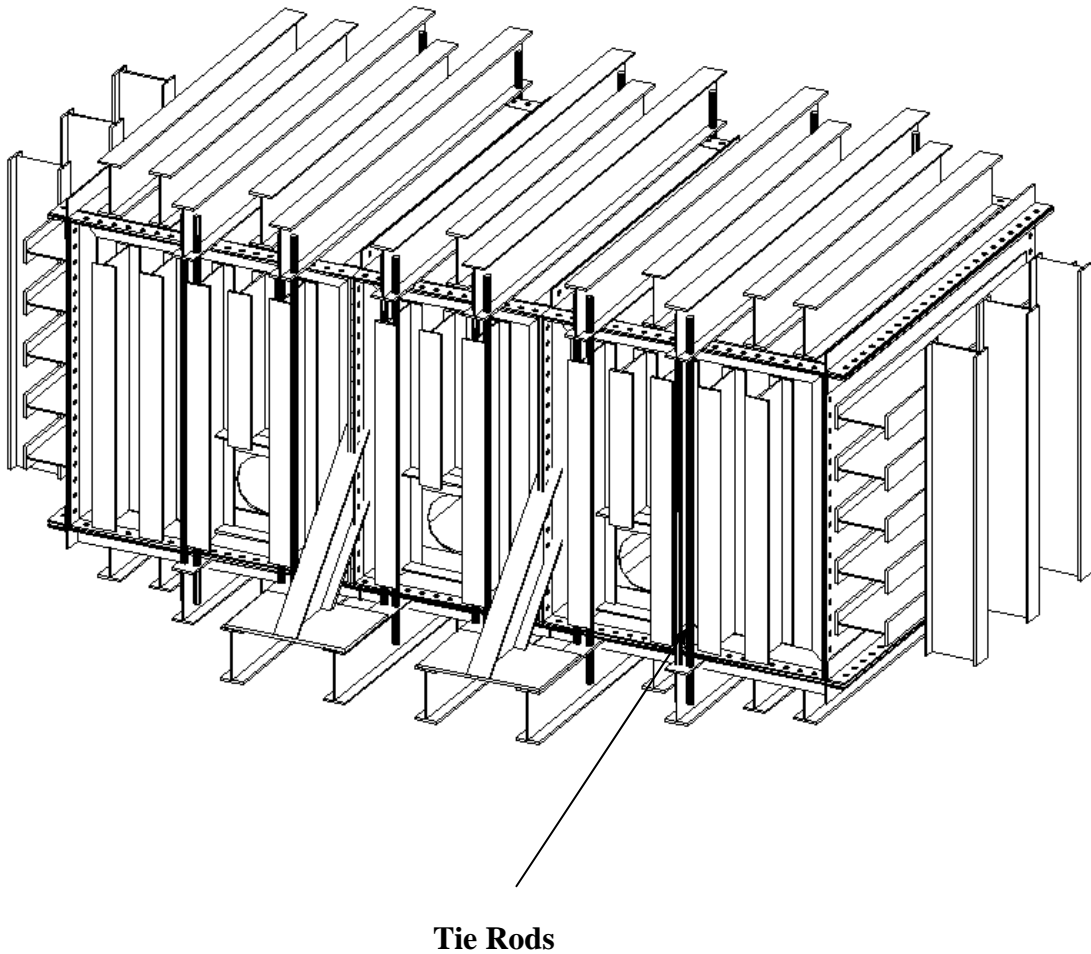


Figure 36. Added tie rods.



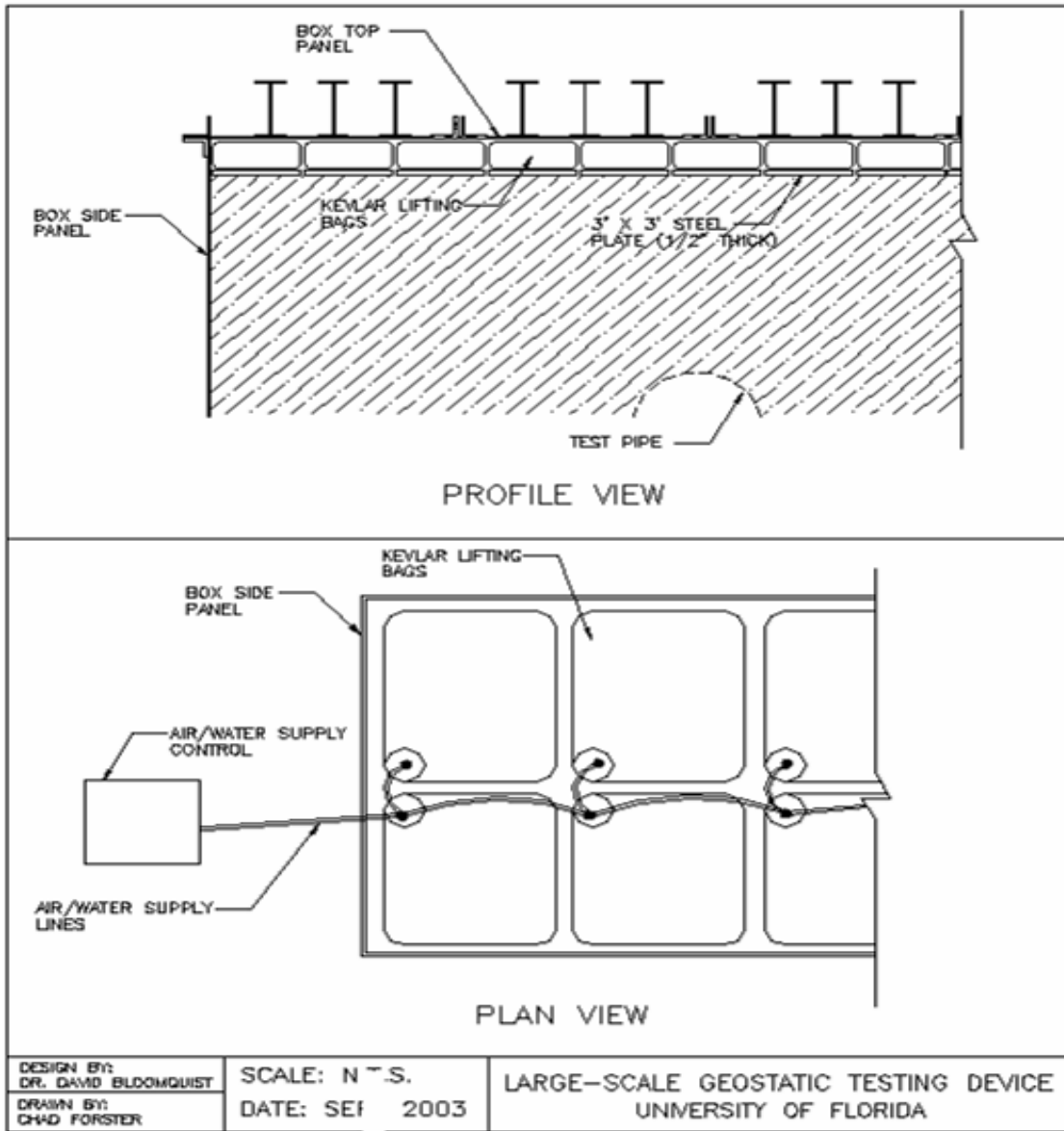
Table 7. Parts List for the Original Box Design

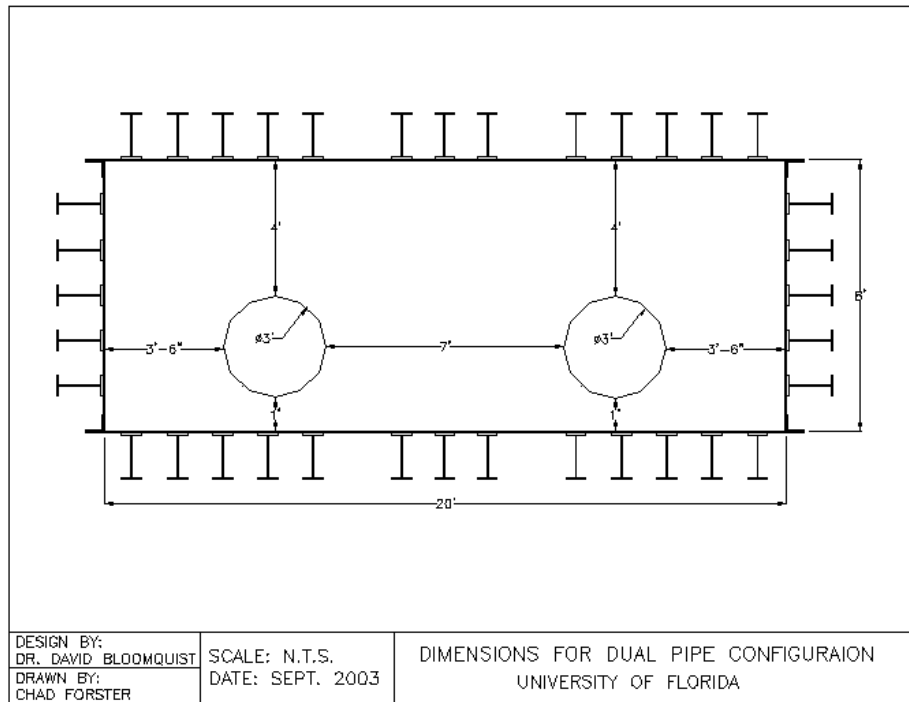
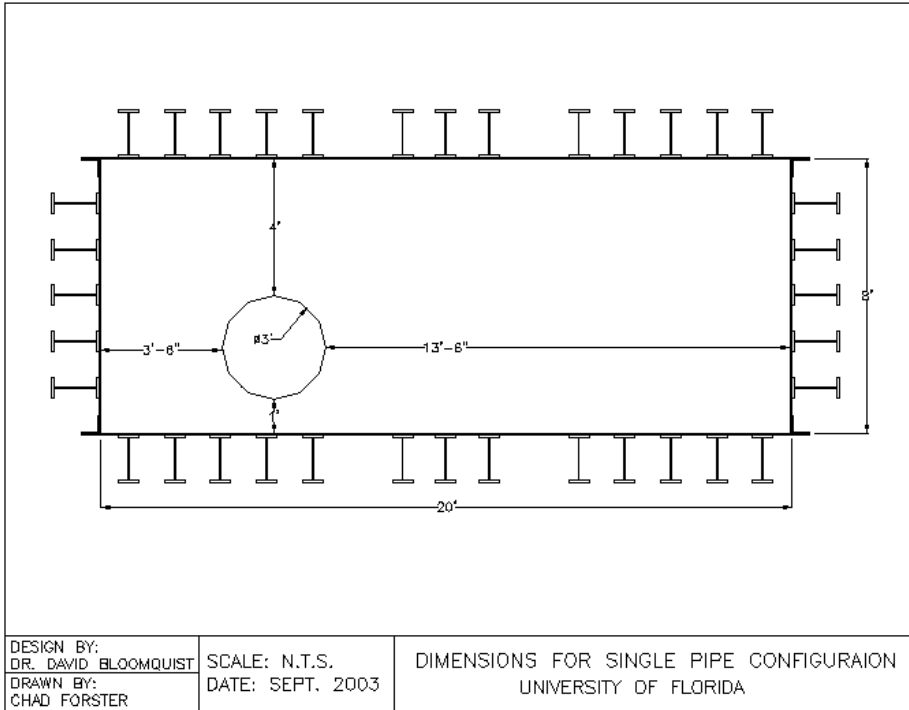
<b>Parts</b>	<b>Materials</b>	<b>Total</b>	<b>Cross Section</b>	<b>Properties</b>
STEEL PANELS	ASTM A36	14	N/A	thickness: 0.5"
I-BEAMS	ASTM A992	20	W16×57	7'-1.0"; vertical; front/back panels
		10	W16×57	10'-1.0"; horizontal; end panels
		13	W16×57	10'-1.0"; horizontal; top panel
		13	W16×57	10'-1.0"; horizontal; bottom panel
BOLTS	ASTM A325	(Approx.) 246	1 1/4" diameter	Bolt holes = 1 1/2" diameter
PIPE COVERS	ASTM A36	6	19" diameter; 17.5" diameter	0.5" thick; 0.5" thick

Table 8. Additional Parts Required for Revised Container

<b>Parts</b>	<b>Materials</b>	<b>Total</b>	<b>Cross Section</b>	<b>Properties</b>
STEEL PANELS	ASTM A36	14	N/A	thickness: 0.5"
		20	W16×57	7'-1.0" long; vertical; front/back panels
		10	W16×57	10'-1.0" long; horizontal; end panels
		13	W16×57	10'-1.0" long; horizontal; top panel
		10	W16×57	10'-1.0" long; horizontal; bottom panel
I-BEAMS	ASTM A992	2	W16×57	Extended (Approx.)19' long; horizontal; bottom panel
		6	W16×57	4' - 4.5" long; vertical; front/back panels

# Miscellaneous Soil Box Details







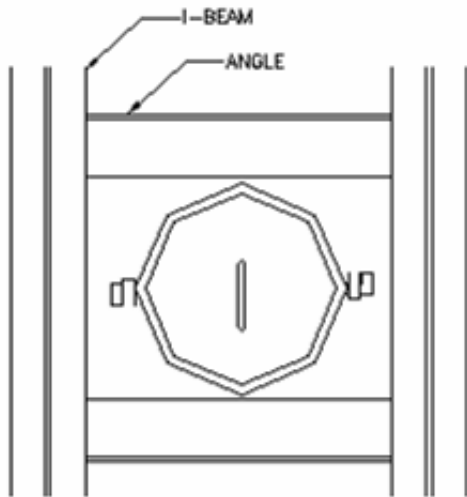
COVER DETAIL

19" DIAMETER X 0.5" THICK PLATE TO FIT AGAINST OUTSIDE OF PANEL

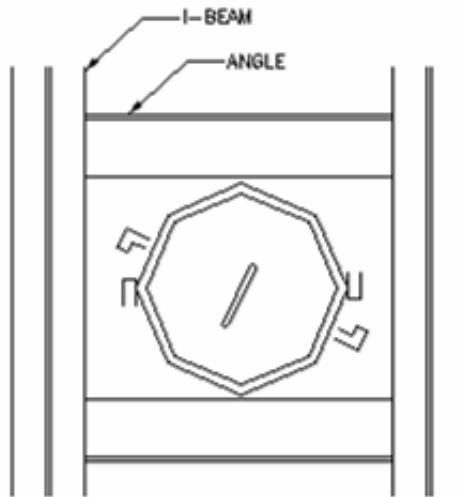
17.5" DIAMETER X 0.5" THICK PLATE WILL FIT IN THE 18" HOLE

THIN LAYER OF NEOPRENE TO BE PLACED AROUND INSIDE OF PANEL HOLE TO ACT AS A GASKET

PROFILE VIEW



LOCKED POSITION

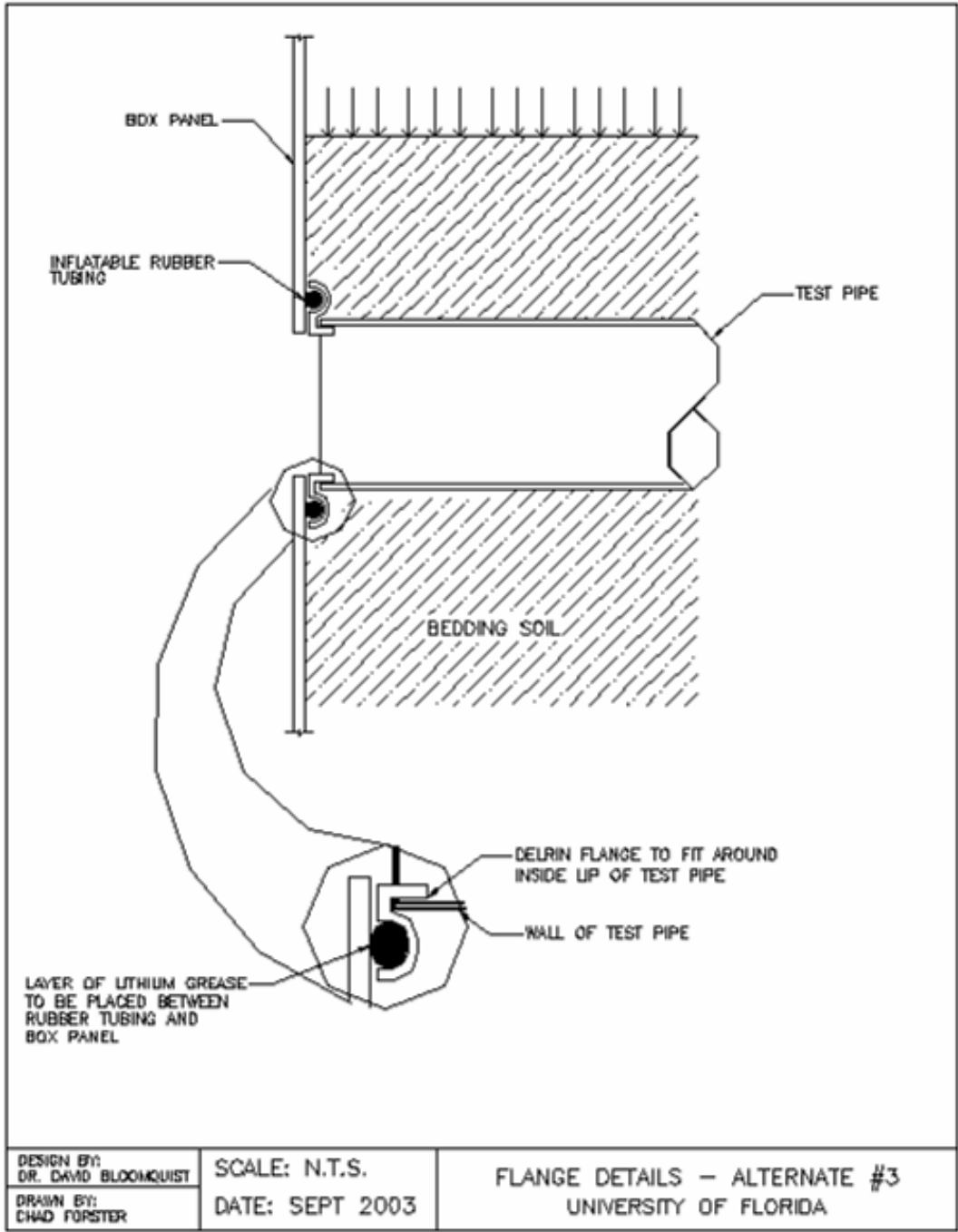


UNLOCKED POSITION

DESIGN BY:  
DR. DAVID BLOMQUIST  
DRAWN BY:  
CHAD FORSTER

SCALE: N.T.S.  
DATE: SEPT 2003

COVER DETAILS  
UNIVERSITY OF FLORIDA



## CHAPTER 5. SOIL BOX CONSTRUCTION

Once the extensive FEM analysis and subsequent reviews by numerous parties were completed, a contract was let for construction of the Soil Box. This proved to be a relatively straightforward operation. The only problem encountered during assembly was the fact that one of the bottom panels was warped excessively. Thus, it was returned to the fabricator who repaired the section in a timely manner.

The other related issue was that the crane used to off load the transport truck and place the pieces inside the Coastal Lab could not maneuver around some small trees. Hence they were removed.

The following are photos showing the sections of the box, including final assembly.

Hence, the Soil Box is now completed and ready for testing. In the future, two projects are anticipated: a polymer density project for FDOT and an elevated temperature testing of HDPE pipe - also for FDOT. Future tests are also anticipated - thus making valuable use of this unique device.



Figure 37. Spacers primed and painted.



Figure 38. Bolts and nuts being cleaned and painted.





Figure 39 Trees removed for crane maneuvering space.



Figure 40. Side panel showing pipe access port.



Figure 41. End panels in foreground and bottom panel in background.



a) Inside view

Figure 42. Soil box – Various views



b) Front view

Figure 42. Soil box – Various views, continued



c) Side view

Figure 42. Soil box – Various views, continued



d) End view

Figure 42. Soil box – Various views, continued



e) Pipe Access hole and cover



f) Close up of fastened nuts and bolts

Figure 42. Soil box – Various views, continued



**APPENDIX A.**

**SUPPLEMENT TO  
FINAL REPORT**

***FINITE ELEMENT ANALYSIS OF A LARGE SCALE SOIL BOX  
TEST FACILITY FOR EVALUATING THE STRUCTURAL  
RESPONSE OF BURIED STRUCTURES***

## BACKGROUND

Two and three dimensional finite element analyses were used to examine the stresses on a laboratory soil box test facility designed to evaluate the structural response of fiber reinforced and standard reinforced concrete pipes. Boundary conditions were examined in attempt to minimize the effects on the concrete pipe tested. The state of stress in the soil due to the applied loading was studied, along with its influence on the concrete pipe. An extensive literature search is presented on the history of soil box testing of pipes. Small and large-scale test facilities have been discussed through previous testing in the literature search. A description of the test facilities, both small and large, is presented. Plaxis, a two and three-dimensional finite element analysis program, analyzes the stresses on the sidewalls for the dimension design of a soil box properly scaled to minimize the boundary effects on the concrete pipe specimens. Comparisons were made between three different proposed box lengths. It was found that as the length increased, the stress concentrations and intensities decreased, thus minimizing the boundary effects.

Sidewall friction and its effects on the test pipe were examined. Two and three dimensional finite element analysis was used to assign a friction angle on the sidewalls in order to model the soil structure interaction. An additional analysis was done to examine the possibility of shear stresses induced on the ends of the pipe. Friction was induced on the front and rear wall to create shear stresses on the ends of the pipe. Shear stresses were induced on the ends of the pipe in the three dimensional analyses but very little difference in displacement occurred. A comparison of soil backfill, between a loose and dense compaction, showed a large difference in overall settlement. Maximum stresses and pipe deflections were approximately double for the loose compaction when compared to the dense backfill.

## TABLE OF CONTENTS

	<u>Page</u>
BACKGROUND .....	A-2
LIST OF TABLES .....	A-5
LIST OF FIGURES .....	A-6
 Chapter	
A-1 INTRODUCTION .....	A-8
A-2 LITERATURE REVIEW .....	A-10
Introduction to Buried Pipes .....	A-10
Concrete Pipes .....	A-10
Concrete Pipe Testing .....	A-11
Three-Edge Bearing Strength .....	A-13
Bedding Factors and Classifications .....	A-14
History of Pipe Testing Facilities .....	A-15
Small Test Facilities.....	A-19
A-3 STANDARD REINFORCED CONCRETE PIPE VS. FIBER REINFORCED CONCRETE PIPE .....	A-28
Background Information on Concrete Pipes.....	A-28
Cracking in Concrete-The Fracture Zone .....	A-28
Modes of Cracking.....	A-29
Standard Reinforced Concrete Pipe - SRCP .....	A-30
Mechanics of SRCP .....	A-32
Reinforcement.....	A-32
Strength .....	A-33
Structural Performance .....	A-33
Fiber Reinforced Concrete Pipe – FRCP .....	A-34
Mechanics of FRCP .....	A-35
Fiber-Matrix Bond .....	A-36
Fiber-Fiber Interaction .....	A-37
Load vs. Deflection in Fiber Reinforced Concrete .....	A-37
Stages of Cracking – Fiber Intervention .....	A-38
Strength .....	A-40
Toughness .....	A-40
FRCP versus SRCP.....	A-41
Manufacturing.....	A-41
Installation.....	A-41
Performance .....	A-42

A-4	INSTRUMENTATION AND TESTING TECHNIQUES.....	A-43
	Crack Detection and Deflection in Concrete Pipes.....	A-43
	Background on Acoustic Emission Testing.....	A-43
	Equipment and Instrumentation.....	A-45
	Sensors .....	A-45
	Preamplifiers .....	A-47
	Postamplifiers and Signal Processors .....	A-48
	Transient Recorders .....	A-48
	Spectrum Analyzers .....	A-49
	LAM – Local Area Monitor.....	A-50
	Data Analysis Software.....	A-52
	Minolta 3D Digitizer – VIVID 900 .....	A-53
	Hardware.....	A-53
	Accessories .....	A-54
	Operation.....	A-55
A-5	PLAXIS VERSION 7.2- FINITE ELEMENT CODE FOR SOIL AND ROCK ANALYSES.....	A-58
	Introduction.....	A-60
	Plaxis – Input .....	A-68
	Plaxis – Calculations.....	A-72
	Plaxis - Output .....	A-78
A-6	FINITE ELEMENT ANALYSIS OF A SOIL BOX TEST FACILITY .....	A-78
	Introduction.....	A-78
	Input Parameters-Finite Element Analysis .....	A-78
	Plaxis 2D.....	A-80
	Box Dimension Selection .....	A-80
	Wall Friction/ Soil Compaction Analysis.....	A-85
	Plaxis 3D-Analysis.....	A-87
	3D Verification of 2D.....	A-88
	Three-Dimensional Wall Friction Analysis .....	A-93
A-7	RECOMMENDATIONS.....	A-97
	APPENDIX A-A Plaxis 2D analysis and results.....	A-99
	Dimension Analysis.....	A-99
	Wall Friction/ Soil Compaction Analysis.....	A-103

## LIST OF TABLES

<u>Table</u>		<u>page</u>
A-3.1	Typical Fiber-Matrix Pullout Strengths .....	A-37
A-4.1	Specifications of Minolta VIVID 900 3D Digitizer .....	A-57
A-6.1	Material Properties of the Soil (Loose & Dense).....	A-79
A-6.2	Material Properties of the 18”-diameter Concrete Pipes (FRCP & SRCP) .....	A-79
A-6.3	Material Properties of the 24”-diameter Concrete Pipes (FRCP & SRCP) .....	A-79
A-6.4	Material Properties of the 48”-diameter Concrete Pipes (FRCP & SRCP) .....	A-80
A-6.5	Wall Friction Analysis-Plaxis 2D Finite Element Analysis .....	A-86
A-6.6	Three Dimensional Analysis Verification of Plaxis 2D Wall Friction Analysis .....	A-93
A-6.7	Displacement of Pipe Length with Shear Stress Induced on the Ends .....	A-95
A-6.8	Extreme Effective Normal Stress Along the Length of Pipe with Shear Stress Induced on the Ends .....	A-96

## LIST OF FIGURES

<u>Figure</u>	<u>page</u>
A-2.1 Early concrete pipe testing (Photo courtesy of Hardie Pipe, Inc.).....	A-11
A-2.2 Three edge bearing test for concrete pipe.....	A-13
A-2.3 Ohio University full scale testing site (Courtesy James Hardie Pipe, Inc.).....	A-18
A-2.4 The Center for Pipes and Underground Structures test facility at Ohio University (Courtesy of James Hardie Pipe, Inc.).....	A-19
A-2.5 Hardie Pipe’s rigid soil box front view (Courtesy of Hardie Pipe Inc.).....	A-21
A-2.6 Hardie Pipe’s rigid soil box full image view (Courtesy of Hardie Pipe).....	A-21
A-2.7 Hardie Pipe flexible soil (Courtesy of Hardie Pipe, Inc.).....	A-22
A-2.8 Hardie Pipe flexible soil box testing conducted at UCF.....	A-23
A-2.9 LVDT’s shown to measure deflection of sidewalls.....	A-24
A-2.10 Flexure crack at the crown of fiber reinforced concrete pipe.....	A-24
A-2.11 Reinforced concrete pipe cracking at the crown.....	A-25
A-3.1 Coordinate system and stress components ahead of crack tip (Mode I displacement) (Mindess, 2003). .....	A-29
A-3.2 Three modes of cracking (Mindess, 2003). .....	A-30
A-3.3 Standard reinforced concrete pipe section cracked.....	A-31
A-3.4 Standard reinforcing steel rebar.....	A-33
A-3.5 Typical fiber reinforced concrete pipe.....	A-35
A-3.6 Typical load-deflection curve for fiber reinforced concrete (Mindess, 2003).....	A-38
A-3.7 Schematic representation of fibers bridging a crack (Mindess, 2003).....	A-39
A-4.1 Burst acoustic emission signal with properties.....	A-44
A-4.2 Acoustic emission process.....	A-45
A-4.3 Pre-amplifiers (PAC).....	A-47
A-4.4 Transient recorder with multiple AE signals.....	A-49
A-4.5 Digital oscilloscope.....	A-50
A-4.6 LAM-Local Area Monitor.....	A-51
A-4.7 Minolta VIVID 900 non-contact 3-d digitizer.....	A-53
A-4.8 Compact flash memory card (40MB and 128MB capacity).....	A-54
A-4.9 Rotating stage set for scanning a full 3-D image.....	A-55
A-4.10 Tripod (left) and tilting base mount (right) for Minolta VIVID 900.....	A-55

A-5.1	Plaxis 7.2 CAD screen used to create modeling analysis. ....	A-59
A-5.2	General setting window in Plaxis 7.2. ....	A-61
A-5.3	Plaxis 7.2 main toolbar. ....	A-62
A-5.4	Tunnel Designer in Plaxis 7.2. ....	A-62
A-5.5	Standard fixities in Plaxis 7.2 shown on a soil box with right half tunnel. ....	A-63
A-5.6	Material sets window in Plaxis 7.2. ....	A-64
A-5.7	Soil input in Plaxis 7.2 – Mohr coulomb model. ....	A-65
A-5.8	Beam properties input window in Plaxis 7.2. ....	A-66
A-5.9	Pore water pressure & initial stress modes in Plaxis 7.2. ....	A-67
A-5.10	Plaxis 7.2 calculations program. ....	A-69
A-5.11	Plaxis 7.2 calculations program – Parameters tab ....	A-70
A-5.12	Plaxis calculations program – Multipliers tab ....	A-71
A-5.13	Plaxis output program with deformed mesh displayed on example model. ....	A-72
A-5.14	Plaxis output effective mean stresses displayed by mean shading. ....	A-73
A-5.15	Plaxis output effective mean stresses displayed by contours. ....	A-74
A-5.16	Stress distribution cross section A-A in Plaxis 7.2 – Output program ....	A-75
A-5.17	Horizontal displacement cross section A-A in Plaxis 7.2 – Output. ....	A-75
A-5.18	Displacements for the pipe and interface – Plaxis 7.2 Output program. ....	A-76
A-5.19	Bending moment for the pipe – Plaxis 7.2 Output program. ....	A-77
A-6.1	Plaxis 2D symmetry model of 24” diameter FRCP ....	A-81
A-6.2	Three different widths modeled in Plaxis 2D: 10, 15, 20 feet wide ....	A-82
A-6.3	Example of cross section used to examine sidewall stresses (20’ Width).....	A-82
A-6.4a	Example FRCP cross section of sidewall stresses (10’ wide box) ....	A-83
A-6.4b	Example FRCP cross section of sidewall stresses (15’ wide box) ....	A-84
A-6.4c	Example FRCP cross section of sidewall stresses (20’ wide box) ....	A-84
A-6.5	Three dimensional view of total displacements for 24” FRCP.....	A-89
A-6.6	Three dimensional view of total displacements for 24” SRCP.....	A-89
A-6.7	Left side interface of soil box model 24” FRCP.....	A-91
A-6.8	18” diameter FRCP friction interface stress shading view. ....	A-91
A-6.9	18” diameter FRCP near zero friction interface shading view. ....	A-92
A-6.10	Plaxis 3D test pipe with shear stress induced on ends of pipe.....	A-94

## CHAPTER A-1 INTRODUCTION

Structural performance testing of small diameter buried pipes dates back to the 1930's. Large scale testing of buried concrete pipes provides useful information in evaluating the soil structure response expected under field conditions. Large scale test facilities are located at Utah State, University of Massachusetts at Amherst, and Ohio University in the United States; the University of Western Ontario in Canada and LGA Geotechnical Institute in Germany (Brachman, 2001). Each of the listed facilities has limitations related to the boundary conditions. Many of the existing test facilities cannot closely approximate the expected field conditions with respect to a stress state associated with small diameter buried pipes. When large scale testing is not applicable for the location, a laboratory test facility is needed to examine the structural response of small buried pipes. A test facility is needed to examine small diameter buried pipes allowing a laboratory assessment of the performance under expected conditions.

Two small test facilities have been designed and built by Hardie Pipe, Inc. and still pending a patent. Laboratory test facilities allow control over monitoring and testing procedures. Boundary conditions such as the method of loading and the geometry of the test facility may significantly influence the results of the test. The structural response of the buried pipe can be influenced by the boundary conditions if the test facility is not designed properly. Proper dimensions are designed under expected loading conditions allowing minimal sidewall deflection and minimizing the boundary conditions. The main concern in the analysis of the design is the boundary conditions must not influence the structural response of the concrete pipe.

A two and three-dimensional finite element analysis program, Plaxis version 7.2 and Plaxis 3D Tunnel, will evaluate the boundary conditions due to service loads. Stresses from the load dissipate throughout the soil applying a load to the pipe surrounded by the backfill. A stress and



sidewall friction analysis will provide dimensional information to minimize the boundary conditions. Two different backfill soils will be evaluated, loose and dense compacted soil.

The objective of this paper is to present the design parameters of a laboratory test facility for evaluating the structural performance of small diameter concrete pipes; fiber reinforced and standard reinforced concrete. The facility will be built of steel and filled with a sandy soil compacted to 98% proctor with minimal deflections occurring on the sidewalls. The soil test box facility will be subjected to loads from inflatable bladders placed on top of the soil. Attention is focused on the influence of the boundary conditions in the soil box and how efficiently it represents field conditions for a small diameter buried pipe. Interests of focus are on the selection of test cell dimensions, influence of sidewall friction and boundary stiffness on the structural performance of the concrete pipes and the performance of the soil.

## CHAPTER A-2 LITERATURE REVIEW

### **Introduction to Buried Pipes**

Buried pipes and/or conduits have improved the standard lifestyle of people since the beginning of civilization. Remnants of such structures from ancient civilizations have been found in Europe, Asia, and even the western hemisphere, where some of the ancient inhabitants of South and Central America had water and sewer systems (Moser, 2001). Buried pipes serve as sewer lines, drain lines, water mains, gas lines, telephone and electrical conduits, culverts, oil lines, coal slurry lines, subway tunnels, and heat distribution lines. In comparing the design used in the 1800's to the design applications we have today, it is apparent that the degree of technology has increased significantly.

Engineers and planners take into account the subsurface infrastructure before developing buildings and houses for a community. The underground water systems serve as arteries to the cities, and the sewer systems serve as veins to carry off the waste (Moser, 2001). High quality drinking water is taken for granted by humans in today's society. To ensure adequate quality, pipes are designed and constructed to prevent any contaminants from entering. The same standards apply to sewer pipes so as to prevent seepage of contaminants into the ground that may reach the water table and aquifers.

### **Concrete Pipes**

Pipes are classified as either rigid or flexible. A flexible pipe is defined as one that will deflect at least 2 percent without structural distress. Flexible pipes, such as those made of polyethylene plastics, are not within the scope of this project. A rigid pipe is one that does not meet the flexible pipe criteria. The two main types of rigid concrete pipes are steel reinforced concrete pipes and fiber reinforced concrete pipes. Parameters of the pipes are analyzed to

design for maximum performance. Rigid pipes have the strength to resist wall stresses due to internal pressure used in the analysis or external load that are considered critical under service conditions. Parameters for design are; strength, stiffness, corrosion resistance, density, durability and ease of joining. A pipe must have sufficient strength and/or stiffness to perform its intended function and also must be durable enough to perform this function throughout its intended service. Strength is the ability to resist stress. Internal pressure, soil pressure, live loads, differential settlement and longitudinal bending moments impose stresses. Stiffness is the material's ability to resist deflection. The modulus of elasticity of the material is directly related to the stiffness, thus affecting deformation of the pipe wall. Durability is the ability to resist corrosion, abrasion and deleterious environmental exposures. Durability is a critical parameter when determining a design service life for performance.

### **Concrete Pipe Testing**

In the early 1900's, concrete pipe testing consisted of placing sand bags on top of a pipe to obtain a static distributed load as shown in Figure A-2.1. In 1913, Marston researched earth

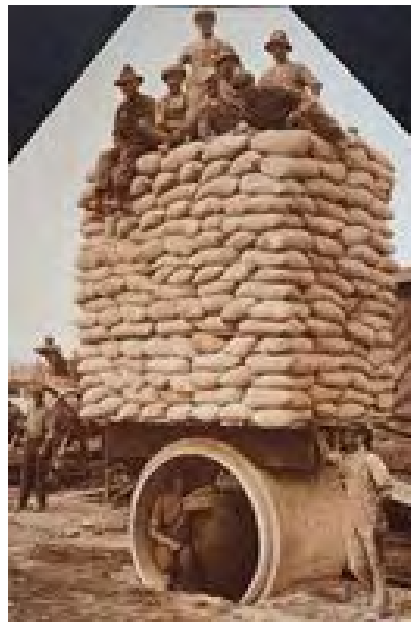


Figure A-2.1 Early concrete pipe testing (Photo courtesy of Hardie Pipe, Inc.).

loads on top of a buried pipe in “The Theory of Loads on Pipes in Ditches and Tests of Cement and Clay Drain Tile and Sewer Pipe.” Marston’s research marked the beginning of the development of an equation for calculating earth loads on buried pipes. Shortcomings included an assumption that the vertical load due to the backfill was uniformly distributed. Results were limited to the technology available and did not include pipe- soil interaction or settlement ratio. The Marston load theory, based on the concept of a prism shaped soil load on the pipe, resulted in what is known today as the Marston load Equation (A-2.1).

$$W_d = C_d \gamma B_d^2 \quad (A-2.1)$$

$W_d$ - load on conduits per unit length (lbs/ft)

$C_d$  - load coefficient for ditch conduits

$\gamma$  - unit weight of the backfill

$B_d$  - horizontal width of ditch at top of conduit in feet

As technology progressed, more test methods were standardized to evaluate the strength of concrete pipe. Spangler conducted research in the 1930’s that proposed four classifications of bedding for pipes covering normal installations in the field. In order to determine the soil-structure interaction, the American Concrete Pipe Association (ACPA) undertook a long-range research program to understand the nature of the loading imposed on a buried pipe (Moser, 2001). This research covered the development of a finite element program to simulate non-linear behavior of buried pipe, validation of the program, and analysis of the soil around the pipe. Full scale testing conducted at the Transportation Research Center in East Liberty, Ohio found the strains along the length of the pipe to be insignificant. The results were symmetric about the vertical plane of symmetry of the pipe, thus validating the plane strain finite element analysis.

### Three-Edge Bearing Strength

Rigid nonpressure pipes are tested for strength in the laboratory using the three-edge bearing test (ASTM C 497). The performance criteria require the pipe to reach laboratory strengths relative to the required service load condition and ultimate strength. Traditional design practice uses the three-edge bearing load that produces a 0.01-inch crack width as the design load. The failure load in three-edge bearing test is defined as the load per length required to cause crushing or critical cracking of the pipe test specimen. The strength obtained is the load failure in the laboratory only, not necessarily the load that will cause failure in the field under buried conditions. Figure A-2.2 shows a schematic diagram of the three edge bearing test for a rigid pipe, where  $W$  represents the distributed load,  $D$  the pipe diameter,  $R$  the radius of wood blocks and  $C$  the clearance beneath the pipe. There are four types of nonpressure rigid pipes covered by ASTM specifications. Testing of nonreinforced concrete pipes are specified in ASTM C 14. Nonpressure reinforced concrete pipe is specified by its “D-load” strength, as

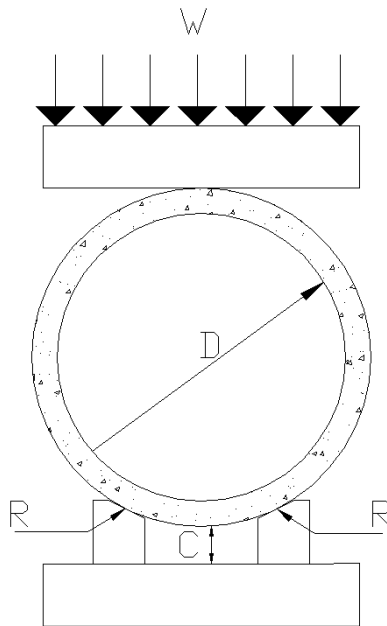


Figure A-2.2 Three edge bearing test for concrete pipe.

determined in ASTM C 76. The D- load is defined as the load applied to a pipe under three-edge bearing conditions, expressed in pounds per linear foot per foot of inside diameter.

### **Bedding Factors and Classifications**

Laboratory testing and field-testing can result in two different strengths for concrete pipes. As previously stated, the strength causing failure in the laboratory does not always cause failure in the soil. Past experiments show that the estimated load required to cause failure according to the Marston load equation is greater than that resulting from the three-edge bearing strength. The most important factor influencing this discrepancy is the method in which the pipe was bedded. Bedding factors are variables that were developed to account for the type of soil in which the pipe is installed. The bedding factor (sometimes called the load factor) is the ratio between the strength of a buried pipe to the strength of the same pipe as determined by in the three-edge bearing test. Bedding conditions affect the bottom reaction under the pipe and the lateral pressure on the pipe. Conduits used in ditch drainage have four bedding classifications. The load factors associated with these classifications are determined empirically and do not take into account any lateral pressures exerted by the backfill. Furthermore, it has been noted that the specified soil compaction cannot be depended upon reliably. Bedding classifications in which a licensed engineer should inspect the installation are Class A, Class B, Class C and Class D.

Class A (also known as Concrete Cradle Bedding) has a load factor of 2-4 and occurs when the lower part of the conduit is bedded in a cradle constructed of 2,000 psi concrete, having a minimum thickness of one-fourth the pipe's internal diameter. The cradle must extend up the sides of the pipe for a height equal to one-fourth its outside diameter.

Class B (also known as First Class Bedding) has a load factor of 1.9 and is where the pipe is carefully bedded on fine granular materials in an earth foundation that is carefully shaped to fit

the lower part of the pipe. The minimum bedding width is 60 percent of its diameter and the remainder of the conduit must be entirely surrounded to a height at least 1 ft above its top by granular materials that are carefully placed in order to completely fill all spaces under and adjacent to the pipe. This fill material must be thoroughly tamped on each side, and beneath the pipe, and placed in layers not exceeding 0.5 ft in thickness.

Class C (also known as Ordinary Bedding) has a load factor of 1.5, and is where a pipe is bedded with “ordinary” care in an earth foundation shaped to fit the lower part of the pipe, with reasonable accuracy, for a width of at least 50 percent of its outside diameter. The remainder of the pipe is surrounded to a height of at least 0.5 ft above its top by granular materials that are shovel-placed and shovel-tamped to completely fill all spaces under and adjacent to the pipe (McGraw-Hill).

Class D (also known as Impermissible Bedding) has a load factor of 1.1. This class is where there is little or no care applied to shaping the foundation to fit the lower part of the pipe or to refill all spaces under and around it. This class of bedding is not recommended for culvert and sewage pipe. Major pipe manufacturing associations recommend bedding factors that correspond to those listed in the Water Pollution Control Federation Manual of Practice, No. FD-5, Gravity Sanitary Sewer Design and Construction (Moser, 2001).

### **History of Pipe Testing Facilities**

A pipe’s insitu performance is based on its material properties, the applied loads, and the soil-structure interaction. Concrete pipe testing dates back to the early 1900’s, when the testing of a concrete pipe involved placing sand bags on top of the pipe to achieve static, distributed load. Traditional concrete design methods are based on research conducted at Iowa State University that date back to the 1930’s. By the 1930’s, Spangler had proposed four

classifications of bedding that covered the range of installations that could be anticipated in normal installations (Hardie, 2001). Some design methods were found to be too conservative as research progressed. Prior to the 1970's, the testing of buried pipes, along with the soil-structure interaction, did not present accurate findings. In 1970, the American Concrete Pipe Association undertook a long-range research program to determine the nature of loading imposed on buried concrete pipe and to develop a reliable design method based upon soil-structure interaction (Hardie, 2001). This research program purported to develop a comprehensive finite element analysis program to simulate non-linear behavior of buried concrete pipe. The results of the research program indicated that stains along the length of the pipe were insignificant. Also it was determined that the results were symmetric about the vertical plane of symmetry of the pipe. This result validates the use of plane strain finite element analysis.

Soil box testing began in the 1960's. This approach can be defined as a three-dimensional box of a known size, containing a pipe and backfilled with soil. Between 1960 and 2000, several researchers conducted large and small scale testing on pipes under simulated insitu conditions. Each of these research programs were formulated to design a test that would yield results similar to those found in the field.

Selander (Hardie, 2001) evaluated reinforced plastic mortar pipe in 1972. His design for the height of overlying soil (approximately 12 feet high) proved later to be overly conservative.

Bland and Sheppard (Hardie, 2001) used research findings from the Transport and Road Research Laboratory and the Clay Pipe Development Association obtained with unrealistic boundary conditions to develop a test for clay pipes using a large test pit in order to investigate structural performance. By using a large test pit, the limitations of unrealistic boundary conditions found in a small soil box test were eliminated.



Bishop's (Hardie, 2001) research tested buried PVC pipes in a soil cell and in an embankment. He proved it is possible to separate the long-term behavior of the pipe from the long-term behavior of the soil. In-situ the load increases with time, whereas the loads applied to the soil cell will decay since the PVC pipe undergoes stress relaxation (Hardie, 2001).

In 1981, Gaube and Miller (Hardie, 2001) designed a sand box with 5mm thick sheet steel to test plastic sewer pipes. They placed a 'water-filled bladder' between the tops of the sand and the soil box lid to apply pressure to the top of the sand. Their design had a box width of eight times the diameter of the pipe. The soil box tests produced results similar to the field tests and indicated that plastic pipe could withstand up to 150 feet of earth fill, assuming that compacted soil was used for the fill.

Molin (Hardie, 2001) tested flexible 200mm diameter PVC pipes in a soil box investigating backfills of sand, compacted clay and uncompacted clay. His results showed that the vertical soil pressure above the pipe increases with increasing pipe stiffness. Molin states that his soil box test results were similar to field tests yet claimed the field tests were more vague. Measured strains were compared to calculated strains and found to be acceptable.

In 1985, Singhal and Veliz (Hardie, 2001) believed that the boundary conditions and edge effects could be eliminated. In other words, the soil surrounding the pipe in the soil box carried stresses and strains that dissipated laterally with distance. Singhal and Veliz tested cyclic torsion, axial pullout and bending on buried pipes. In the same year Todres and McClinton (Hardie, 2001) used a soil box constructed of 19mm plywood panels pinned through steel channels and angles. A 4-inch diameter steel pipe was tested for performance by measuring strains on the pipe's walls. A controlled load placed on top of the fill allowed them to compare the measured bending stresses with calculated stresses and obtained a reasonable correlation.

In 1995, Zanzinger and Gartung (Hardie, 2001) implemented finite element analysis into the design of a soil box test facility. Their design was based on the drop in modulus of elasticity of the pipe over time. When loading the surface of the soil, stresses from the pipe are distributed to the soil surrounding the pipe. A finite element analysis approach can be used to determine the required soil box width needed to eliminate stresses acting on the sides of the box. During the 1000-hour test, a laser was used to measure pipe deformation.

The size of a testing facility determines whether one needs to design a laboratory test site to simulate field conditions. Some research centers are equipped with field sites where results are what you would expect in a field because the research is done in a field test site. The Center for Pipes and Underground Structures was developed by both the Ohio University and ORITE and is shown in Figures A-2.3 and A-2.4. This facility is one of the largest test facilities. When a large test site similar to the Center for Pipes and Underground Structures developed by Ohio University and ORITE is not available, a smaller facility or soil box is needed to recreate tests in laboratory conditions. Laboratory tests provide better control of the test and conditions. James



Figure A-2.3 Ohio University full scale testing site (Courtesy of James Hardie Pipe, Inc.).



Figure A-2.4 The Center for Pipes and Underground Structures test facility at Ohio University.  
(Courtesy of James Hardie Pipe, Inc.)

Hardie with Hardie Pipe conducted research on buried pipes with a small test facility. Hardie has tested both rigid and flexible soil boxes.

### **Small Test Facilities**

As stated earlier, Ohio State University is home to one of the largest in situ test facilities. Small test facilities are needed for researchers unable to gain access to such large test pits. Brachman (Hardie, 2001) states that boundary conditions, such as the geometry of testing facilities and the method of load application, may significantly affect test results. An advantage of soil box testing is the control provided and the access allowed for instrumentation.

R. W. I. Brachman, I. D. Moore, and R. K. Rowe conducted research entitled “Interpretation of Buried Pipe Test: Small-Diameter Pipe in Ohio University Facility.” A small diameter leachate collection pipe was analyzed using two and three-dimensional analyses. Numerical analysis provides one way to assess boundary conditions on measured results when laboratory

tests are conducted. Tests were done at Ohio University for small diameter high-density polyethylene leachate collection pipes. Boundary conditions of the test facility along with stress states in the soil and the response of the pipe to the soil interaction was investigated.

Two large hydraulic cylinders were used to apply vertical force to a loading platform thus loading the soil and pipe underlying. Backfill surrounding the pipe of crushed stone over a bedding of clay was used to simulate waste for a leachate collection system. The most important boundary condition for this study was the method of load application onto the soil. A platform of eight W-shaped steel beams welded together provided a rigid footing for the load applied. Results from the finite element analysis clarified the state of stress in the soil due to the overburden load from the platform loading. The facility results were compared to the expected results from the field installation.

The results from the facility testing were complex and require careful interpretation before drawing conclusions about pipe performance under landfill for leachate collection. The stresses occurring from the rigid platform differed from the expected uniform load in a landfill. It was found that at low levels a portion of the backfill material in the interface of the pipe yielded due to the crushed stone behaving as a beam in bending. This effect resulted in a reduction of the lateral support to the pipe increasing pipe deformations and altering the mode of the pipe deflection. The deflections the facility measured were higher than expected in a landfill situation. Careful care must be taken when interpreting the results from facility testing. Numerical analysis can be successful when interpreted correctly to evaluate boundary conditions.

James Hardie with Hardie Pipe Research tested a *rigid* soil box constructed with lateral sides of 9mm angle iron. The angle iron effectively restricts any lateral movement. James Hardie's *rigid* pipe is shown in Figures A-2.5 and A-2.6.



Figure A-2.5 Hardie Pipe's *rigid* soil box front view (Courtesy of Hardie Pipe Inc.).



Figure A-2.6 Hardie Pipe's *rigid* soil box full image view (Courtesy of Hardie Pipe).

Hardie also developed a flexible soil box (shown in Figure A-2.7) after realizing the rigid box was restrictive and did not accurately represent in situ conditions. The new box was designed with moving lateral walls. Leaf springs supported the walls of the soil box to simulate in situ stiffness. The flexible soil box provides the option of changing the sidewall's lateral stiffness to reflect different burial conditions (Hardie, 2001).



Figure A-2.7 Hardie Pipe's flexible soil (Courtesy of Hardie Pipe, Inc.).

Testing using the flexible soil box was observed on November 13, 2002 at the University of Central Florida (UCF) in Orlando, Florida as seen in Figure A-2.8. Hardie Pipe is conducting tests at the University of Central Florida with the fiber reinforced concrete pipes and reinforced concrete pipes. The research will compare the soil box test results to insitu results. Two different types of reinforced concrete pipes were tested in the flexible soil box. Hardie Pipe's fiber reinforced concrete pipe was tested using a dry cross section and a saturated cross section.

The other concrete pipe tested in the flexible soil box was the standard reinforced concrete pipe. The backfill used in the box was coarse sand. Two sheets of Teflon were used to line the walls inside the box reducing friction. The box was loaded using a concrete platform on top of 2 x 4's for the mechanical load to simulate a uniform distributed load. The load was monitored with a personal computer.



Figure A-2.8 Hardie Pipe flexible soil box testing conducted at UCF.

During the test, LVDT's are shown set up in Figure A-2.9 to measure the deflection of the sidewalls due to the loading applied. The loading is stopped once the first crack is seen with the naked eye. The flexible soil box is equipped with a viewing port of plexi-glass to monitor the loading of the pipe. Surfaces of the crown and invert of the pipe are visible from the viewing port. Cracking of the fiber reinforced concrete pipe is shown in Figure A-2.10 looking through the viewing port of the flexible soil box. Each of the tests loaded until the first crack occurred



Figure A-2.9 LVDT's shown to measure deflection of sidewalls.



Figure A-2.10 Flexure crack at the crown of fiber reinforced concrete pipe.



and then continued loading until the crack propagated across the crown and invert or in flexure of the pipe. For the dry and saturated conditions of fiber reinforced concrete pipes, the pipe was loaded until cracking occurred in flexure.

Standard reinforced concrete pipes were also tested with the flexible soil box. Compaction of the backfill followed the same procedure as the fiber reinforced concrete pipes. Cracking of the reinforced concrete pipe is shown in Figure A-2.11 occurring at the crown of the pipe. The loading procedure was the same for the reinforced concrete pipe resulting in a much lower maximum load when compared to the fiber reinforced concrete pipe. The testing observed on November 13, 2002, was only a portion of the testing to be conducted in the future. Small test facilities of soil box testing will allow the ability to conduct test and compare to the large scale testing of insitu performance.



Figure A-2.11 Reinforced concrete pipe cracking at the crown.

Brachman discussed the design of a laboratory facility and the testing of buried pipe performance. Their study considered a limiting applied pressure of 1000kPa, based on a burial length of 50 meters and a soil density of 20kN/m<sup>3</sup>, and then used finite element analysis to determine the effect of sidewall friction on the soil. Symmetry about the vertical diameter of the pipe was assumed so that only one half of the test facility need be modeled. The load was applied as a uniform pressure. The soil box contained a 2000mm<sup>2</sup> soil prism that extended to a height of 1600mm. These dimensions allowed only small horizontal deflections under large vertical pressures. The distance from the pipe to the sidewalls is a result an attempt to provide lateral stiffness, while at the same time not altering pipe behavior. Hardie stated that the effect of sidewall friction should be considered with respect to the pipe's response and not to the soil box wall. Brachman stated that sidewall friction reduces the amount of load experienced by the pipe, thus resulting in a reduction in vertical deflection of the pipe diameter. Based on a finite element analysis, Brachman concluded that a sidewall friction angle of 5 degrees best simulates in situ conditions. In order to obtain a friction angle of 5 degrees, Brachmann used polyethylene sheets lubricated with DC44 silicone grease. This research highlighted the importance of recognizing that the pipe distributes both horizontal and vertical stresses and that a reasonable model of the soil stresses can be achieved when the top and bottom of the soil is at least a distance of one diameter from the pipe. Research conducted by the University of Florida will achieve a depth below the pipe of one diameter length.

In the early years of soil box testing, the boundary conditions induced by the equipment caused poor correlation with in situ condition results. Boundary conditions were later revised to better represent in situ conditions. From the literature review conducted, it has become apparent that boundary conditions and pipe installation technique are of high importance when trying to

simulate in situ performance with pipes tested in a soil box. When designing a soil box, boundary conditions and soil stiffness are fundamental to producing accurate and acceptable results.

CHAPTER A-3  
STANDARD REINFORCED CONCRETE PIPE  
VS. FIBER REINFORCED CONCRETE PIPE

**Background Information on Concrete Pipes**

Presently, concrete pipes are fabricated in a variety of sizes, ranging from 4 inches to over 16 feet of inner diameter. Concrete pipes are used to transport liquids under gravity flow and are implemented as highway culverts, storm drains and sanitary sewers. The evaluation of concrete pipes for use as storm drains under gravity flow is the focus of this project.

Concrete pipes are reinforced against crushing when the inner diameter is greater than 24 inches. Standard reinforced concrete pipes (SRCP) are fabricated in accordance with ASTM C76 “Standard Specification for Reinforced Concrete Culvert, Storm Drain, and Sewer Pipe.” ASTM C76 covers a size range from 12 inches to 108 inches, with an exception for larger size pipe diameters. SRCP are heavy and require lifters capable of proper placement and installation. The SRCP used for this research will come from Rinker Materials, Inc., Ltd., etc. Hardie Pipe introduced fiber reinforced concrete pipes (FRCP) into the civil construction market for large drainage pipes in early 2002 under the company’s trademark Fiber Reinforced Concrete Speed Drain Pipes.

Concrete properties for each pipe to be discussed include compressive strength, density, absorption, water-cement ratio, cementitious materials, aggregates and versatility.

**Cracking in Concrete-The Fracture Zone**

Cracking in concrete begins at the micro level. The fracture zone is defined as the state when the stress or the strain is increased ultimately until the atomic bonds within the matrix are broken and the solid is cracked or fractured. As the stress load increases cracks will develop and propagate. Cracks will propagate under tensile loads due to the low tensile strength of concrete.

The tensile strength is most often not considered in design but is the origin for crack propagation. Failure of concrete in tension is due to tensile stresses occurring under load and or environmental changes. Concrete failure is a result of microcracking associated with the interfacial region between the cement and aggregates and or the cement and fibers. Cracks are initially localized but increase in size as the stress is increased. In certain circumstances cracks can propagate very fast. Cracks occur in three different modes.

### Modes of Cracking

Modes of cracking are classified as plane strain modes and anti-plane strain modes. Mode I and Mode II deformation are of plane strain and Mode III is anti-plane strain. The deformation of the crack is discussed using the following coordinate system shown for Mode I displacement in Figure A-3.1 below. A description of the three modes of cracking will follow the coordinate system shown in Figure A-3.2. In Figure A-3.1 an isotropic solid is shown with the origin of the coordinate system at the tip of the crack. It is important to note that the solid shown in Figure A-3.1 represents an isotropic solid only. Anisotropic solids are quite complicated when

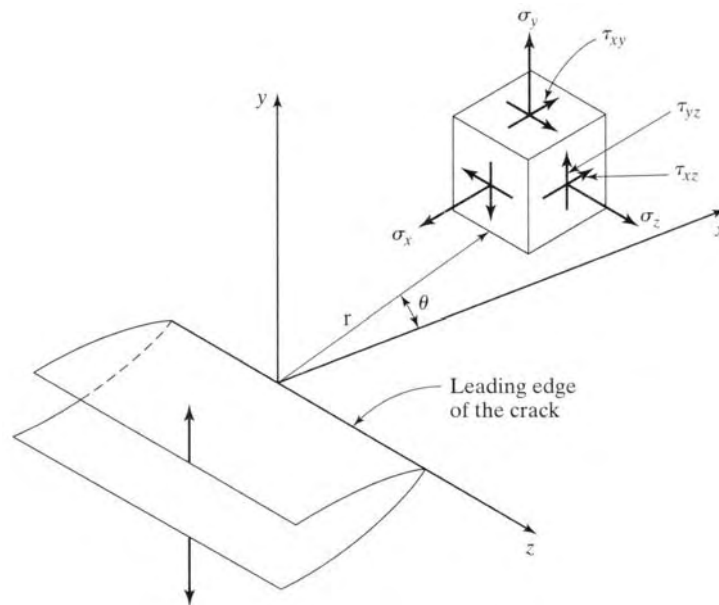


Figure A-3.1 Coordinate system and stress components ahead of crack tip (Mode I displacement) (Mindess, 2003).

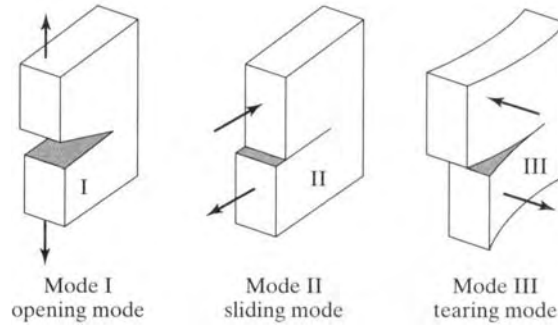


Figure A-3.2 Three modes of cracking (Mindess, 2003).

analyzing the fracture of the solid. Mode I deformation occurs when a transverse plane stress is applied to the crack forcing the crack to open up along the y-axis. Mode I is the most important when considering cracking in a brittle material. Mode II deformation is a result of a shear stress applied on the cracked solid making the faces of the crack slide over one another parallel to the xy plane. Mode III is an anti-plane strain mode of deformation. This mode occurs when a shear stress is applied resulting in the crack faces sliding over each other perpendicular to the xy plane. Cracking of concrete occurs in different stages beginning at the micro level.

### **Standard Reinforced Concrete Pipe - SRCP**

SRCP are widely used in the construction market today. Uses include highway culverts, storm drains and sanitary sewers. Pipes without reinforcement are used where the application is suitable for such products. Majority of applications require reinforcement to increase the overall strength of the pipe in order to resist loads applied over the service life of the pipe. For example, a highway culvert located under a bridge would be subjected to cycling of live loads from traffic. Reinforcement would increase the amount of live load capability prior to failure.

SRCP use steel rebar for reinforcement. The rebar is oriented in the pipe as either in a longitudinal spiral or linear section placed around the perimeter, parallel to the length of the pipe.

Welded wire mesh is also used for additional reinforcement, allowing for increased bonding of the concrete to the rebar reinforcement. A SRCP is shown in Figure A-3.3 with the steel reinforcement visible. This pipe section was tested in Hardie Pipe's soil box apparatus located at the University of Central Florida, Orlando, Florida. The aggregates are also visible, along with the cracking that occurred due to the load applied.



Figure A-3.3 Standard reinforced concrete pipe section cracked.

Properties that will be discussed for SRCP include durability, such as the ability to resist corrosion of rebar and proper bonding of the concrete to the rebar. Without sufficient bonding of

the concrete and rebar, the reinforcement cannot properly carry the tensile stresses and prevent the concrete from cracking.

### **Mechanics of SRCP**

Different sizes of steel rebar are used to reinforce cement based concrete structures. In this research, concrete pipes will be tested for ultimate strength. Concrete is weak in tension strong in compression. When tensile stresses are induced in the concrete, the use of steel bars or wires are used as reinforcement to carry the tensile stresses. Steel rebar left open to the environment will corrode resulting in a loss of strength. Steel rebar, with concern to concrete pipes, is placed within the concrete matrix in prevention from corrosion. The bond between concrete and steel is necessary to carry the stresses on the concrete.

Stress in concrete is distributed throughout the cement matrix including the steel reinforcement. The structural performance of SRCP relies on the bond between the steel and concrete. Stresses are absorbed through the concrete and supported by the structural steel embedded in the concrete. Steel reinforcement is primarily used to carry tensile stresses within the concrete matrix. Steel design for concrete structure is specified in ACI 318.

### **Reinforcement**

Concrete is used together with steel bars or wires that resist the tensile stresses because concrete is weak in tension. The most common used reinforcement for non-prestressed members are hot-rolled deformed bars and wire fabric. Steel, hot-rolled deformed bars are basically round in cross section with lugs or deformations rolled into the surface to aid in anchoring the bars. Steel reinforcement bars are manufactured according to ASTM specifications: ASTM A615-85 Specification for Deformed and Plain Billet-Steel Bars for Concrete Reinforcement; ASTM A616 Specification for Rail-Steel Deformed and Plain Bars for Concrete Reinforcement; ASTM



A617 Specification for Axle-Steel Deformed and Plain Bars for Concrete Reinforcement; ASTM A706 Specification for Low-Alloy Steel Deformed Bars for Concrete Reinforcement.

### **Strength**

Reinforcing steel bars are manufactured in three grades; 40, 50, 60, with yield strengths of 40, 50 and 60 kilo pounds per square inch (ksi). The 40-ksi bar is the most ductile of the three. This bar size is most used in structures not of buildings and bridges. Hot rolled steel bars are shown in Figure A-3.4. Steel reinforcement is classified by their nominal diameter expressed in eighths of an inch.



Figure A-3.4 Standard reinforcing steel rebar.

ASTM specifications for reinforcing bars define the yield strength as the stress at a strain of 0.005. ACI Sections 3.5.3.2 and 3.5.3.4 to 3.5.3.6 define the yield strength as the stress at a strain of 0.0035. ACI's definition is based on the strain at which concrete crushes when bars are in compression as in columns where a strain of 0.005 may never be reached. ASTM specifications for yield strength are based on mill tests that are carried out at a high rate of loading.

### **Structural Performance**

Structural performance is affected by several factors such as bonding, temperature and surrounding environment conditions. The bond between the concrete matrix and the steel

defines the stress transfer within the concrete. Tensile stresses are absorbed by the structural steel providing strength within the concrete. Cracking usually occurs around the steel bars due to the lack of bond between the concrete and steel. Debonding of the concrete and steel results in a lower strength and overall performance of the concrete. Temperature affects the overall strength of steel. The concrete cover in the structure prevents the temperature of the steel from getting hot and losing strength. Exposed steel exceeding about 850°F results in a significant drop in both yield and ultimate strength.

Environment conditions cause corrosion of the steel reinforcing bars decreasing the performance of the steel. Water absorption into the concrete from the surrounding soil increases the possibility of steel corrosion. Concrete pipes, serving as storm drains, are susceptible to water absorption by the concrete on both the inside and outside of the pipes. Increasing strain on the pipe will induce stresses resulting in cracks forming throughout the pipe. Once a crack occurs, channels are created throughout the concrete pipe allowing water to enter and start to corrode the steel. Once the steel is corroded the strength of the concrete overall is decreased.

### **Fiber Reinforced Concrete Pipe – FRCP**

Fiber reinforcement in concrete pipes serves as the reinforcement used to carry the tensile stresses. A diameter range of 12” to 48” is produced, with a standard length of 16’. Pipe strengths for each size are divided into five different classes, I – V, with I being standard and V extra heavy. FRCP pipe is manufactured in accordance with standard ASTM C1450 and FDOT standard 941 and designs from AASHTO Section 17 or LRFD Section 12. A typical FRCP is shown in Figure A-3.5.



Figure A-3.5 Typical fiber reinforced concrete pipe.

### **Mechanics of FRCP**

Different types of fibers are used to reinforce cement-based matrices. Fibers offer a more economical means of reinforcement for concrete structures of small size. Economically, fibers are cheaper than the usual steel reinforcing bars used, although fibers are not to be considered a complete replacement for traditional reinforcement of massive structures. Structurally, design code ACI 318 is based solely on concrete strength for design criteria looking at only the peak loads a structure can withstand. Fibers are used very little with structural steel due to the lack of design for post peak behavior, as fibers are most effective in the post peak time of loading. The performance of fibers begins after the first crack occurs.

Fibers are generally distributed throughout the cross section. Most fibers are short and closely spaced within the matrix allowing a bond between the fiber and the matrix. Stresses are sometimes transferred from fiber to fiber within the matrix, thus resulting in fiber-fiber interaction.

Fibers are primarily used to control cracking by bridging across the cracks as they begin to open when the strain has exceeded ultimate capacity of the matrix. An important factor used to determine fracture is the stress intensity factor. Cracking occurs after the critical value of the stress intensity factor is reached. Without going into detail of derivations and matrices used to solve for the stress intensity factor, a simple overview will explain the importance. The stress intensity factor noted as  $K$  is considered as a single-parameter description of the stress and displacement fields in the region of a crack tip (Mindess, 2003). When the stress intensity factor reaches a critical value, unstable fracture will occur resulting in cracks forming.

Fibers contribute to a more ductile concrete matrix. Fracture toughness is increased with the bridging of fibers across the crack. After loading is applied, fibers absorb the maximum amount of energy as possible before unstable behavior of the matrix occurs.

### **Fiber-Matrix Bond**

In properly designed cement composites for maximum performance, fibers are discontinuously dispersed throughout the matrix. The fiber matrix bond is a result of the fiber properties and the bonding between the matrix and fibers embedded. Fiber matrix bond strength is obtained from fiber pull out tests reported as an average value over fiber surface area. Stresses are induced upon the fiber-matrix bond resulting in fiber pull out or debonding from the matrix after the maximum strength is reached. Typical Fiber-Matrix Pullout Strengths are shown in Table A-3.1. When using cement as a matrix, the fiber-cement interface can become complicated if a chemical reaction occurs between the cement and fiber. Formation of water around the fibers can occur due to bleeding from fresh concrete mixing and insufficient packing of the cement grains around the fibers. The matrix is more porous around the surface of the fibers than in the bulk cement paste. In comparison, fibers serve as tensile reinforcement the

same as steel reinforcement although not a complete replacement where high tensile strength is needed for massive concrete structures.

Table A-3.1 Typical Fiber-Matrix Pullout Strengths (Mindess, 2003)

<i>Matrix</i>	<i>Fiber</i>	<i>Pullout Strength</i> <i>MPa (lb/in.<sup>2</sup>)</i>	
Cement paste	Asbestos	0.8-3.2	(115-460)
	Glass	6.4-10.0	(930-1450)
	Polycrystalline alumina	5.6-13.6	(810-1970)
	Steel	6.8-8.3	(990-1200)
Mortar	Steel	5.4	(780)
Concrete	Steel	3.6	(520)(first crack)
		4.2	(610) (failure)
	Nylon	0.14	(20)
	Polypropylene	1.0	(150)

### **Fiber-Fiber Interaction**

A high ratio of fiber modulus of elasticity to matrix modulus of elasticity facilitates stress transfer from the matrix to the fiber. Fiber to fiber interaction occurs when stress is transferred between fibers. Fibers absorb the tensile stress contained by the fibrous composite material. Stress concentrations will arise at the ends of the fibers if the fibers are discontinuous. The tensile stress assumed by the fiber without the discontinuity must be taken up by the surrounding fibers in the composite. The effect of fiber-fiber interaction on stress transfer is described by Riley's theory (Beaudoin, 1990). The theory states that discontinuous fibers can contribute a maximum of only 6/7 of their strength to the strength of the composite, decreasing the ratio to 1/2 for badly flawed fibers.

### **Load vs. Deflection in Fiber Reinforced Concrete**

As the load increases on a material such as fiber reinforced concrete, the strain will eventually after increasing the load exceed ultimate capacity thus resulting in deflection. A typical stress-strain curve is shown in Figure A-3.6. Point A is where the first crack occurs in the matrix known as the first crack strength. The stress at which the first crack occurs is the same in

both fiber reinforced concrete and plain reinforced concrete represented by the line segment OA. The strength of fiber reinforced concrete in the post-cracking zone comes from the transfer of loads across the cracks increasing the strength of fiber reinforced concrete over that of the matrix. Fibers increase the toughness by providing energy absorption mechanisms through the gradual debonding and pull out of the fibers bridging across the cracks (Mindess, 2003).

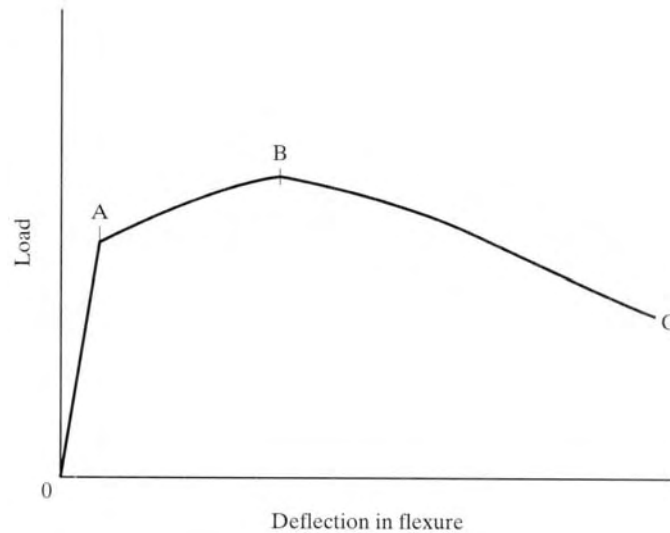


Figure A-3.6 Typical load-deflection curve for fiber reinforced concrete in flexure (Mindess, 2003).

### **Stages of Cracking – Fiber Intervention**

The first stage of cracking is the development of microcracks. The cracks are distributed randomly throughout the concrete. Microcracks occur due to loading on the concrete mass. Secondly, the microcracks are located leading to the creation of one or more macrocracks. The final stage corresponds to the propagation of cracks. Much research has been done to find out how the fibers intervene during the stages of cracking. During the first stage the fibers respond to the uniformly distributed microcracking creating a stitching effect on the micro cracks thus preventing the propagation. The intervention of the fibers is to retard the microcracking location phase and the creation of macro cracks. If stage two develops with macrocracks, fibers will

bridge across serving as reinforcement similar to the steel in reinforced concrete. Bridging across cracks is illustrated in Figure A-3.7.

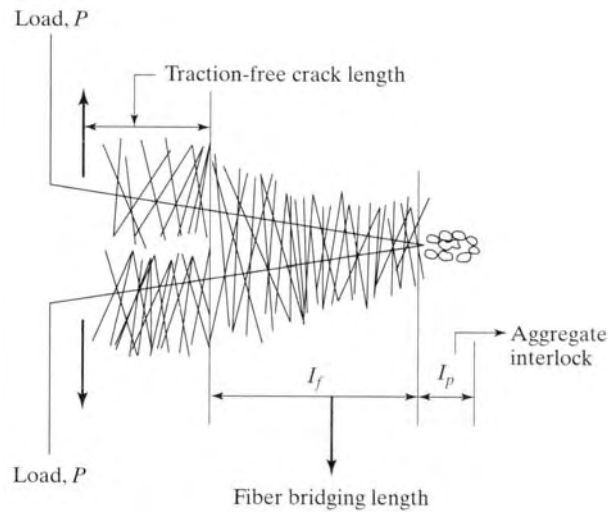


Figure A-3.7 Schematic representation of fibers bridging across a crack (Mindess, 2003).

Fibers bridge across the cracks as they open within the matrix. The stress field around the crack is shown along with the traction-free crack length, fiber bridging length and the aggregate interlock. Stresses are absorbed by the fibers in three different areas shown in Figure A-3.7. The traction free zone is where fibers have pulled out due to the crack opening up wide enough to overcome the pull out strength. Stresses are absorbed by the fibers and transferred across the fibers by frictional slip in the fiber-bridging zone. Aggregates also absorb stresses interlocked to the matrix itself in the microcracked matrix process zone.

As stated previously, fibers intervene at two levels, the material level with macrocracking and at the structural level during location phase. In order for the fibers to respond, fiber dimensions have to be optimized for the material. The percentages of fibers according to the mechanical properties also need to be optimized for the material performance. Two possibilities are considered for the mix design. Based only on discontinuous fibers, one possibility is to mix in a high percentage of short fibers resulting in an increase of strength of material, as the

dimension scale of the fibers is the same as the microcracks. Another possibility is to mix in a low percentage of long fibers resulting in improved ductility of the structure. This is effective with regard to macrocracking having sufficient anchoring length as the crack opens across the fibers.

### **Strength**

The role of fibers in concrete is not to increase the overall strength. Some minimal increase in strength will occur for compression and flexure. Research shows that in direct tension, where it would be expected that fibers would be most effective in terms of strength, it is indicated that only about a 30% increase in strength for a steel fiber volume of 1.5% (Mindess, 2003). Fibers are reported to have no major effect on shear and torsional strength or elastic modulus.

### **Toughness**

Fibers have an enormous effect on toughness. If the fibers are equipped with strength, stiffness and have bonded with the matrix well, they will minimize cracking allowing the fiber reinforced concrete to withstand significant stresses over a relatively large strain capacity in the post-cracking (or strain-softening) stage thus providing a considerable amount of post-cracking ductility (Mindess, 2003). Certain fibers have a better effect on increasing the toughness of the fiber reinforced concrete. Deformed fibers have a greater effect on increasing the toughness as they bond to the matrix better increasing the overall pull out strength. Mindess shows that steel fibers are more effective than polypropylene fibers in toughness increase because of their higher stiffness. More energy is required to pull out a fiber from the matrix than to break the fiber across a crack.



## **FRCP versus SRCP**

Performance of a pipe is based on the ability of the pipe to maintain shape under service loads, prevent cracking from applied stresses, and to resist deterioration of the pipe material. Concrete drain pipes are subjected to a number of deterioration mechanisms. Stresses will induce microcracking that eventually coalesce into macrocracks within the concrete matrix. These cracks provide openings for chemicals and water penetrate into the concrete. Water damage to a concrete pipe results in corrosion of the steel reinforcement, leading to a decrease in the ultimate strength of the pipe. A comparison of the properties and characteristics of FRCP and SRCP will be discussed.

### **Manufacturing**

FRCP is manufactured under high pressure. Higher strength is achieved under high-pressure autoclaving. SRCP are manufactured with a low water to cement ratio and depend upon the strength of the aggregate to prevent abrasion to the surface of the pipe.

### **Installation**

The unit weight of a concrete pipe has a significant impact on the installation process. A lighter pipe is easier and quicker to install than a heavy pipe. FRCP is half the weight of SRCP and therefore easier to install and handle.

The standard length of SRCP is six feet. FRCP, on the other hand, come in a standard length of 16 feet. The installation work of FRCP, compared to SRCP, is cut in half with the longer standard length. FRCP is also easy to cut for length adjustments, requiring less time than SRCP.

An important part of the installation of concrete pipes is the joint seal at the ends of the pipes. Rubber gaskets are placed on both pipes for a tight seal, preventing as best as possible the penetration of liquid into, and from, the pipe system.

### **Performance**

An important property affecting overall performance is the bond of the concrete to the reinforcement. Steel rebar is more difficult to bond to than cellulose fibers, which are randomly dispersed throughout the concrete mix. This random dispersion allows for increased bondage due to the size of the fibers. Most of which are of hair-like size in the concrete mix. Fiber reinforcement is not considered a complete replacement of reinforcement for concrete structures.

Both FRCP and SRCP will be tested in the soil box designed by the University of Florida for research funded by the Florida Department of Transportation. FRCP will come from Hardie Pipe, Inc. while Rinker Materials, Inc will provide the SRCP. Following the design and construction of the soil box testing apparatus, each type of pipe will be tested to determine in situ performance.

## CHAPTER A-4 INSTRUMENTATION AND TESTING TECHNIQUES

### **Crack Detection and Deflection in Concrete Pipes**

Durability of a concrete pipe is defined as the ability to withstand the effects of service conditions to which it will be subjected, such as weathering, chemical action and wear. With advances in technology, crack detection is more easily accomplished using different techniques. The deflection of a concrete pipe is an observation of the pipe's deformation while subjected to an applied load. There are many test methods used today to detect cracks and measure deflection of a structure under load. After construction of the soil test cell, two novel methods will be used to detect cracks within the concrete pipe on both the micro and macro scale, and to observe and record pipe deflection due to the subjected load. These two techniques are Acoustic Emission monitoring and Minolta 900 imaging. Each of the methods will be defined and discussed below.

### **Background on Acoustic Emission Testing**

Acoustic emission is defined as an acoustic wave generated by a material when subjected to an external stimulus causing an irreversible change in the material. There are two types of acoustic emission signals, continuous and burst signals. A continuous emission is a sustained signal level produced by rapidly occurring emission events such as plastic deformation. A burst emission is a discrete signal related to an individual emission event occurring in the material, such as a crack forming or propagating in concrete. The concrete pipes tested in this research will produce acoustic emission burst signals representing cracking within the pipe wall. An acoustic emission burst signal is shown in Figure A-4.1 below. Acoustic emission signal is often used interchangeably with acoustic emission. An acoustic emission signal is defined as the electrical signal received by the sensor in response to the acoustic wave moving through the

material. The emission is received by the sensor and transformed into a signal, then analyzed by acoustic emission instrumentation, and resulting in information about the material that generated the emission.

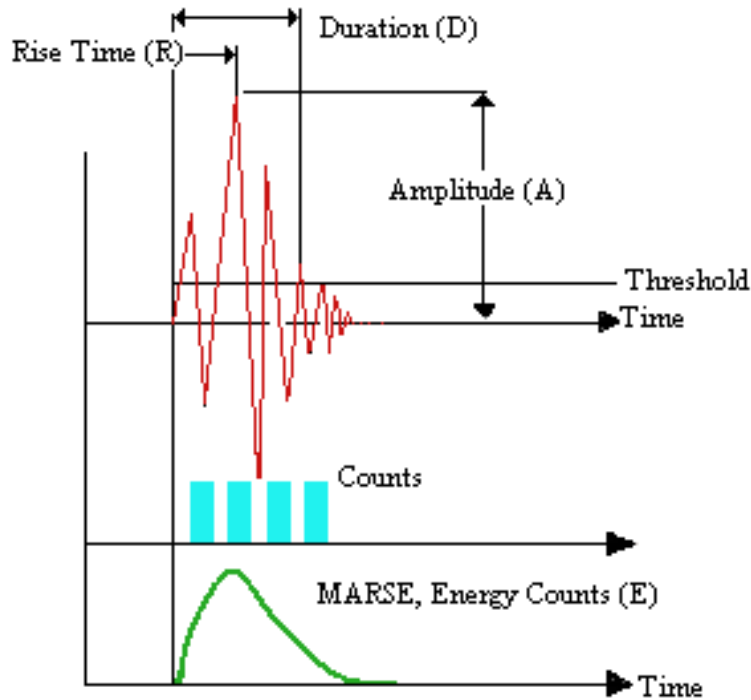


Figure A-4.1 Burst acoustic emission signal with properties.

Acoustic emission is a passive, non-destructive monitoring technique. This means there is no input from an outside source; the technique purely monitors the material being tested.

Acoustic emission is used to detect cracking, delamination (slip between concrete and steel reinforcement), failure of strands in prestressing tendons, and fracture or debonding of fibers in fiber reinforced concrete. A typical acoustic emission system setup is shown in Figure A-4.2.

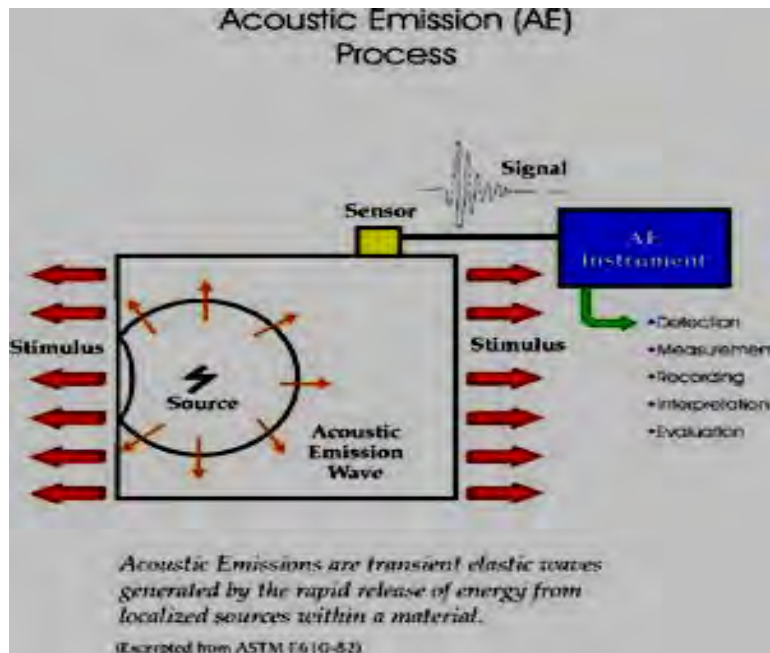


Figure A-4.2 Acoustic emission process.

### Equipment and Instrumentation

An Acoustic emission system includes at least one sensor and a preamplifier. Most systems also include postamplifiers and signal processors. The acoustic emission system to be used in this research is a LAM – Local Area Monitor that consists of eight sensors, which will be mounted on the pipe while undergoing load testing. More specialized equipment often associated with such a system include transient recorders, spectrum analyzers, tape recorders, distribution analyzers and spatial discrimination circuits (Beattie, 1993). Microprocessor based systems have become more widely used in recent years that can perform single channel analysis along with source location for up to eight AE channels.

### Sensors

The Acoustic emission sensor is the most important part of the instrumentation and must be properly mounted to assure the required sensitivity. Selection of sensors and or transducers will depend on test parameters and desired results. Sensors are calibrated using test methods

stated by societies. ASTM states that annual calibration and verification of pressure transducer, AE sensors, preamplifiers (if applicable), signal processor (particularly the signal processor time reference), and AE electronic simulator (waveform generator) should be performed. Equipment should conform to manufacturer's specifications. Instruments should be calibrated with National Institute for Standards and Technology (NIST). An AE electronic simulator, used in making evaluations, must have each channel respond with a peak amplitude reading within  $\pm 2\text{dBV}$  of the electronic waveform output. A system performance check should be done immediately before and after an AE examination. A preferred technique is the pencil lead break test. Description of the test is in ASTM E 570. Another important factor of sensors is location.

Determination of the number of sensors required for the test, their placement strategy and location on the part to be monitored is needed. A single sensor used near the expected source of AE is sufficient when background noise can be controlled or does not exist. When background noise is limited, the use of a single AE data sensor near the expected source plus a guard sensor(s) near any background source will suffice. ASTM defines a *guard sensor* as sensors whose primary function is the elimination of extraneous noise based on arrival sequences. The guard sensors will effectively block noises that emanate from a region closer to the guard sensors than to the AE data sensor. Another technique involves the placement of two or more sensors to perform spatial discrimination of background noise and allow AE events to occur. ASTM defines *spatial discrimination* as the process of using one or more (guard and data) sensors to eliminate extraneous noise based on arrival sequences.

In situations where irrelevant noise cannot be controlled during testing and could be emanating from any and all directions, a multiple sensor location strategy should be considered. Using a linear or planar location strategy will allow for an accurate source location of the

acoustic emission. Applications of spatial filtering and/or spatial discrimination will only allow data emanating from the region of interest to be processed as relevant AE data.

### **Preamplifiers**

Preamplifiers as shown in Figure A-4.3 are used to prevent loss in sensor activity. Loss occurs when one sensor is connected through a long coaxial cable to an amplifier. The amplifier is split into a fixed gain preamplifier located close to the sensor. The preamplifier consists of a low noise input stage, bandpass filters and a low impedance output stage capable of driving a 50-ohm cable (Beattie, 1993). Power for the preamplifier is received from the main instrument group. AE preamplifiers are designed to have a relatively flat frequency response between about 20 kHz and 2MHz, without the bandpass filters (Beattie, 1993).

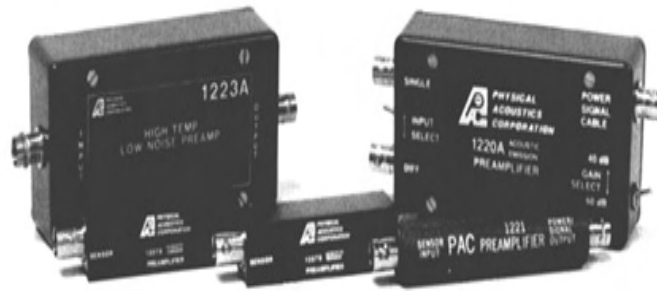


Figure A-4.3 Pre-amplifiers (PAC).

Preamplifiers can be included in the sensor package. The advantages of this arrangement are elimination of cable capacity effect and being able to tailor the preamplifier characteristics to match the sensor. The disadvantages of such units, besides their higher cost, are that they are restricted to temperatures near 20°C (the preamplifier will not work properly at high or low temperatures) and that a separate preamplifier has to be purchased for each sensor (Beattie, 1993).

## **Postamplifiers and Signal Processors**

Most AE systems use variable gain postamplifiers. This allows the use of signal processors with fixed input ranges or threshold in conjunction with fixed gain preamplifiers (Beattie, 1993). The systems total gain is the sum of the preamplifier and postamplifier in decibels. Additional noise reduction can be achieved through postamplifiers from bandpass filters.

Signal processors are found included the system's capabilities. These include voltage controlled gates that allow data to be collected only on certain portions of a load cycle, envelope processors which attempt to filter out high frequencies leaving only the signal envelope to be counted, logarithmic converters which allow the output of the signal analyzer electronics to be plotted in logarithmic form and a unit which allows the combination of outputs from several preamplifiers so that several sensors can be monitored by one channel of electronics (Beattie, 1993).

## **Transient Recorders**

Transient recorders are used to study individual AE burst signals. A signal is digitized in real time, and then stored into memory. A transient recorder is used in sequence with an oscilloscope or spectrum analyzer to display AE signals at visible speeds. Digital rates vary on transient recorders. The fastest rate of the recorder is the limiting rate with some instruments sampling up to 1 word/ns (Beattie, 1993). Sampling rates can be modified for testing purposes. One advantage of transient recorders is an additional mode of triggering and pretriggering, where the input signal is continuously digitized and the data stored in the memory (Beattie, 1993). This feature allows a digitized picture of the signal to be displayed as it is received. More advanced recorders allow recording of two or more signals simultaneously. The recording of more than one AE signal is shown in Figure A-4.4 below.



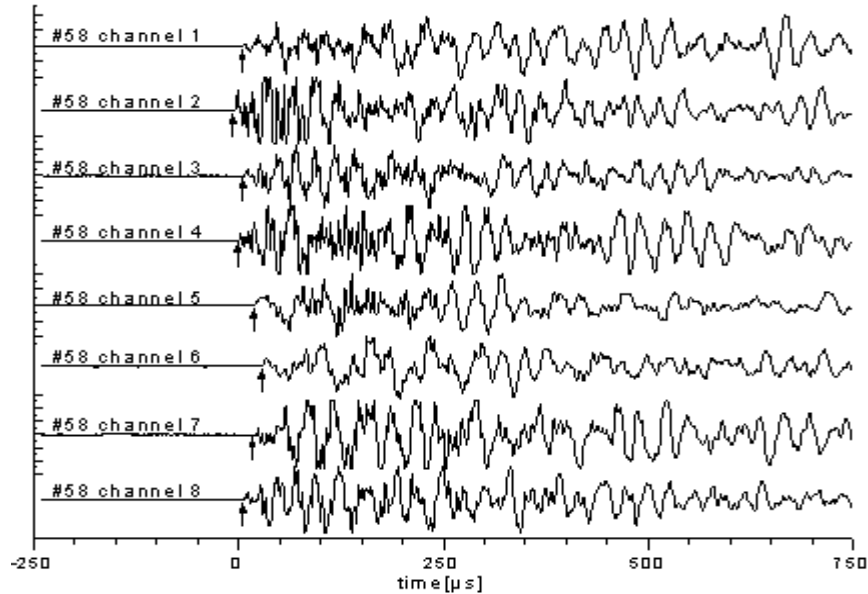


Figure A-4.4 Transient recorder with multiple AE signals.

### Spectrum Analyzers

The ideal spectrum analyzer has horizontal and vertical signal outputs, allowing an X-Y plot of the signal output. Spectrum analysis is done either directly with analog electronics or by digitally viewing a continuous signal. A local oscillator signal is mixed with the input signal and the highest frequency is passed through a chain of intermediate frequency (I.F.) amplifiers, after which it is measured by a voltmeter (Beattie, 1993). The oscillator is swept through a frequency range so that the frequency components of the signal selected by the I.F. amplifier are continuously changing (Beattie, 1993). The voltmeter output is plotted on the vertical axis of the oscilloscope. A typical oscilloscope is shown in Figure A-4.5. A synchronized signal is displayed for the horizontal axis through the local oscillator frequency. The final result is a plot of signal strength vs. frequency.

Spectrum analyzers range in frequencies from at least 10kHz to 2MHz. The width and speed of the local oscillator and the sharpness of the I.F. amplifier filters are all under the direct

control of the operator (Beattie, 1993). An AE burst signal emission is not suitable for spectrum analysis. AE burst signals must be captured on a tape recorder and played repetitively onto the spectrum analyzer for analysis. This will simulate a continuous signal for spectrum analysis.



Figure A-4.5 Digital oscilloscope.

### **LAM – Local Area Monitor**

LAM is the world's first acoustic emissions system to allow remote condition monitoring of structures. Physical Acoustics Corporation developed the LAM, as shown in Figure A-4.6, in conjunction with the U.S. Federal Highway Administration. The system is portable and easy to handle weighing only 25 pounds including one battery pack. Features of the LAM used in this research project are:

- Modular 8 channel DSP-based AE system with 16-bit A/D
- User-friendly software
- AC/DC powered
- 4 high-speed and 8 low-speed parametrics
- Digital AE features and waveforms processed simultaneously
- Software programmable filters
- Resistant to harsh environmental conditions



Figure A-4.6 LAM-Local Area Monitor.

The LAM is useful for monitoring many structures including bridges for defects, chemical/ petrochemical tanks for leaks and deterioration, transformers for partial discharge and most structures (including concrete pipes) during fatigue tests.

The LAM was originally designed for monitoring defects in steel bridges. The LAM's modularity lends itself to many other applications, as stated before, to monitor fatigue cracks and other discontinuities in structures, pressure vessels and transformers. This research will use the LAM to monitor microcracking in the walls of fiber reinforced and steel reinforced concrete pipes. LAM offers up to 8 channels of digital AE for short – term condition monitoring, long – term integrity monitoring, laboratory fatigue testing or incipient failure detection monitoring through user selections. The LAM unit operates from an external 12 Volt DC battery power or 110 Volt AC power supply. An optional feature is remote access through traditional phone line or cellular phone. This feature allows the user to monitor the apparatus from an office or other location remote from the test site.

Advantages of the LAM over other acoustic emission instrumentation include a reduction in the extensive cabling normally required for operation. The unit is placed on site with the structure/ object to be monitored. The set up is easy and operated at leisure. For this project, the concrete pipes will be instrumented with the eight sensors to monitor microcracks occurring inside the walls. Data analysis for this research will be performed with the NOESIS 3.1 software published by Physical Acoustics Corporation.

### **Data Analysis Software**

NOESIS 3.1 is windows based advanced data analysis pattern recognition and neural networks software used for acoustic emission applications. It provides all necessary tools for analyzing, filtering and classifying acoustic emission hits and waveforms that are acquired with the LAM unit. NOESIS is equipped to handle data saved in DTA file format coming directly from the LAM unit. The software utilizes PAC (Physical Acoustics Corporation) file libraries to load and save data in DTA file format.

NOESIS allows multiple DTA files to be loaded simultaneously for direct comparison, statistics and filtering or merging. Direct export of data files to MS EXCEL and MS WORD is also possible. Any number of windows can be displayed, limited only by the resolution of the viewing window for adequate visibility. Navigation throughout the program, along with data selection, is done with the mouse. Data point selection is available using the mouse on scatter plots, cumulative plots, waveform plots, FFT plots and data tabular views. NOESIS allows graphs and plots to be customized for presentation of data and analysis.

Waveforms and AE hits can be selected and displayed on any graph or data table. Comparison of the data can be superimposed or viewed in three dimensions. Graphical and other data filtering are applied to waveform views presenting the collected data. Any changes made to hardware settings are immediately reflected in the waveforms.

## Minolta 3D Digitizer – VIVID 900

Minolta is the world's largest manufacturer of 3-D non-contact digitizing instruments providing a 3-D scanner with a simple point and shoot camera that scans 300,000 points in less than 3 seconds. This project will use Minolta's newest 3-D scanner, the VIVID 900, shown in Figure A-4.7. The VIVID 900 is an easy to use scanner with simplicity, flexibility and portability. Minolta offers simplicity by a point and shoot camera with excellent results. The VIVID 900 includes interchangeable lenses applying to variable scanning volumes for flexibility. The camera unit is compact, measuring 8-3/8"x 16-1/4"x 10-11/16" and weighs only 24 lbs. Scans can be saved and stored on a compact flash memory card or viewed immediately after scanning on the rear-panel's color LCD viewfinder. Color images are equivalent to a 3 CCD digital camera displaying full 24-bit color depth.



Figure A-4.7 Minolta VIVID 900 non-contact 3-D digitizer.

### Hardware

The Minolta VIVID 900 offers variable volumes for digitizing between 110 x 80- x 40 mm and 1200 x 900 x 750 mm. There are three interchangeable lenses included as a standard accessory for scanning; telephoto, medium and wide angle. The VIVID 900 is an independent instrument that does not require a host computer for operation. Scanned images are saved to a

flash memory card (Figure A-4.8) and are viewed immediately after the scan is complete on the LCD viewfinder on the rear of the instrument. The Minolta VIVID 900 also offers an autofocus function that eliminates the need to move the unit back and forth to achieve optimal focus for the scan.



Figure A-4.8 Compact flash memory card (40MB and 128MB capacity).

### Accessories

Minolta offers accessories to improve the outcome of the scan. When scanning a complete 360° view of an object, the rotary specimen stage shown in Figure A-4.9 will prove helpful. A rotating disc is set to rotate at a specified speed while the VIVID 900 scans the object, resulting in a full 3-D image of the object. To ensure level scans and stability, Minolta offers a tripod accessory with the option of a tilt mounting base unit as shown in Figure A-4.10. Other accessories available are a PC card adapter allowing transfer of the scanned images to a personal computer for analysis.



Figure A-4.9 Rotating stage set for scanning a full 3-D image.



Figure A-4.10 Tripod (left) and tilting base mount (right) for Minolta VIVID 900.

### Operation

Minolta's VIVID 900's basic theory of operation is described through LASER triangulation. A laser source from the VIVID 900 emits a horizontal light stripe through a

cylindrical lens onto the object being scanned. The plane of light is swept across the field of view by a rotating mirror. The light is reflected from the scanned object, captured, and observed by a single frame through the CCD camera. Once received by the CCD, the light is converted through triangulation into distance information. Each scan line is captured and observed by the CCD camera. The shape of the image of each reflected scan line is derived to produce the contour of the surface. The selected area in the view is captured in 2.5 seconds (0.3 seconds in FAST mode), and the surface shape is converted to a lattice of over 300,000 vertices (connected points) (Minolta, 2001). The VIVID 900 produces a polygonal-mesh with all connected information, eliminating geometric ambiguities while improving detail. Minolta's VIVID 900 uses an X, Y, Z coordinate axis. The x coordinate is the horizontal dimension of the focal plane, the y is the vertical axis and the z coordinate is the distance from the sensor. The VIVID 900 produces no parallax error. Specifications for the VIVID 900 are displayed in Table A-4.1 below.



Table A-4.1 Specifications of Minolta VIVID 900 3D Digitizer

Type	Non-contact 3D digitizer VIVID 900
Measuring method	Triangulation light block method
AF	Image surface AF (contrast method), active AF
Light-Receiving Lens (Exchangeable)	TELE: Focal distance f=25mm MIDDLE: Focal distance f=14mm WIDE: Focal distance f=8mm
Image Input Range	0.6 to 2.5m (2m for WIDE)
Measurement Input Range	0.6 to 1.2m
Laser Output	“Eye-safe”, Class I (FDA), Class 2 (IEC), Maximum 30mW 690 nm
Laser Scan Method	Galvano mirror
Input Time	0.3 sec (FAST mode), 2.5 sec (FINE mode), 0.5 sec (FINE mode)
Transfer Time to Host Computer	Approx. 1 sec (FAST mode, 1.5 sec (FINE mode)
Ambient Light Condition	Office Environment, 500 lx or less
Imaging Element	3-D data: 1/3-inch frame transfer CCD (340,000 pixels) Color data:3-D data is shared (color separation by rotary filter).
Number of Output Pixels	3-D data : 640 x 480 (for FINE mode); 320 x 240 (for FAST mode) Color data : 640 x 480
Output Format	3-D data : Minolta format, & (STL, DXF, OBJ, ASCII points, VRML) (Converted to 3-D data by the Polygon Editing Software/ standard accessory) Color data:RGB 24-bit raster scan data
Recording Medium	Compact Flash memory card (128MB)
Data File Size	Total 3-D and color data capacity: 1.6MB per data (for FAST mode), 3.6MB per data (for FINE mode)
Viewfinder	5.7-inch LCD (320 x 240 pixels)
Output Interface	SCSI II (DMA synchronous transfer)
Power	Commercial AC power 100 to 240V (50 to 60Hz), Rated current 0.6A (when 100Vac is input)
Dimensions (WxHxD)	213 x 413 x 271 mm (8-3/8 x 16-1/4 x 10-11/16 in.)
Weight	Approx. 11 kg.
Operating environment	Temperature: 10-40°C (50-104°F); relative humidity 65% or less with no condensation, Pollution degree:2, Installation category:II
Storage Temperature	-10 to 50°C (14-122°F); relative humidity 85% or less (at 35°C/95°F) with no condensation

CHAPTER A-5  
PLAXIS VERSION 7.2- FINITE ELEMENT CODE FOR SOIL AND ROCK ANALYSES

**Introduction**

Plaxis was developed in 1987 at the Technical University of Delft initiated by the Dutch Department of Public Works and Water Management. Initially, Plaxis was developed to analyze river embankments along the soft soils of the lowlands of Holland. Throughout the development and improvements, Plaxis extended its development to cover most of the geotechnical engineering. Plaxis excelled over the years forming a company in 1993, Plaxis BV.

Plaxis is a computer program designed to provide a practical analysis tool for use by engineers who are not specialist in finite element analysis. Non-linear finite element computations done without a computer can be too time consuming for regular analyses. Plaxis 7.2 is a window-based program with easy to use tabs to navigate one through the analysis.

This finite element program, is designed for the analysis of deformation and stability in geotechnical engineering projects. Geotechnical engineering uses advanced models for the simulation of non-linear and time dependent behavior of soils. Soil is a multiphase material with properties that can change with a changing environment. It is equipped to deal with hydrostatic and non-hydrostatic pore pressure in the soil. Even though modeling of the soil itself is important, modeling of soil – structure interaction is the situation seen in many engineering projects today. Plaxis is also equipped with features to analyze a number of aspects dealing with complex geotechnical structures.

Plaxis is made up of four internal programs, Input, Calculation, Output and Curves. Graphical input of geometry models consists of soil layers, structures, construction stages, loads and boundary conditions all created with drawing procedures on a CAD (Computer Aided Drawing) screen as shown in Figure A-5.1. CAD allows accuracy and detail modeling of real

engineering situations. From the geometry entered, a finite element mesh is generated. The automatic mesh generation feature allows for fully automatic mesh generation of unstructured finite element meshes.

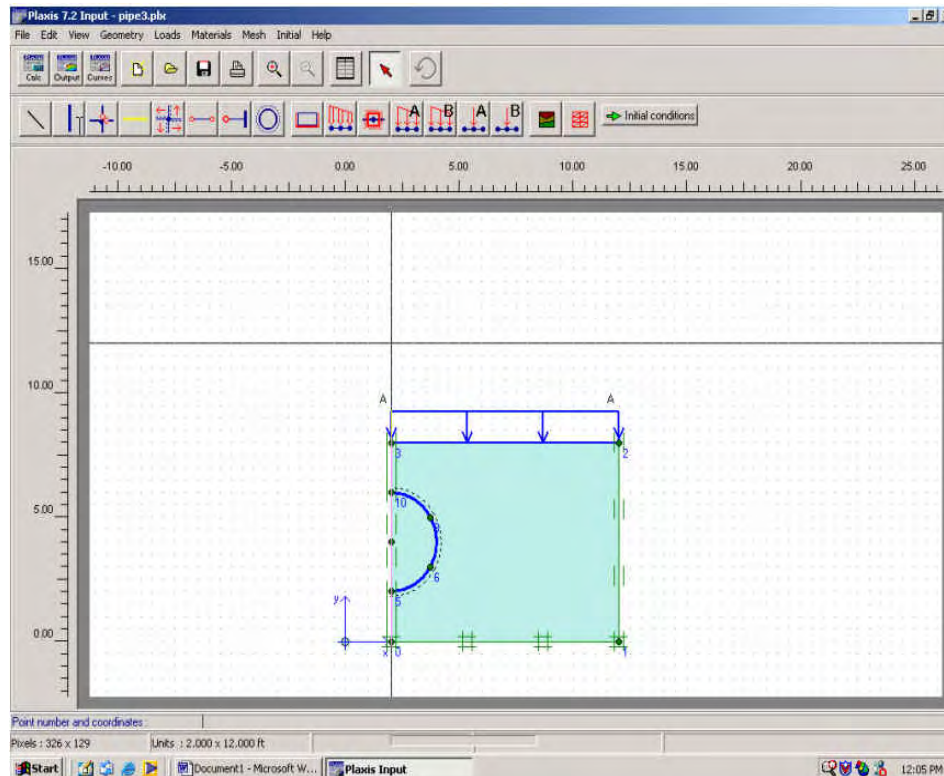


Figure A-5.1 Plaxis 7.2 computer aided drafting screen used to create modeling analysis.

Beam elements are used to model retaining walls, tunnel linings and other structures such as pipes, which are modeled using the tunnel feature. Behavior of each element is defined as flexural rigidity, normal stiffness and/or ultimate bending moment. Assigned to the beam elements are a feature called interfaces. Interfaces are joint elements used in calculations of the soil – structure interaction. For example, interfaces can simulate a zone of intense shearing material located at the contact of footings, piles, geotextiles, retaining walls and soil – pipe interaction. Values such as friction angle and adhesion can be assigned to the interface elements. Anchors and geotextiles are additional features available for modeling. The tunnel feature option

creates circular and non – circular tunnels composed of arcs. Beams and interfaces may be added for analysis on tunnel lining and interaction with the surrounding soil.

A number of soil models are used in Plaxis for analysis of the soil performance. Mohr – Coulomb, a simple non – linear model, is the most used soil model based on soil parameters encountered in everyday practical situations. Other advanced soil models are available for analyses. Pore pressures are analyzed within the Plaxis model.

Steady state and excess pore pressures are defined by the water table location in the model. There are two approaches for steady state pore pressures. Complex pore pressure distributions are generated on a basis of a two – dimensional groundwater flow analysis. For simple conditions, multi – linear pore pressure distributions can be directly generated by a simple phreatic line in the model. Excess pore pressures are computed during plastic calculations when pores are full of water and subjected to loads.

A typical analysis through Plaxis finite element modeling involves input parameters and specifications of model types. The input model is then run through the calculation phase to produce output results for analysis. Plaxis is also equipped with a curves program that produces graphs for analysis such as stress/strain curves and load/displacement curves.

### **Plaxis – Input**

The input program is the beginning of analyses in Plaxis. At the start of a new project the General Settings window appears as shown in Figure A-5.2 prompting the user to set the basic parameters of the project. The general settings window has two tabs: Project and Dimensions. The project tab allows for a description of the project, the type of model used such as plane strain and the number of nodes to use in finite element analysis (i.e., 6 and 15 node). The dimensions tab specifies units of length (ft), force (lbs.) and time (day); and the geometry dimensions for the CAD screen and grid spacing.

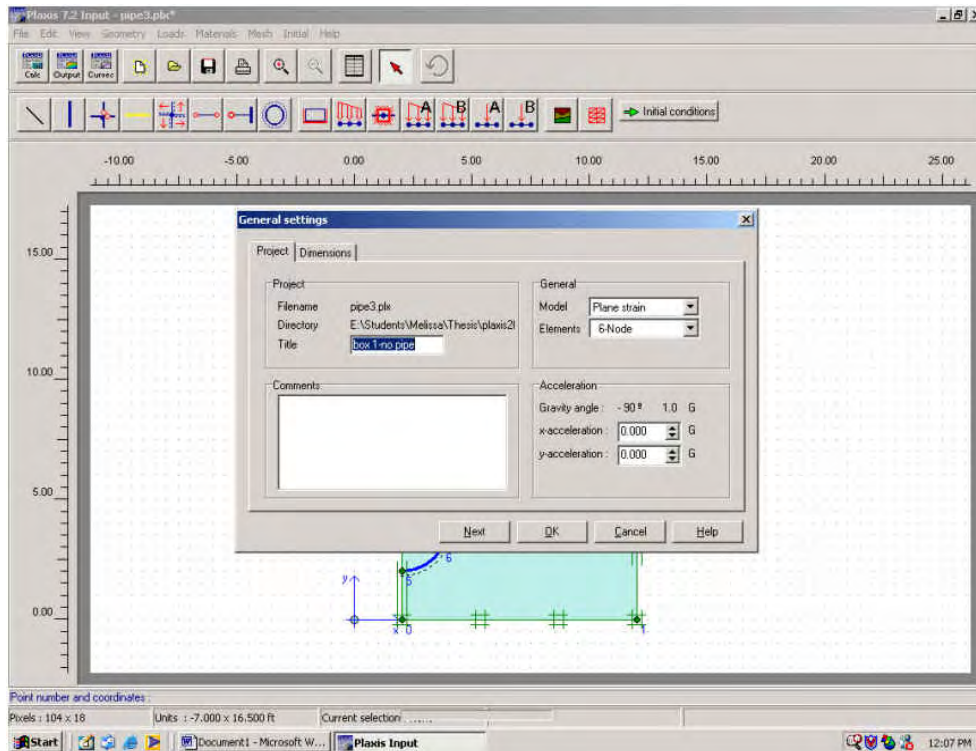


Figure A-5.2 General setting window in Plaxis 7.2.

Once the general setting parameters are entered into Plaxis, the CAD screen appears for geometry creation of the model. An example of a tunnel model used in this research will be used to demonstrate a typical run through of Plaxis 7.2 finite element modeling. The tunnel model can be used to model buried pipes for analyses. The model described in the example is a four-foot diameter reinforced concrete pipe to be modeled in a soil box. A steel framed box will be designed to test concrete pipes modeling the soil structure interaction and analyzing the stresses applied to the side walls and pipe thus defining the design of the box.

After the general settings are complete, the geometry of the model is created in the input drawing area using the points and lines feature. With the windows based program the creation of a model is done by working from left to right with the icons at the top of the screen as shown in Figure A-5.3.



Figure A-5.3 Plaxis 7.2 main toolbar.

Points and lines are used to create an enclosed box of dimensions 20' x 10' x 10'. The tunnel option is then used to create a circular tunnel representing the two-foot diameter concrete pipe composed of arcs defined by a radius and a radial increment (angle). By clicking on the tunnel feature the user is prompted with a choice to use a whole tunnel or a half tunnel. After the choice is made a window is opened as shown in Figure A-5.4 to input the radius and radial increment.

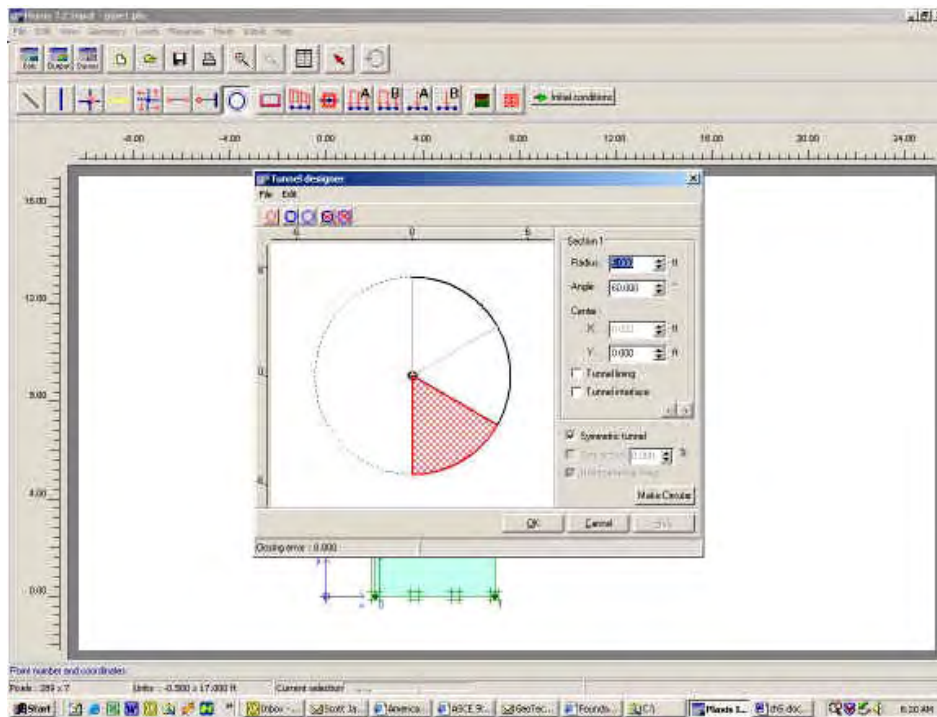


Figure A-5.4 Tunnel designer in Plaxis 7.2.

In this same window an interface and material lining is assigned to the tunnel modeled as a pipe. For the example a radius of 2 foot is entered and a tunnel and interface lining is assigned to the tunnel. An interface is used to model soil-structure interaction and the material lining provides the option for assigning concrete properties to the tunnel lining. The next step in the model is load and boundary conditions.

The load and boundary conditions used for this model are standard fixities and traction loads (distributed loads). Both features are chosen from the standard toolbar as shown in Figure A-5.3. The soil box will be modeled as a rigid box with minimal deflection. Fixities are prescribed displacements equal to zero. These fixities can be applied to points and lines. By clicking on the standard fixities button on the toolbar, the two sidewalls and bottom of the box were assigned both horizontal and vertical fixities as shown in Figure A-5.5 below.

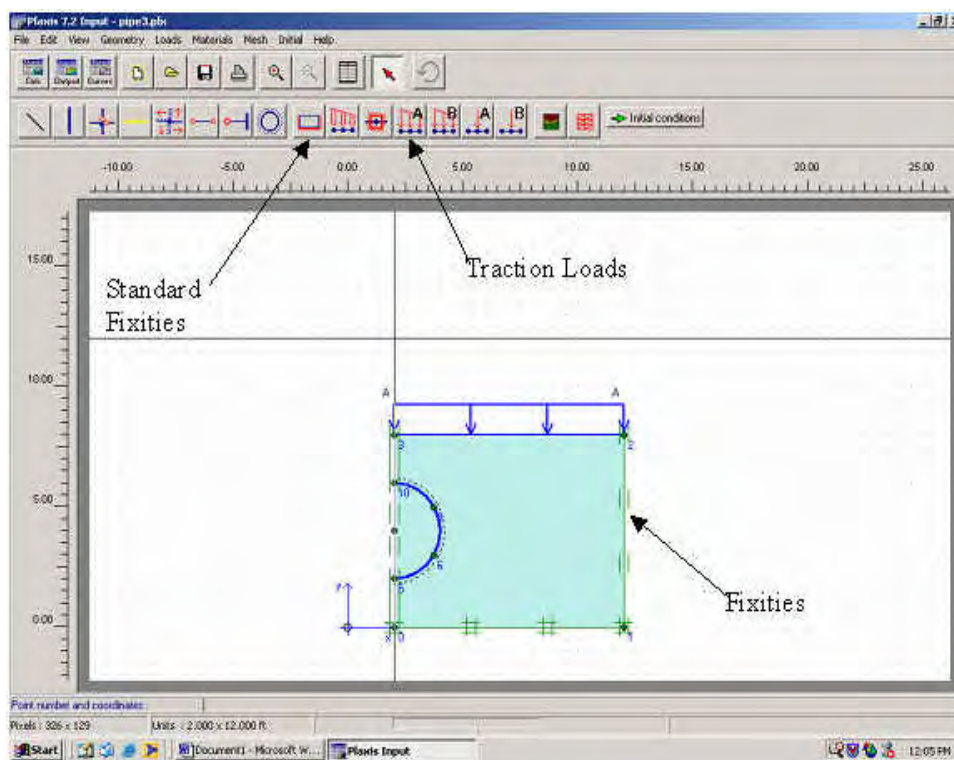


Figure A-5.5 Standard fixities in Plaxis 7.2 shown on a soil box with right half tunnel.

After the standard fixities are assigned, moving to the left on the toolbar, the loads are assigned through the traction icon as shown in Figure A-5.5. A distributed load was assigned using traction A, assigning the load to the two top points of the box on the CAD drawing area. Plaxis will ask the user to enter a multiplier for loading steps in the calculation phase. The default is 1.00 representing a true value for the load entered in the calculation phase. A multiplier of 1.00 was used in the example.

Once the model is finished geometrically with all beam elements added, fixities assigned and loads added, the material properties need to be specified and added to the model. Material data sets for soil, interfaces and beams are entered using the material data set icon located on the main toolbar. When the icon is clicked on, a window will open labeled Material sets with choices for the project database as shown in Figure A-5.6.

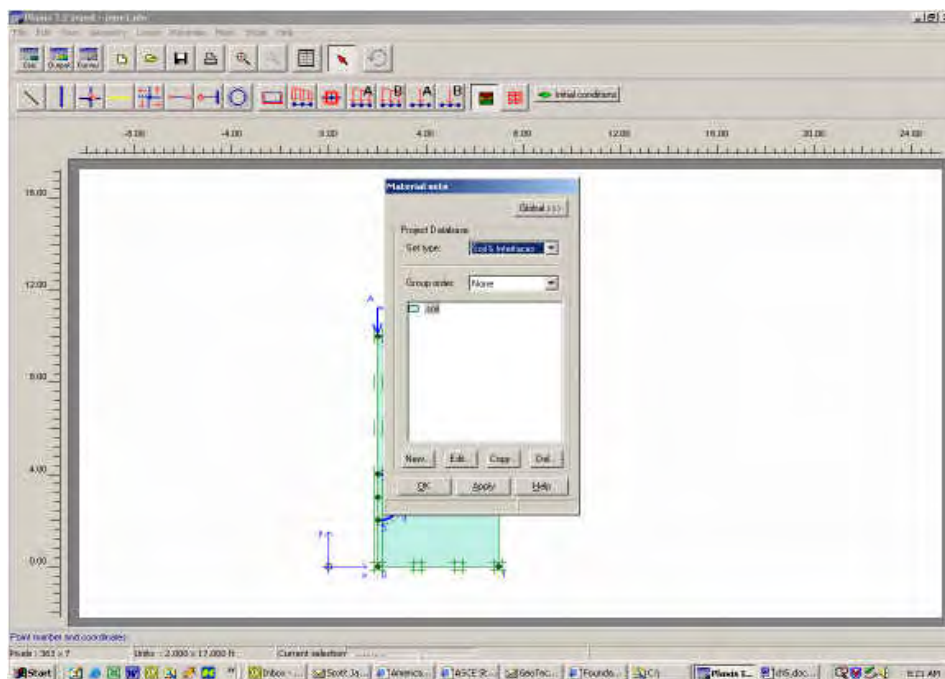


Figure A-5.6 Material sets window in Plaxis 7.2.



The example requires material data sets for soil & interfaces and beams. The first step is to set the parameters for the soil & interfaces. Input parameters for the soil are entered in the window shown in Figure A-5.7 such as material model, unit weight, permeability, stiffness, Poisson's ratio, cohesion, friction and dilatancy angles and interface properties.

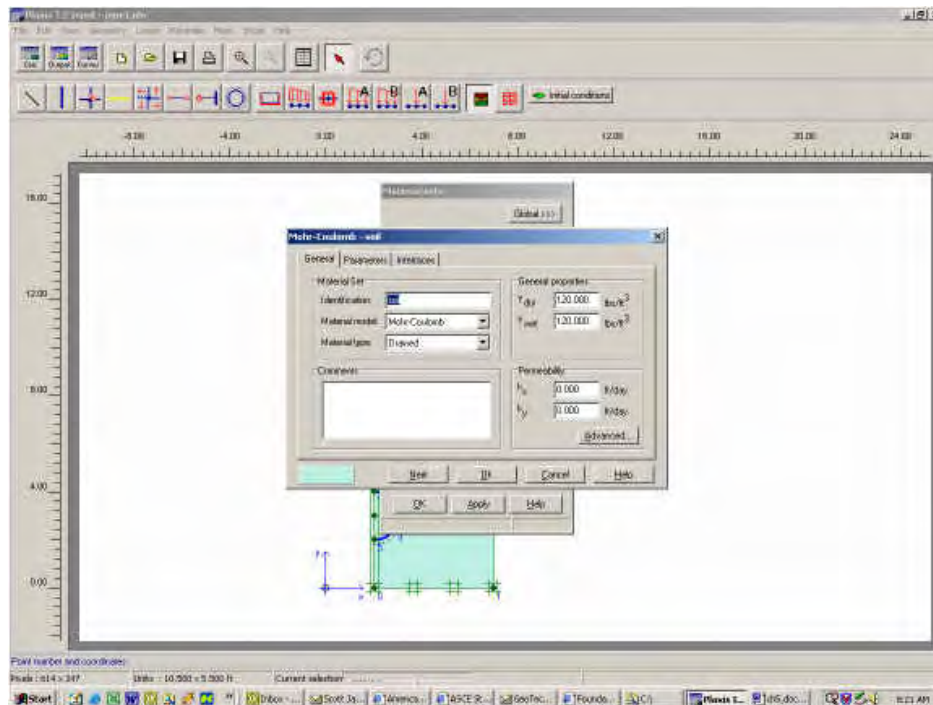


Figure A-5.7 Soil input in Plaxis 7.2 – Mohr coulomb model.

The input parameters used for the example soil model are:

- Model used: Mohr Coulomb
- Material type: drained
- Unit weight: 120 pcf
- Permeability: 0 (both vertical and horizontal)
- Stiffness (E): 489,600 psf
- Poisson's ratio (ν): 0.3
- Cohesion (c):  $1 \times 10^{-5}$
- Phi angle (φ): 35.00°
- Dilatancy angle (ψ): 5.00°

Specified along with the input parameters for the soil model are the settings for the interfaces.

The soil interfaces are specified as rigid or a manual setting. This feature is used for soil-

structure modeling. The example model shown is modeling the soil-structure interaction between the soil and a concrete pipe. Both rigid and manual settings for the interface are used. Rigid assigns the same properties of the soil to the interface and manual allows the user to specify a friction angle for modeling two different friction angles next to one another such as concrete and soil or steel and soil.

The material set for beams is specified when the user selects beams from the material set window and assigns the parameters. Input parameters are entered in the window as shown in Figure A-5.8.

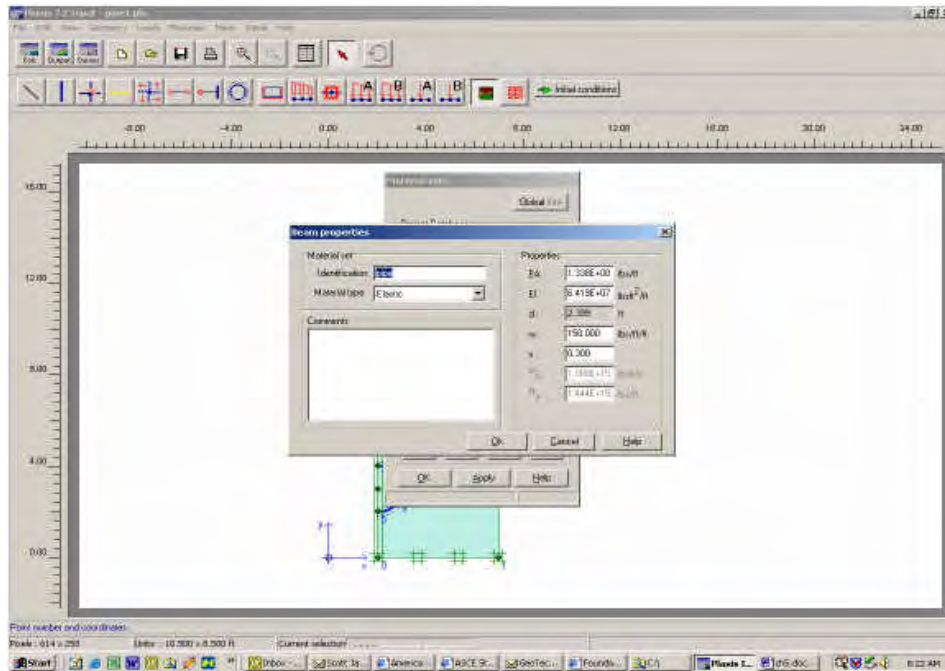


Figure A-5.8 Beam properties input window in Plaxis 7.2.

The input parameters used for the beam material model representing the concrete pipe are:

- Axial Stiffness (EA):  $107.3 \times 10^6$  lb/ft
- Flexural Rigidity (EI):  $193.5 \times 10^6$  lb-ft/ft
- Unit weight: 150 pcf
- Poisson's ratio: 0.15

The axial stiffness and the flexural rigidity are calculated using the modulus of elasticity and the cross sectional area of the concrete pipe along with the moment of inertia of the pipe.

The unit weight is referenced in a concrete manual.

After the material parameters are assigned to the model the material sets window appears once more to click and drag the material properties onto the model. Once this task is complete the window is closed. At this point all of the model setup is complete. In order for a finite element analysis to occur, the geometry must be divided into elements called a finite element mesh. The mesh generation icon is the last icon on the main tool bar located on the far right with an image of mesh on it. Plaxis is equipped with a self-generating mesh tool. Once the mesh is generated, a plot is displayed through the output program. The mesh can be defined as very coarse, coarse, medium, fine and very fine. A finer mesh is used where large stress contributions might be seen due to loading. After the mesh is generated the initial conditions are entered as shown in Figure A-5.9.

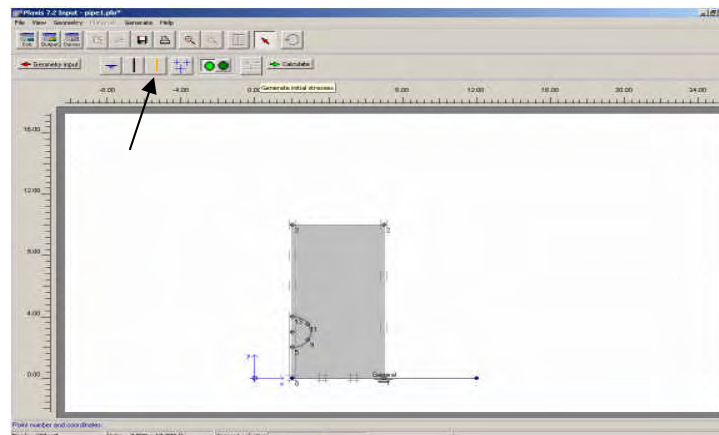


Figure A-5.9 Pore water pressure and initial stress modes in Plaxis 7.2.

Initial conditions involve an initial stress state before loading and an initial situation. This process is still part of the input program. The initial conditions consist of two different modes:

One mode for the generation of initial water pressures (water conditions mode) and one mode for the specification of the initial geometry configuration and the generation of initial effective stress field (geometry configuration mode) (Plaxis, 2001). Switching between these two modes is done by means of clicking on icons as shown in Figure A-5.9.

Water conditions are specified by means of the water weight and phreatic lines. The model used for example was in a dry state thus there were no phreatic line and no water pressures to generate. The switch is made to initial geometry configuration. In this step the example model is shown with the soil box and concrete pipe inside the box. The initial geometry configuration allows the user to select geometry objects that are not active in the initial situation. This means the beam elements are turned off to initiate the initial stresses before the construction/ addition of the concrete pipe is done. The initial stresses are calculated using the  $K_0$  procedure with a default value of 0.426 when the stress icon is chosen on the tool bar. An initial vertical stress is calculated using the coefficient of lateral earth pressure  $K_0$ . Once the initial stresses are generated, a window is displayed with the initial stresses showing the plane of direction. Once the input stage is completed, the next step is the calculation stage.

### **Plaxis – Calculations**

After the finite element mesh is generated, the finite element calculations can be specified and executed in the calculations program. In this program each type of calculation is defined to be performed along with the type of loading activated during the calculation. Initiating the calculation program will open a window as shown in Figure A-5.10. The three tabs, general, parameters and multipliers, will navigate the user through to the end calculate command. The only settings to define in the calculation program are the calculation type, selecting the calculation phases and multipliers. The other input areas in the calculations program are set to default and were used as default for the example model.

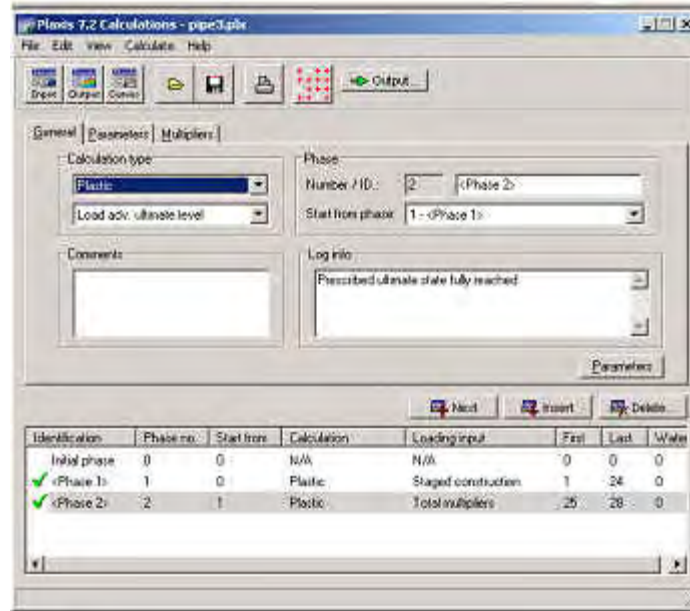


Figure A-5.10 Plaxis 7.2 calculations program.

In the calculation program under the general tab the calculation type is specified along with the setup of the calculation phase(s) using the insert button as seen in Figure A-5.10. The insert button will add additional phases for calculation. In the example model three phases were setup, initial phase, phase 1 and phase2. Phases are assigned parameters and multipliers when highlighted in the phase display box located at the bottom of the calculations window. The initial phase represents the initial situation of the project as defined in the initial conditions mode of the Input program. For the example model two phases were added: staged construction and total multipliers. The stage construction represents the installation of the concrete pipe with loading from overburden soil above the pipe. The total multipliers stage is where the assigned distributed load is activated and applied to the model.

Under the parameters tab as shown in Figure A-5.11 the default modes are used. The parameters tab is where the staged construction phase is defined. The loading input group is

used to specify which type of loading is considered in a particular calculation phase. Loading input is set to staged construction. The define button, located at the bottom right, will open the input window of the model allowing the user to deactivate and activate soil clusters and structural objects which define the construction of the model used for calculations. After the staged construction phase is defined the update key will return the user to the calculation program.

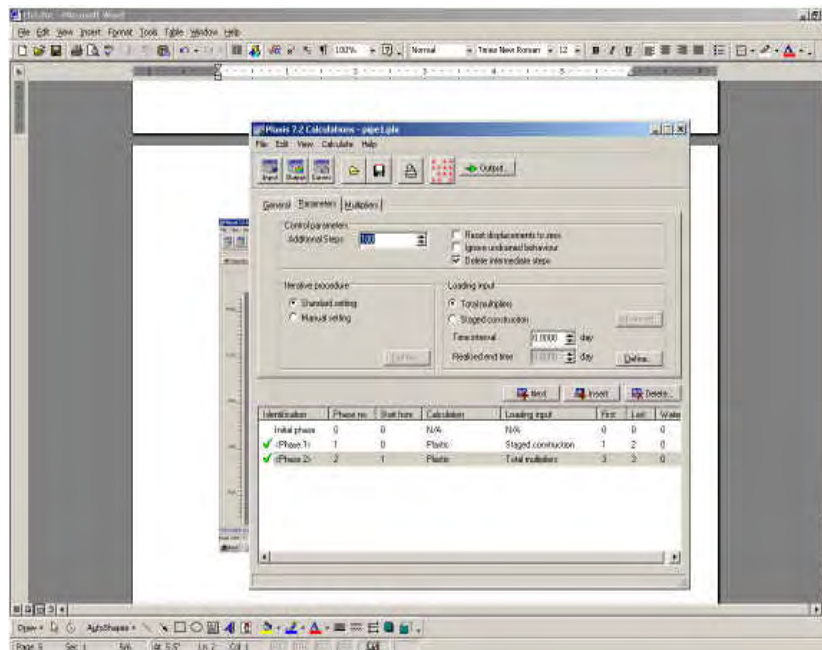


Figure A-5.11 Plaxis 7.2 calculations program – Parameters tab.

The multipliers tab is where loads are assigned for the total multipliers stage. There are two types of multipliers: incremental and total as shown in Figure A-5.12. In the example model shown, the total multiplier assigned in the input program is  $\Sigma MloadA$  at a value of 16,000 with units of pounds per square foot.  $\Sigma MloadA$  controls the magnitude of the traction loads as entered in the load system A in the input program.

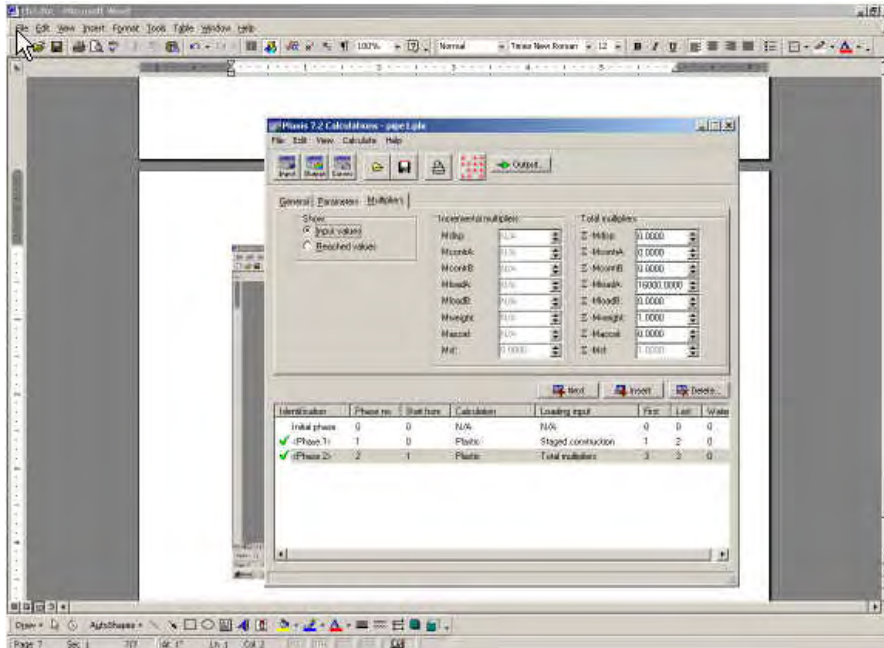


Figure A-5.12 Plaxis calculations program – Multipliers tab.

Another feature in the calculation phase sets up points for curves generated in the curves program. The points can be entered by selecting the *Select points for curves* option from the *View* menu or by clicking on the corresponding button in the tool bar. Selection occurs when the output program opens showing a plot of the finite element mesh with all of the nodes. Nodes are selected by clicking the mouse on the node of interest. Each node selected is characterized in the curves program by an alphabetical letter. A node can also be deselected by clicking on it again with the mouse. In the example model shown, points were selected to create curves for load displacement and stress/strain curves. After selecting the points for curves the calculate button will run the calculation program. A window is opened to view the loading increments displaying different properties. Once the calculation is completed the calculation window appears with green checks beside the phases of calculation. Output of the calculation is viewed through the output program opened by clicking on the output button located at the top of the window of the calculation window.

## Plaxis - Output

The main output quantities of a finite element calculation are the displacements at the nodes and the stresses at the stress points. When a finite element model as the example model used involves structural elements, structural forces are calculated in these elements. The output program is equipped with many facilities to display the results of a finite element analysis. The output program window is displayed in Figure A-5.13 showing the deformed finite element mesh due to loading from the calculation program.

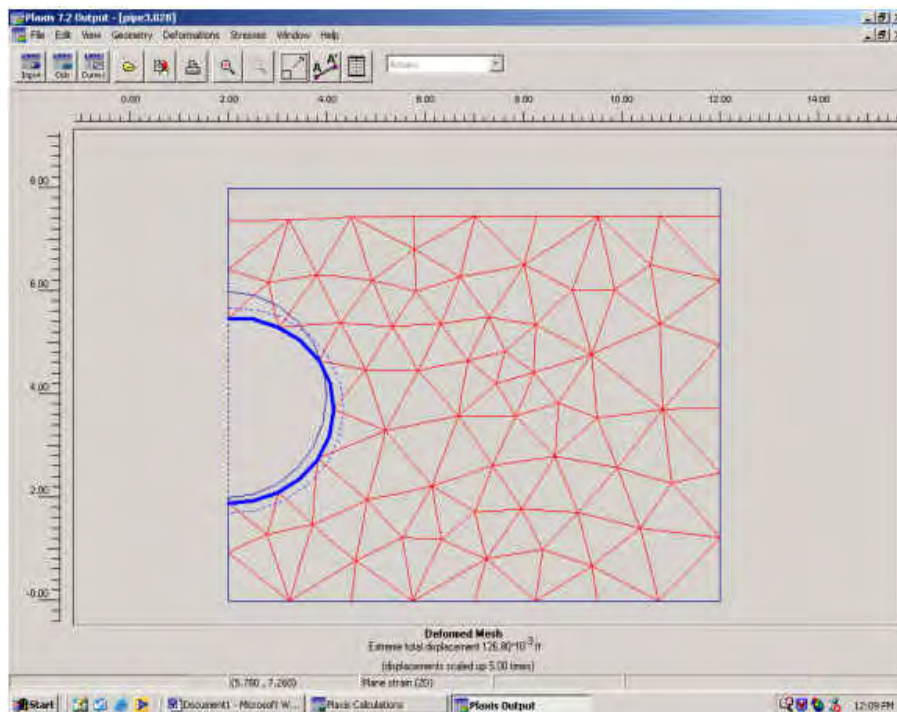


Figure A-5.13 Plaxis output program with deformed mesh displayed on example model.

Output results are viewed through the output program displaying deformations, deformed mesh, total displacements, total increments, total strains, incremental strains, stresses, effective stresses, total stresses, plastic points, active pore pressures, excess pore pressures, groundwater head, flow field, structures and interfaces, beams, geotextiles, interfaces and anchors. In the example model, a four foot diameter concrete pipe modeled in a 20' x 10' x 10' soil box, the



only output of interest are deformed mesh, total displacements (how much the pipe and soil settled), stresses, structures and interfaces and beams (concrete pipe). Each of the output results can be viewed in a picture, table and curve.

The first plot the user views in the output program is the deformed mesh plot as seen in Figure A-5.13. From this plot the user can navigate to other results by selecting from the menu at the top of the output window. In the example model, the first thing to analyze is the stress distribution throughout the soil contained in the box. Figure A-5.14 displays the stress distribution throughout the soil box by means of shading. The red zone is where the highest of the stresses are concentrated. Mean shading provides a colorful way of presenting results for effective mean stresses.

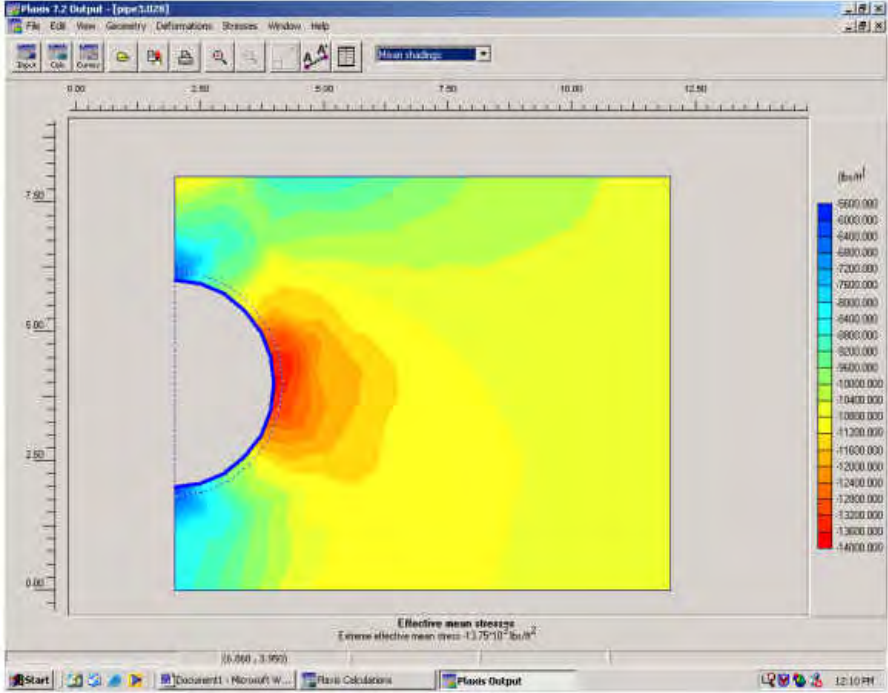


Figure A-5.14 Plaxis output effective mean stresses displayed by mean shading.

Another way to display stress distribution results is through the contour plot of effective mean stresses as shown in Figure A-5.15. The contour plot displays a legend on the right side of

the window identifying the contour when a scan line, that labels the contours with respect to the legend on the right side.

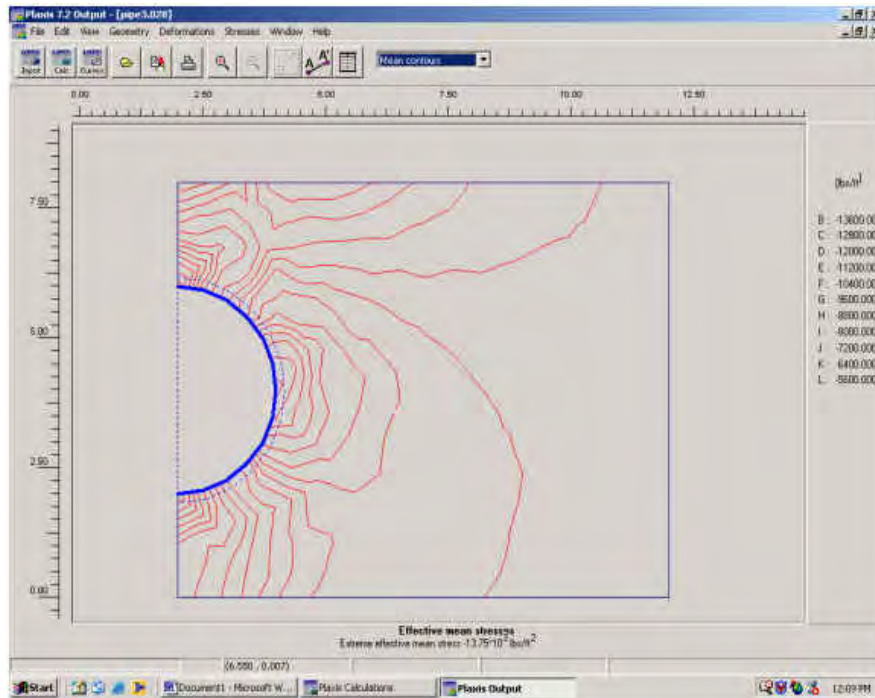


Figure A-5.15 Plaxis output effective mean stresses displayed by contours.

Cross sections through the model are features presenting results of displacement and stress distributions. Viewing output in a cross section allows the user to gain insight in the distribution of a certain quantity of the model. Cross sections are created in the model by selecting the cross section button and clicking and dragging a line through the model where a cross section is desired. In the example model stress distribution on the sidewalls was researched requiring a plot of stress distribution along the sidewalls of the soil box. The cross section on the sidewall is shown in Figure A-5.16. Also shown with the cross section tool are the horizontal displacements along the cross section shown in Figure A-5.17.

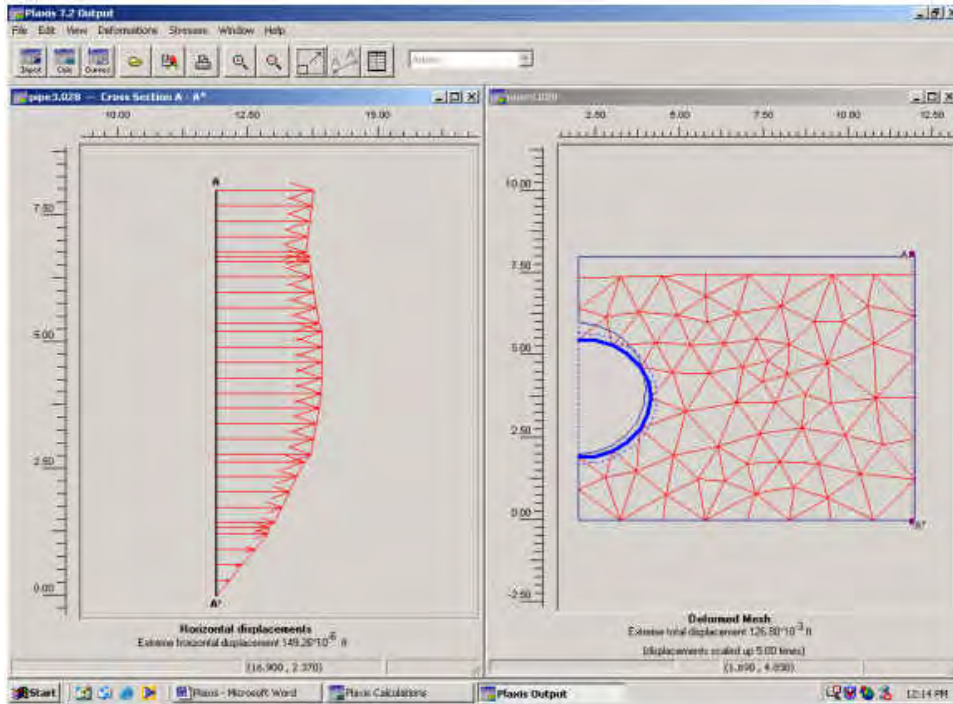


Figure A-5.16 Stress distribution cross section A-A in Plaxis 7.2 – Output program.

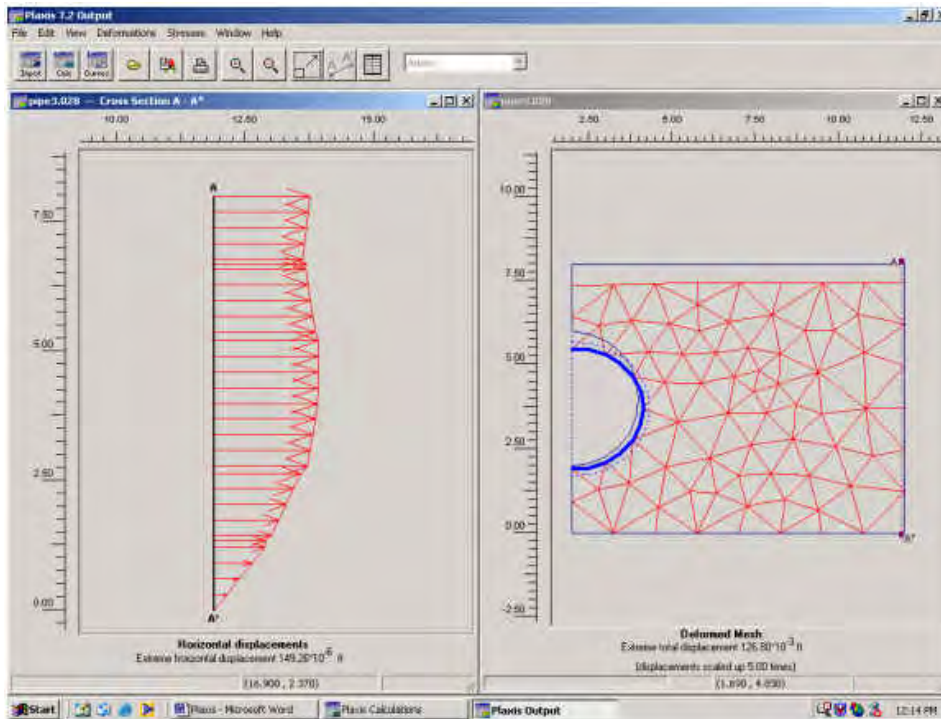


Figure A-5.17 Horizontal displacement cross section A-A in Plaxis 7.2 – Output program.

Beam elements as created in the input program are viewed in the output program with element results and interface results. Element results are the beam forces, displacements and bending moments. Interfaces assigned to the element will show displacements and stresses acting within the interface. Displacement output for the beam element – concrete pipe and the interface assigned to the concrete pipe are shown in Figure A-5.18. Plaxis will specify the extreme displacement for the beam elements and the interfaces. The bending moment of the concrete pipe in the example model is shown in Figure A-5.19. Beam element properties are displayed in the output program by double clicking on the element itself. The choice of what to display is activated from the sub menu found at the top of the screen.

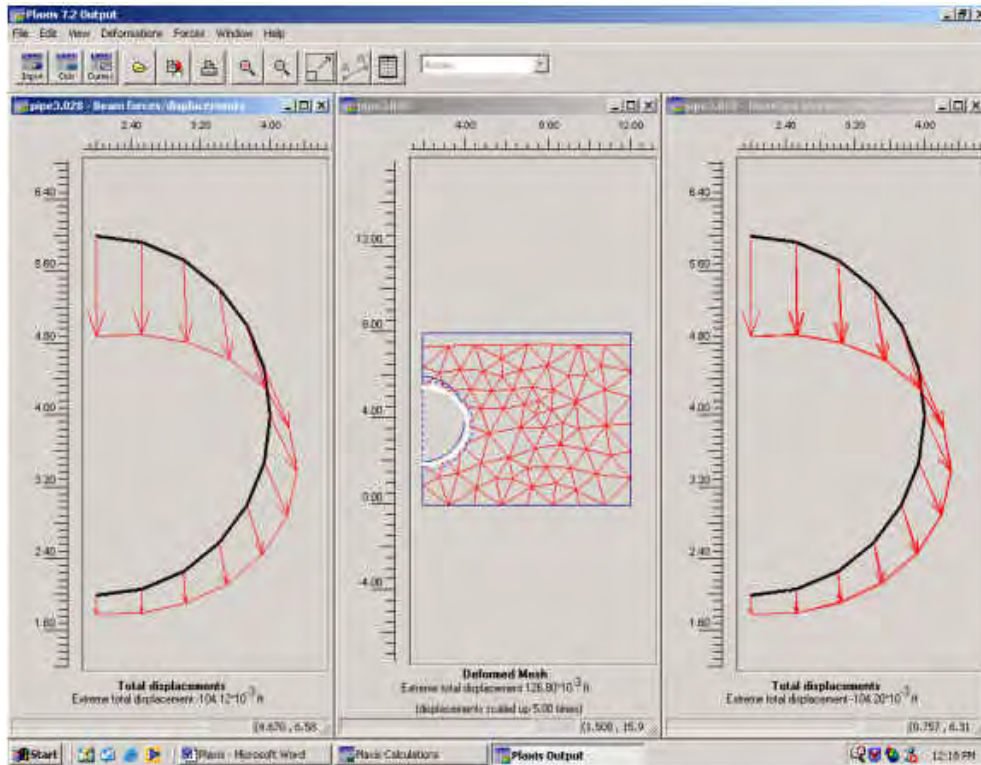


Figure A-5.18 Displacements for the pipe and interface – Plaxis 7.2 – Output program.

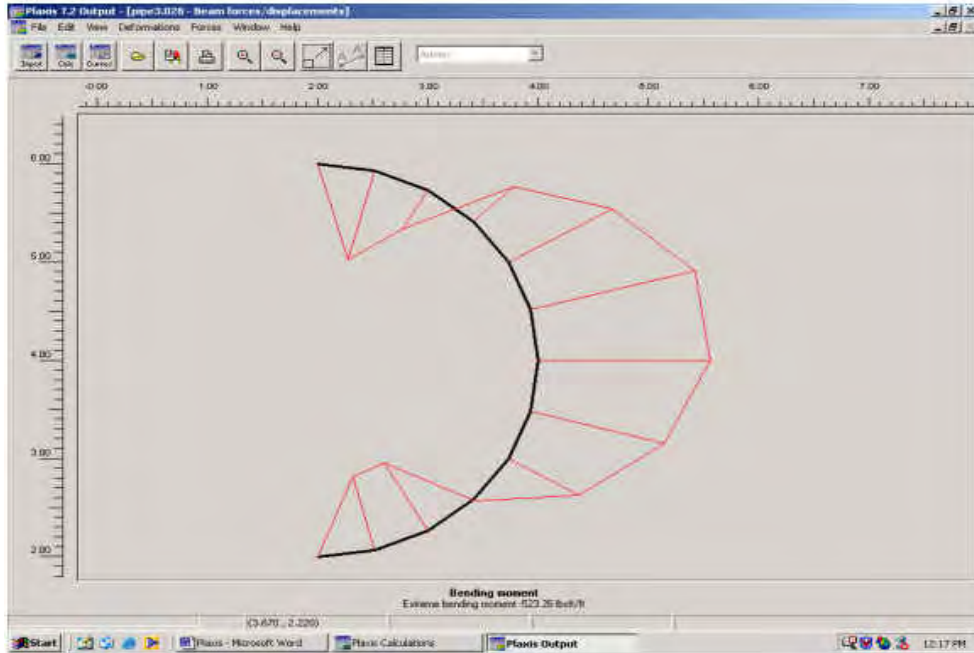


Figure A-5.19. Bending moment for the pipe – Plaxis 7.2 – Output program.

The output program is also equipped with tabular data for analysis. For all types of graphical output the numerical data can be viewed in output tables by clicking on the Table button in the main tool bar or by selecting the Table option from the View menu. A view is opened in which the corresponding quantities are presented in tables. A menu is available to view selections of other quantities. Tables available in Plaxis are tables of displacement, stresses and strains, and stresses and forces in interfaces and structures. In the research example used, tabular data was not used directly. Output data was put into the curves program generating different curves.

CHAPTER A-6  
EXTENDED FINITE ELEMENT ANALYSIS OF PIPES IN A SOIL BOX TEST FACILITY

**Introduction**

A soil box will be designed to test two different concrete pipes, fiber reinforced and standard reinforced, and simulate in-situ conditions. Two and three dimensional finite element analyses were done to evaluate the stress on the sidewalls due to the applied load and the effect of boundary conditions, i.e. friction on the sidewalls. The soil box will be constructed out of steel and filled with compacted soil similar to the soil in the State of Florida right-of-ways. The two-dimensional program used, Plaxis 2D, is a finite element analysis for soil and rock. Plaxis 2D evaluated the stresses on the sidewalls and the soil structure interaction between the soil and concrete pipes as well as the soil and steel structure sidewalls. From the two dimensional analysis, the box dimensions were selected and the stresses evaluated using an interface between the soil and concrete pipe and the soil and the steel sidewall. In the research performed, boundary conditions were eliminated as to not reflect stresses back onto the pipe during loading. A three-dimensional finite element analysis, Plaxis 3D, was used in addition to address the two-dimensional analysis and stresses in the z direction, the third dimension. Displacements of the concrete pipes were evaluated with and without friction on the sidewalls. Stresses were examined along the length of the pipe to ensure that no shear stresses were induced on the ends of the pipes near the front and rear walls.

**Input Parameters-Finite Element Analysis**

Two different manufactured concrete pipes are to be tested inside the soil box, fiber reinforced and standard reinforced concrete pipes. The proposed pipe diameters to be used for testing are 18” and 24” with a possibility of a 48” diameter pipe. In order to ensure proper bedding, a depth of at least one diameter below the pipe inside the soil box will be used in the

analysis and research. For example, the 24” diameter pipe will need two feet of soil beneath resulting in an approximate height of four feet above the crown of the pipe to the top of the box. An overburden soil depth of six feet will allow the distribution of stresses simulating in-situ conditions. The maximum load applied on the soil will be 16,000 lbs/ft<sup>2</sup>. Loose and dense compacted soil defines the two types of backfill used in the analysis shown in Table A-6.1. The loose compacted soil has a Young’s Modulus value of 216,000 lbs/ft<sup>2</sup> and the dense compacted soil with a Young’s Modulus value of 489,600 lbs/ft<sup>2</sup>. Input parameters for the SRCP and FRCP different size diameter pipes are displayed in Tables A-6.2 through A-6.4.

Table A-6.1 Material Properties of the Soil (Loose & Dense)

Parameter	Name	Loose	Dense	Unit
Material Model	Model	Mohr-Coulomb	Mohr-Coulomb	-
Type of material behavior	Type	Drained	Drained	-
Soil weight above phr. level	$\gamma_{\text{unsat}}$	120	120	lbs/ft <sup>3</sup>
Soil weight below phr. level	$\gamma_{\text{sat}}$	120	120	lbs/ft <sup>3</sup>
Young’s modulus	$E_{\text{ref}}$	216,000	489,600	lbs/ft <sup>2</sup>
Poisson’s ratio	$\nu$	0.3	0.3	-
Cohesion	$c_{\text{ref}}$	0.00001	0.00001	lbs/ft <sup>2</sup>
Friction angle	$\phi$	35	35	DEG.
Dilatancy angle	$\psi$	5	5	DEG.

Table A-6.2 Material Properties of the 18”-diameter Concrete Pipes (FRCP & SRCP)

Parameter	Name	FRCP	SRCP	Unit
Type of behavior	Material type	Elastic	Elastic	-
Normal stiffness	EA	147,372,845	280,303,765	lbs/ft
Flexural Rigidity	EI	38,138,787	66791264	lbs-ft <sup>2</sup> /ft
Weight	W	150	150	lbs/ft <sup>3</sup>
Poisson’s ratio	$\nu$	0.15	0.15	-

Table A-6.3 Material Properties of the 24”-diameter Concrete Pipes (FRCP & SRCP)

Parameter	Name	FRCP	SRCP	Unit
Type of behavior	Material type	Elastic	Elastic	-
Normal stiffness	EA	198,636,143	382,227,687	lbs/ft
Flexural Rigidity	EI	93,303,588	168,720,067	lbs-ft <sup>2</sup> /ft
Weight	W	150	150	lbs/ft <sup>3</sup>
Poisson’s ratio	$\nu$	0.15	0.15	-

Table A-6.4 Material Properties of the 48"-diameter Concrete Pipes (FRCP & SRCP)

Parameter	Name	FRCP	SRCP	Unit
Type of behavior	Material type	Elastic	Elastic	-
Normal stiffness	EA	665,723,216	1,228,267,715	lbs/ft
Flexural Rigidity	EI	1,263,829,838	2,322,073,435	lbs-ft <sup>2</sup> /ft
Weight	W	150	150	lbs/ft <sup>3</sup>
Poisson's ratio	v	0.15	0.15	-

Young's Modulus for the FRCP and SRCP were determined using referenced literature. The SRCP modulus value was calculated using the American Concrete Institute (ACI 318). Compressive strength for concrete pipe normally ranges from 4000 lbs/in<sup>2</sup> to 6000 lbs/in<sup>2</sup> (Rinker Materials, 2003). Elastic modulus for the SRCP was calculated using Equation A-6.1 with a compressive strength ( $f'_c$ ) of 4000 lbs/in<sup>2</sup>. Elastic modulus for the FRCP to determine normal stiffness and flexural rigidity of the concrete pipe used was  $3.62 \times 10^6$  lbs/in<sup>2</sup>.

$$E_c = 57,000 * \sqrt{f'_c} \quad (\text{A-6.1})$$

## Plaxis 2D

### Box Dimension Selection

A finite element analysis was conducted with and without the pipe inside the soil box to determine the box dimensions. In the two-dimensional analysis, an approximate height of ten feet was determined based on the proper bedding needs of the 24" diameter pipe. Three different widths of the box were analyzed, ten, fifteen and twenty feet. Each analysis was first run with no pipe inside the box and then with each of the 18" and 24" diameter concrete pipes. Symmetry was used in the size analysis of the box including only the right half of the pipe modeled shown in Figure A-6.1.



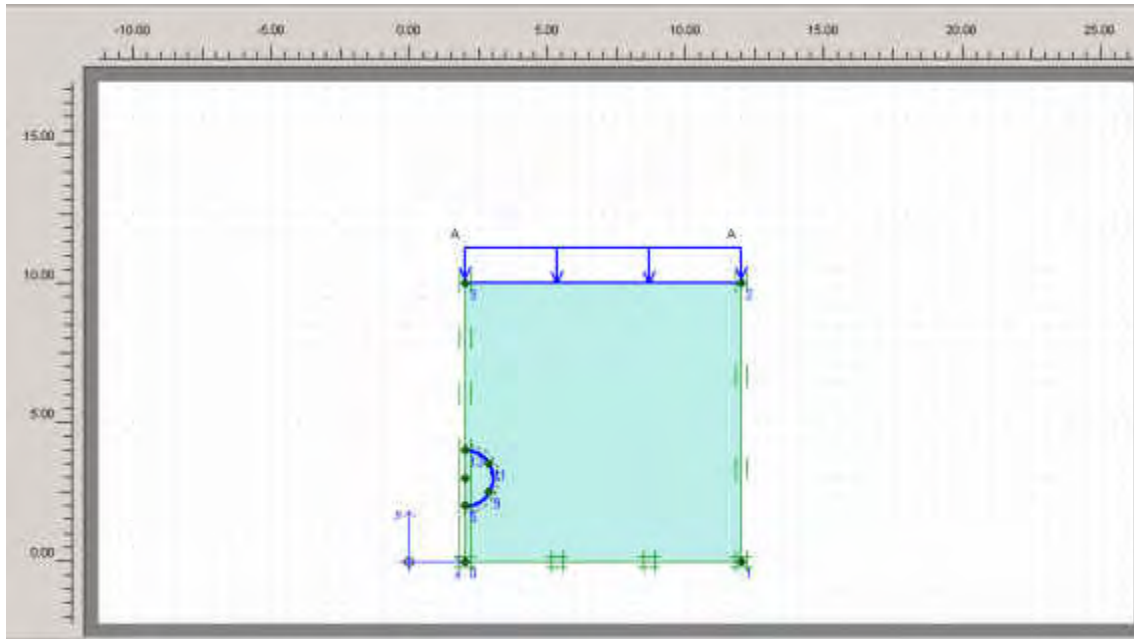


Figure A-6.1 Plaxis 2D symmetry model of 24" diameter FRCP.

Plaxis 2D was examined to minimize the sidewall stresses using the maximum load of 16,000 lbs/ft<sup>2</sup>. The first analysis involved three different widths with no pipe in the box, just the backfill soil. Figure A-6.2 shows the schematic of all three box analyses, each width, executed in Plaxis 2D. Results showed the same extreme value for the sidewall stresses for each width, ten, fifteen, and twenty at 7,270 lbs/ft<sup>2</sup>. Modeling in only two dimensions, stresses are a direct result of the load applied and the unit weight of the soil. Plaxis 2D modeled with uniform compaction results in a uniform stress distribution along the sidewall. In order to obtain the sidewall stresses, a cross section was taken along the sidewall displaying the extreme effective normal stress. An example is shown in Figure A-6.3.

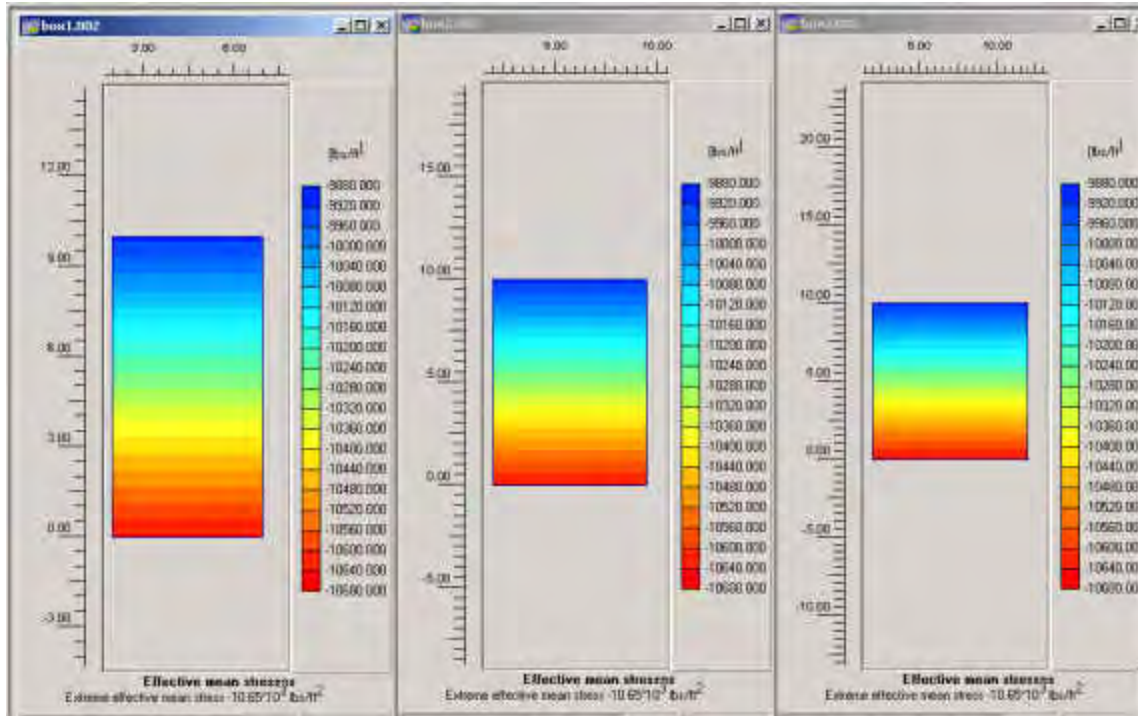


Figure A-6.2 Three different widths modeled in Plaxis 2D: 10, 15, 20 feet wide.

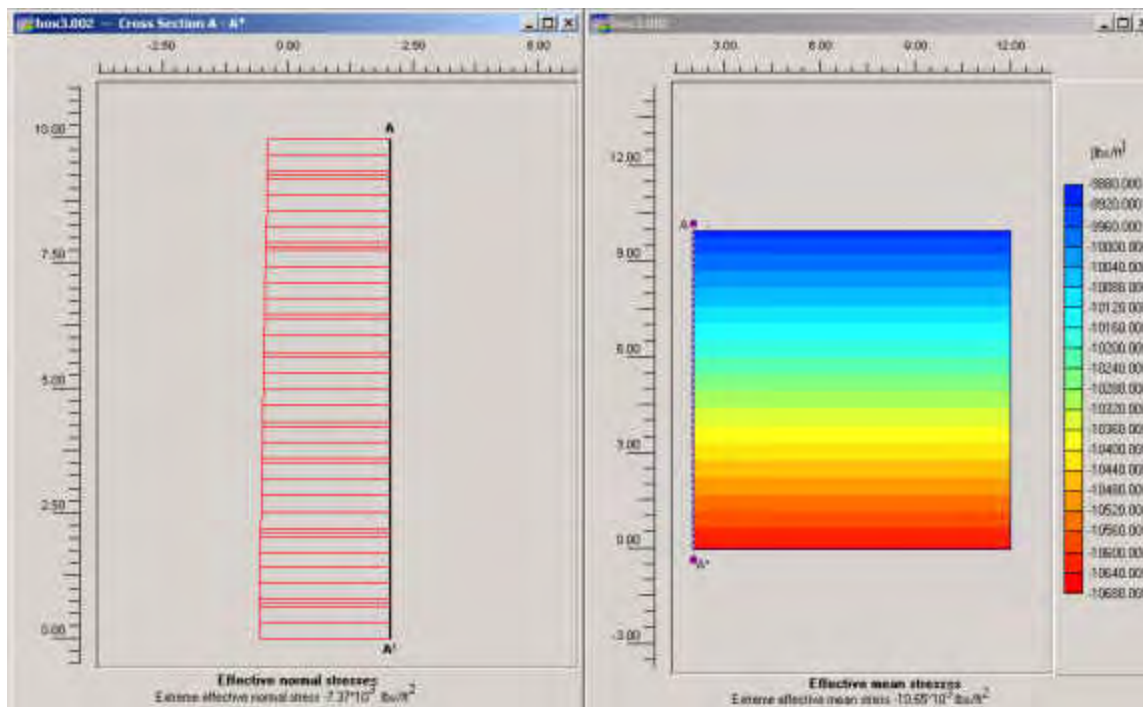


Figure A-6.3 Example of cross section used to examine the sidewall stresses (20' width).

A two-dimensional analysis was done with a concrete pipe inserted in the soil box. A 24” diameter of each of the SRCP and FRCP were used to examine the stresses on the sidewalls in determining the box dimensions. The 24” diameter pipes were used because the stresses on the sidewalls increase as the diameter of the pipe increases. Symmetry was used modeling only the right half of the concrete pipe. Again, three different widths were examined with the right half of each of the FRCP and SRCP inserted into the soil model. For example, stresses along the sidewalls for the ten, fifteen and twenty foot wide models with the FRCP are displayed in Figures A-6.4a through A-6.4c. FRCP is used for display in the figure only, both FRCP and SRCP were analyzed resulting in similar stresses along the sidewalls. Results show that the stresses decrease as the width increases reporting a maximum stress on the sidewall for the twenty-foot width of 7,300 lbs/ft<sup>2</sup>.

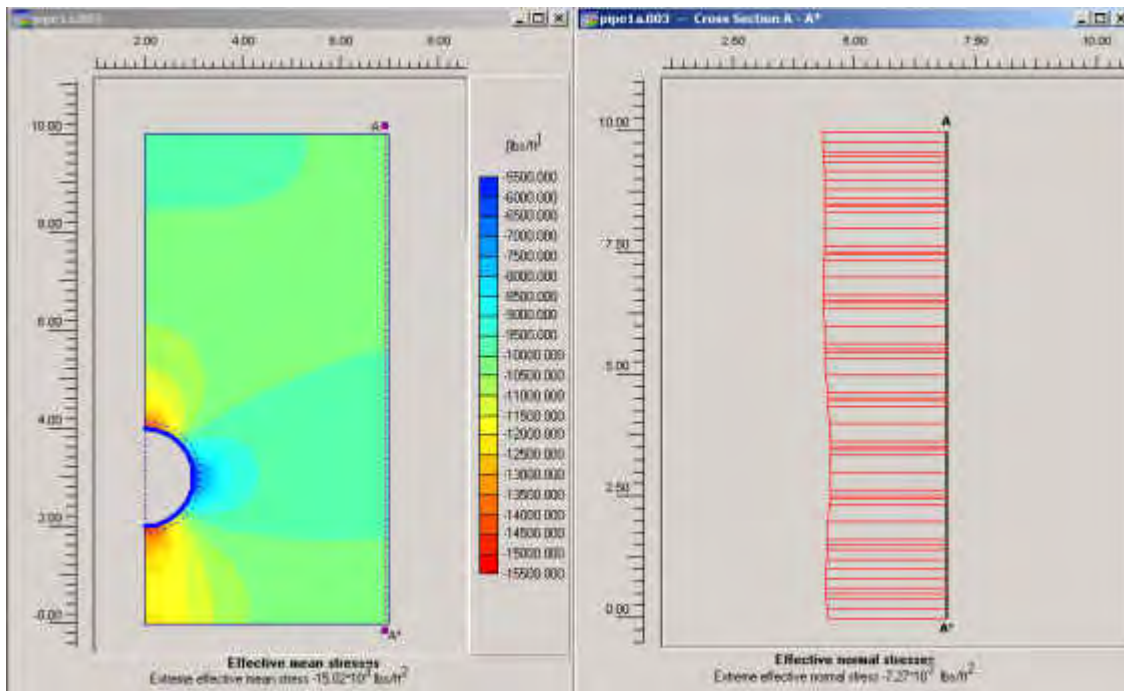


Figure A-6.4a Example FRCP cross section of sidewall stresses (10’ wide box).

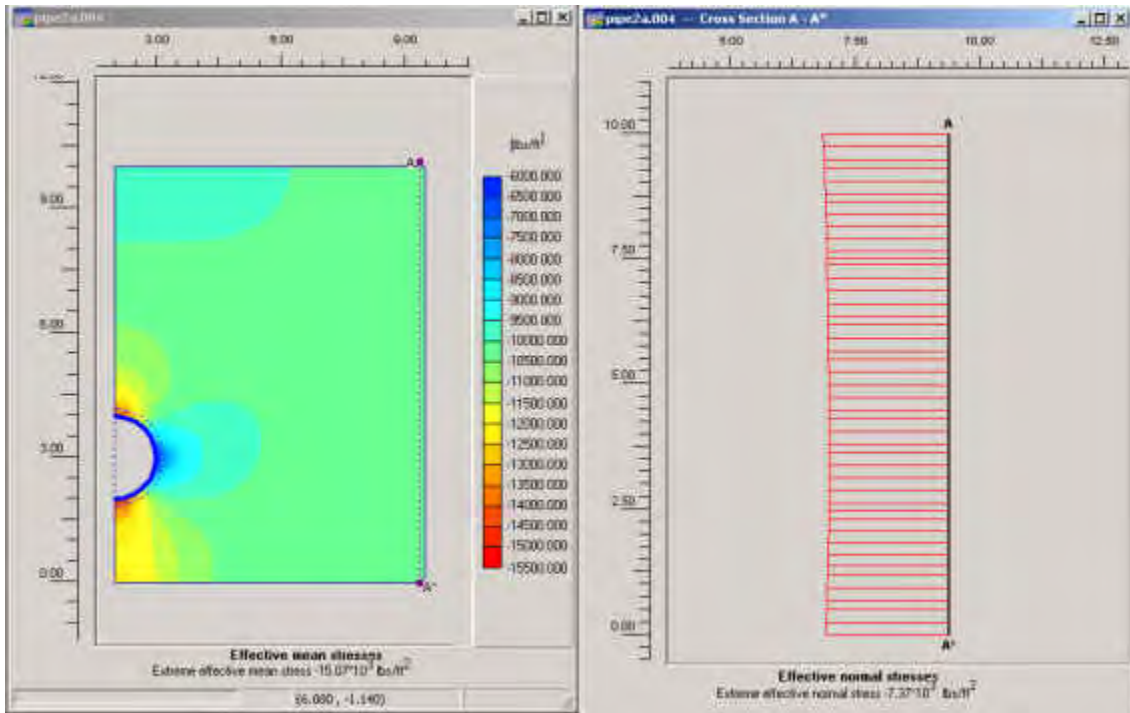


Figure A-6.4b Example FRCP cross section of sidewall stresses (15' wide box).

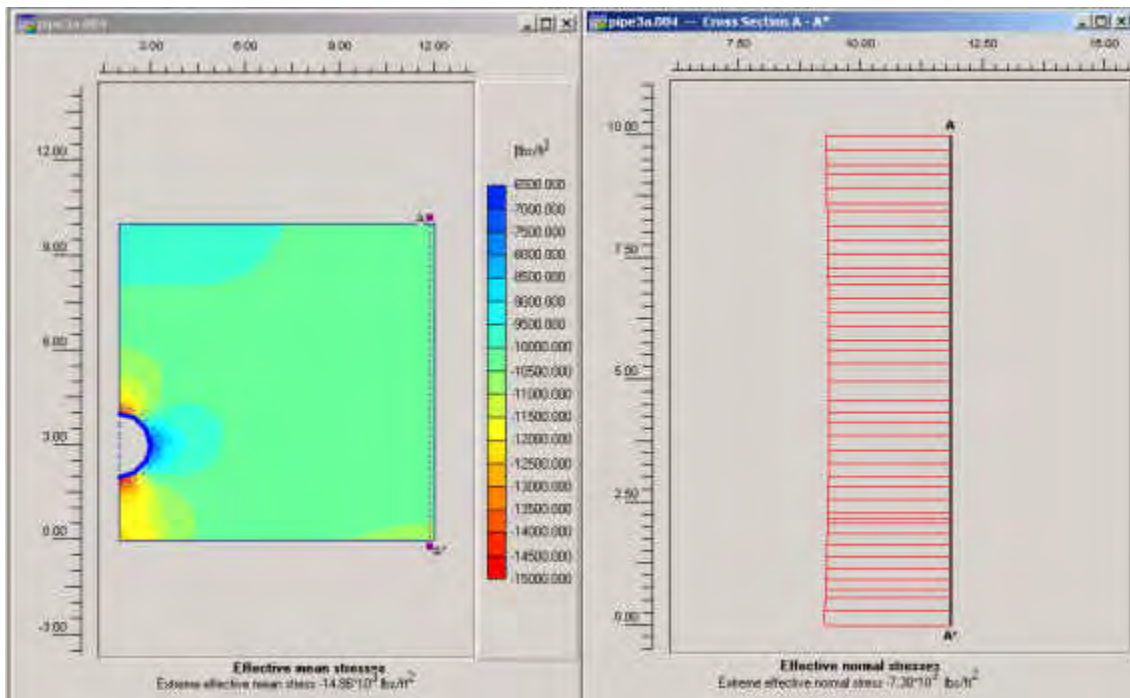


Figure A-6.4c Example FRCP cross section of sidewall stresses (20' wide box).

For verification, a full-scale finite element analysis was done for the twenty-foot wide soil box model. The full-scale model reported the same stresses on the sidewalls as did the model using symmetry and the right half of the SRCP and FRCP. From the 24" diameter pipe analysis, the results showed that the stresses and boundary conditions were best minimized for the box dimension of 20'x10'x10'.

### **Wall Friction/ Soil Compaction Analysis**

A two-dimensional analysis from Plaxis examined the sidewall friction of the selected box dimension width of twenty feet, altering the friction angle of the soil structure interface with the sidewalls and the perimeter of the pipe using two different compacted backfills. As described in Chapter A-5, an interface is region assigned to the steel beam on the sidewalls modeling the soil structure interaction. An interface was also assigned to the perimeter of the concrete pipe to model the soil structure interaction. Stresses and displacements are analyzed throughout the soil and along the interfaces. Two different friction angles were assigned to the interface; a friction angle representing the same friction as the soil and a friction angle less than five degrees allowing the soil to move freely along the sidewall. I. D. Moore conducted research, as stated in Chapter A-2, that minimizing the friction angle below five degrees helps to reduce boundary effects from inducing lateral stresses on the test pipe. The purpose is to simulate in-situ conditions minimizing the boundary conditions effect on the structural response of the test pipe. A total of 24 different analyses were done to examine the wall friction and the effects of different compacted soils on the structural response of the test pipe. Three different pipe size diameters were analyzed, 18", 24", and 48", with two types of concrete pipes, FRCP and SRCP, embedded in two different compacted backfills, loose and dense. Full-scale analyses were done to eliminate any questions of the results. The extreme value results are presented in Table A-6.5.

Table A-6.5 Wall Friction Analysis-Plaxis 2D Finite Element Analysis

Pipe	D <sup>1</sup>	C <sup>2</sup>	R <sup>3</sup>	EPS <sup>4</sup>	EMS <sup>5</sup>	Disp <sub>1</sub>	IEWS <sup>6</sup>	IEPS <sup>7</sup>	Disp <sub>2</sub>	PM <sup>8</sup>	Disp <sub>3</sub>
SRCP	24"	Loose	1	-24560	-14720	0.523	-7360	-24990	-0.157	-10550	0.151
FRCP	24"	Loose	1	-24550	-14710	0.523	-7450	-24990	-0.157	-11100	0.152
SRCP	24"	Dense	1	-24550	-14710	0.231	-7380	-24980	-0.069	-10550	0.067
FRCP	24"	Dense	1	-24530	-14700	0.230	-7260	-24970	-0.070	-10950	0.067
SRCP	24"	Loose	0.05	-26430	-14760	0.755	-4790	-5800	-0.442	-2090	0.257
FRCP	24"	Loose	0.05	-26430	-14760	0.755	-4790	-5800	-0.442	-2190	0.257
SRCP	24"	Dense	0.05	-26430	-14760	0.333	-4790	-5800	-0.195	-2090	0.113
FRCP	24"	Dense	0.05	-26430	-14760	0.333	-4790	-5800	-0.194	-2190	0.113
SRCP	18"	Loose	1	-23690	-13850	0.535	-7340	-24660	-0.135	-5780	0.129
FRCP	18"	Loose	1	-23680	-13840	0.535	-7340	-24660	-0.135	-6070	0.129
SRCP	18"	Dense	1	-23680	-13840	0.236	-7340	-24650	-0.059	-5770	0.057
FRCP	18"	Dense	1	-23660	-13840	0.236	-7340	-24640	-0.059	-6070	0.057
SRCP	18"	Loose	0.05	-24430	-15400	0.750	-4840	-4590	-0.325	-884	0.204
FRCP	18"	Loose	0.05	-24430	-15400	0.750	-4840	-4590	-0.324	-961	0.204
SRCP	18"	Dense	0.05	-24430	-15400	0.331	-4840	-4590	-0.143	-884	0.090
FRCP	18"	Dense	0.05	-24430	-15400	0.331	-4840	-4590	-0.143	-941	0.090
SRCP	48"	Loose	1	-23300	-13840	0.483	-7120	-22920	-0.289	-40150	0.283
FRCP	48"	Loose	1	-23290	-13840	0.482	-7120	-22920	-0.289	-41560	0.282
SRCP	48"	Dense	1	-23290	-13840	0.213	-7120	-22910	-0.127	-40140	0.125
FRCP	48"	Dense	1	-23280	-13840	0.213	-7120	-22910	-0.127	-41550	0.125
SRCP	48"	Loose	0.05	-30550	-17710	1.230	-5130	-11990	-1.130	-18600	0.624
FRCP	48"	Loose	0.05	-30550	-17710	1.230	-5130	-11990	-1.130	-19370	0.624
SRCP	48"	Dense	0.05	-30550	-17710	0.541	-5130	-11990	-0.499	-18600	0.275
FRCP	48"	Dense	0.05	-30550	-17710	0.540	-5130	-11990	-0.499	-19240	0.275

\*\*All values reported are extreme values (i.e. the maximum values).

1. D is the pipe diameter in inches.
  2. C is the compaction of the backfill.
  3. R is the interface value of strength. A value of 1 represents a friction angle the same as the backfill soil. A value of 0.05 represents a friction angle less than five degrees.
  4. EPS is the effective principal stress for the entire model box in lbs/ft<sup>2</sup>
  5. EMS is the effective mean stress for the entire model box in lbs/ft<sup>2</sup>
  6. IEWS is the interface effective normal wall stress in lbs/ft<sup>2</sup>
  7. IEPS is the interface effective normal pipe stress in lbs/ft<sup>2</sup>
  8. PM is the pipe bending moment in lbs-ft/ft
- Disp<sub>1</sub> is the total displacements for the entire box in feet.  
 Disp<sub>2</sub> is the total displacements for interface around the perimeter of the pipe in feet.  
 Disp<sub>3</sub> is the total displacement of the concrete pipe in feet.

It is apparent from the finite element modeling; the results show the dense compaction to be more stable than the loose compaction. Referring to the total displacement in Table A-6.5, the displacement is twice as large for the loose compacted soil. Dense compacted soil will provide better bedding conditions for the pipe to sustain a load. For the dense compacted soil, it is modeled using a soil modulus value compacted 90% proctor. In comparing both of the FRCP and SRCP, the difference in results overall were very minimal. The properties examined around the pipe, such as, interface properties and the pipe properties, showed minimal changes between the FRCP and SRCP. In comparing the interface variation in friction angle, the friction angle equal to the soil friction angle resulted in effective normal stress along the sidewall twice the effective normal stress of the model with a friction angle less than five degrees. Note the negative stress values are representing compression.

### **Plaxis 3D-Analysis**

A three-dimensional analysis was performed to verify the results obtained from the two-dimensional analysis as well as analyze the stress and displacement in the third dimension. Plaxis 3D introduces a third dimension of analysis allowing stresses in the z-axis to be examined. From the two-dimensional analysis, results showed the use of well compacted soil, 90% proctor, provided proper stability with half as much settlement as the loose compacted soil examined. It is important to obtain proper compaction during installation of the pipe to allow maximum performance from the pipe. Proper bedding is a result of good compaction in the bedding of the pipe trench. Three-dimensional finite element analysis will be used to verify eight analyses examined by the two-dimensional finite element program. Verification of the stresses and displacements throughout the soil box will be done for the 18" and the 24" diameter FRCP and SRCP. The 48" diameter pipe is questionable for testing in the soil box dimensions selected due

to the limited amount of soil cover on top of the test pipe. Other concerns to be addressed using a three dimensional finite element analysis are stresses along the length of the pipe as a result of a possible shear stress induced on the ends of the pipe due to wall friction and displacement of the entire pipe as a result of both wall friction and service load.

### **3D Verification of 2D**

Verification of the 18” and 24” diameter pipe was done using a three dimensional version of Plaxis. Four different analyses of the 18” and 24” pipe were done using dense compacted soil varying the friction angle within the interface between the SRCP and FRCP. The three-dimensional analyses differed very little from the two-dimensional analyses. The three dimensional analysis provides better stress distribution throughout the soil box into the third dimension. Varying the friction angle from a value equal to the soil friction angle to near zero through use of the interface doubles the amount of total displacements throughout the whole soil box. Assigning a value of near zero friction to the interface, the soil contained in the box is displaced more upon load. Friction on the sidewalls equal to that of the soil results in a total displacement of 0.236’ and an near zero friction value on the sidewalls results in a total displacement of 0.433’. In comparing the 18” and the 24” diameter pipes, the total displacements are the same. Figure A-6.5 shows the total displacements for the 24” FRCP and Figure A-6.6 shows the total displacement for the 24” SRCP having a friction angle equal to that of the soil. It is apparent visually on the sidewalls that there is friction. The load is distributed throughout the third dimension and the friction along the wall is visible through the displacements.



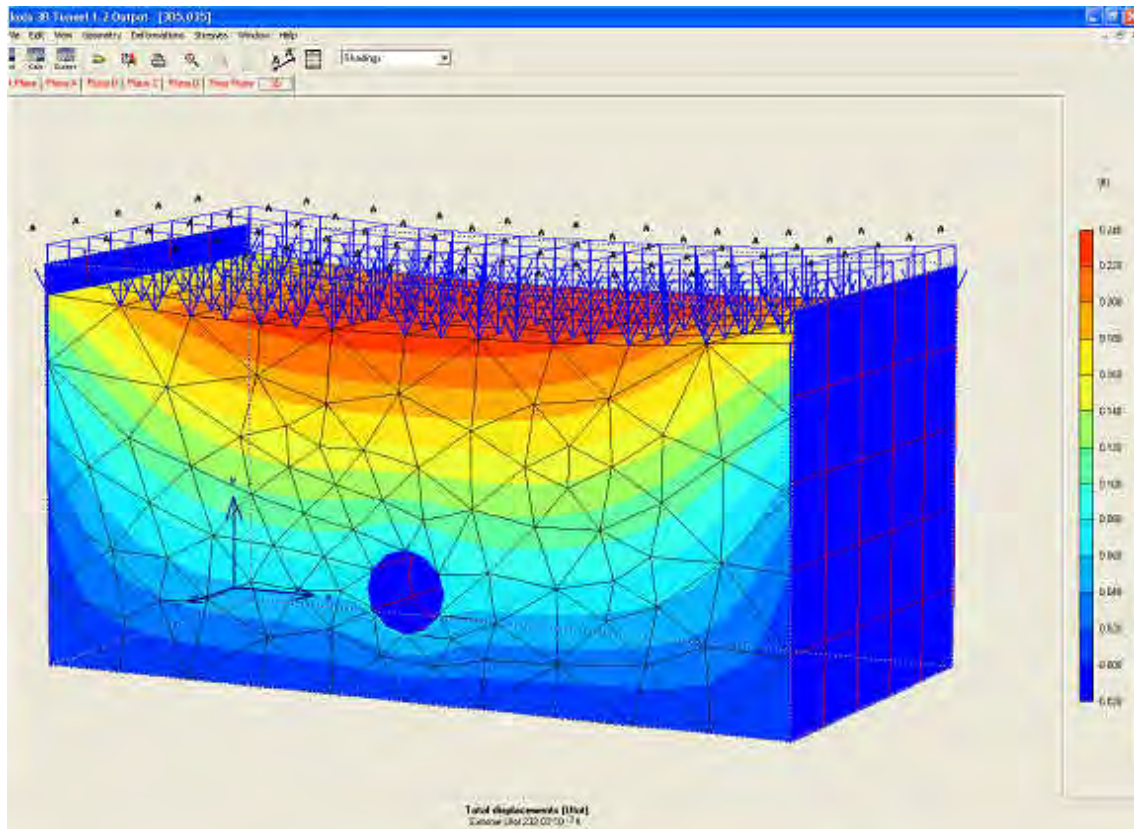


Figure A-6.5 Three dimensional view of total displacements for 24" FRCP.

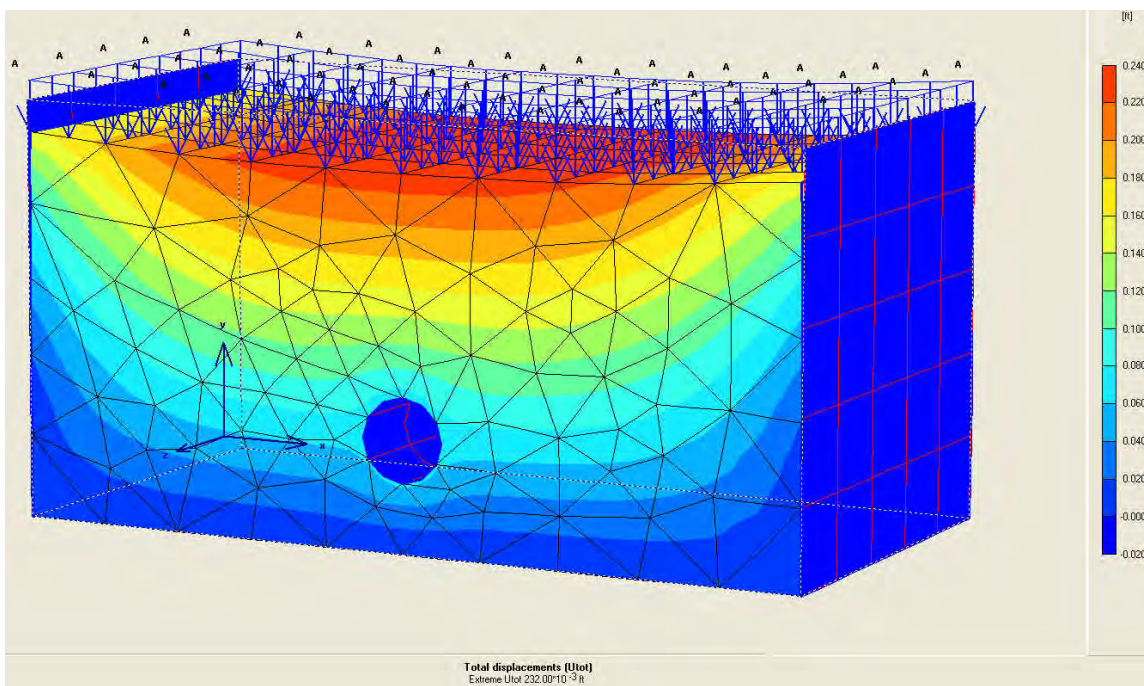


Figure A-6.6 Three dimensional view of total displacements for 24" SRCP.

The effective mean stress reported from the three-dimensional analysis differed little compared to the two-dimensional analysis. For example the extreme effective mean stress for the 18" SRCP, friction sidewalls, measured 12,690 lbs/ft<sup>2</sup> in the two-dimensional and 12,520 lbs/ft<sup>2</sup> in the three-dimensional analysis. The three-dimensional analysis distributes the stresses more efficient in the z direction, i.e. the third dimension.

The design of the box was based on the maximum stress on the sidewalls as a result of the 16,000-lbs/ft<sup>2</sup> load. Each of the two-dimensional wall friction analyses examined the effective mean stress on the sidewalls. Verified by the three-dimensional finite element program, the sidewall stresses were slightly smaller. Sidewall stresses examined through the interface along the sidewall increased when friction was assigned the same value as the soil to the interface. For example, the interface wall stress for the 18" diameter SRCP with friction was 7,070-lbs/ft<sup>2</sup> compared to an interface with near zero friction having a sidewall stress of 4,470-lbs/ft<sup>2</sup>. The soil was unable to move freely upon load application therefore creating higher stress applied to the sidewall. Figure A-6.7 shows the left side interface of the soil box displaying the effective normal stresses.

An interface was also assigned to the pipe inside the soil box for soil-structure interaction modeling. The interface assigned to the perimeter of the pipe varied the friction angle in the same manner as the sidewalls. The extreme effective mean stress around the pipe and extreme total displacement around the pipe are reported for each of the tests. There was very little difference between the FRCP and the SRCP modeled. In varying the friction angle in the interface around the perimeter of the pipe, the effective mean stress increased greatly, from -2,860 lbs/ft<sup>2</sup> to -27,870 lbs/ft<sup>2</sup>, when a friction angle of the same value as the soil was assigned to the interface compared to near zero friction in the interface as shown in Figures A-6.8 and A-6.9.

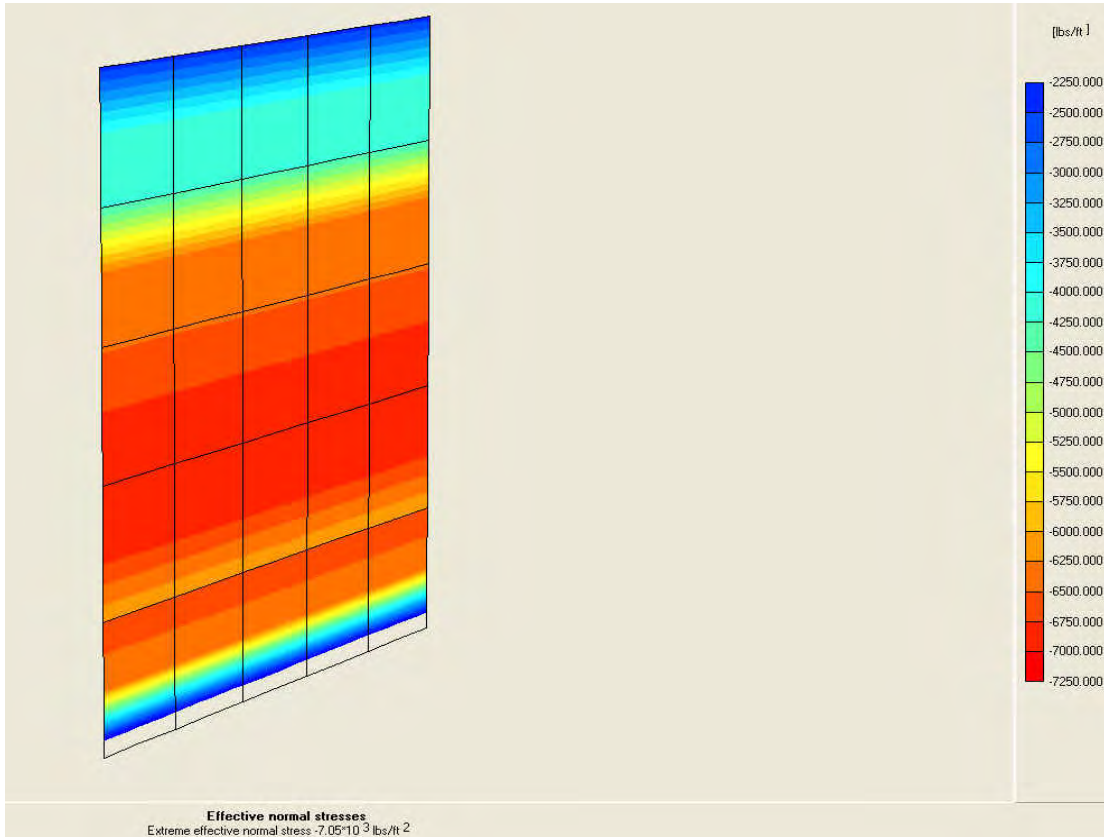


Figure A-6.7 Left side interface of soil box model 24" FRCP.

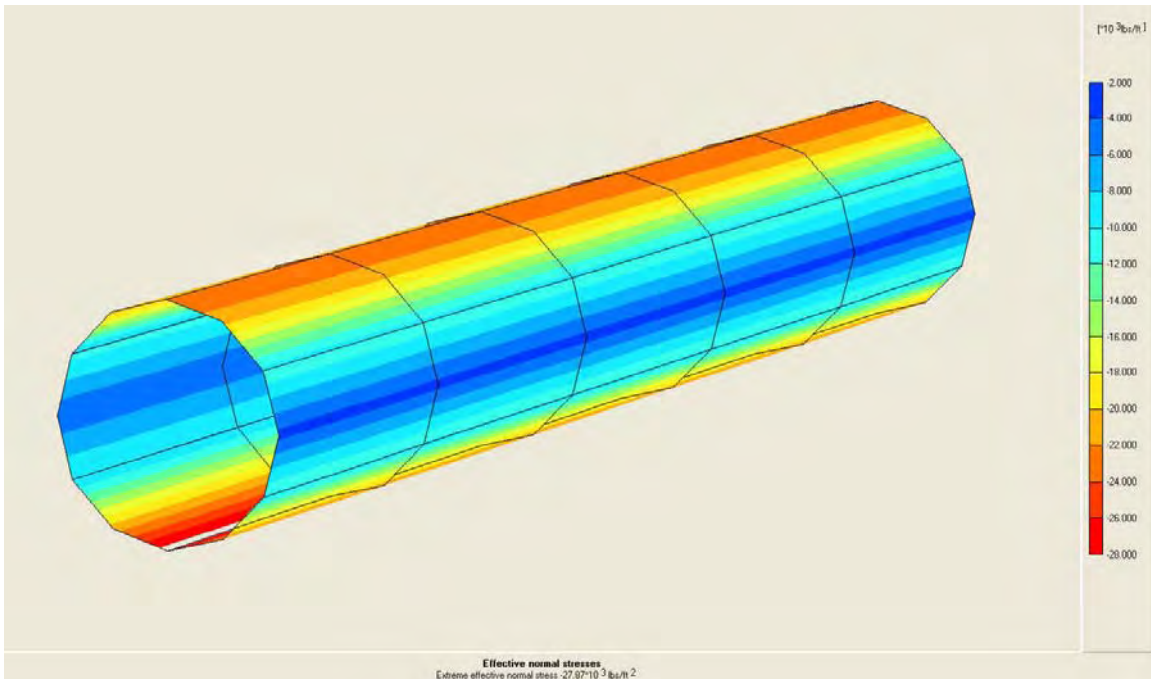


Figure A-6.8 18" diameter FRCP friction interface stress shading view.

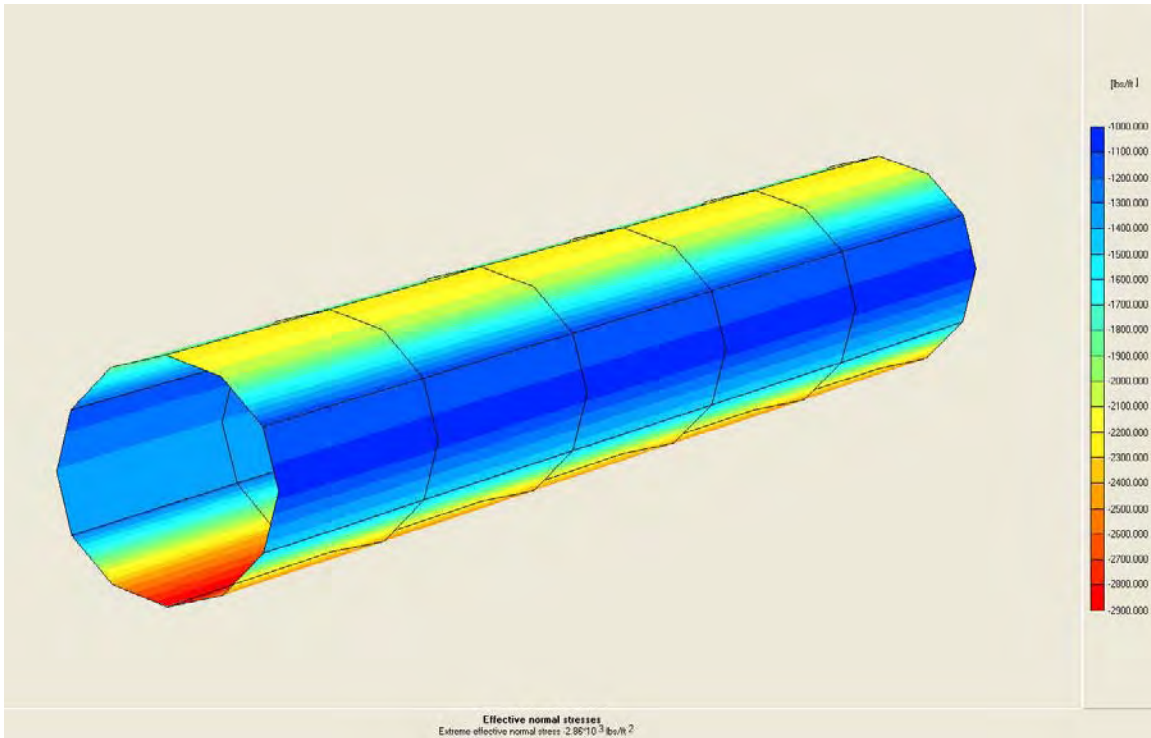


Figure A-6.9 18” diameter FRCP near zero friction interface shading view.

In situ conditions reflect a soil interacting with a concrete surface and soil-soil interaction around the pipe. In attempt to model this, the friction analysis along the wall is justified but the friction around the perimeter of the pipe is questionable. It is impossible to have near zero friction around the perimeter of the pipe thus resulting in the stress decrease as seen in the three-dimensional analysis for a near zero friction angle around the perimeter of the pipe. FRCP is a smoother pipe when compared to the SRCP, yet the friction will not be near zero, thus the results of the friction angle equal to that of soil around the perimeter of the pipe produce more justified results. More stress is induced as friction is encountered throughout the soil depth under the load. The displacement for the interface reacted in the same manner increasing, for example, from 0.072’ to 0.211’ when the friction angle was assigned a value equal to that of the soil friction angle. This is a direct result of the soil encountering a rough friction surface along the

pipe. Table A-6.6 shows the results of the three-dimensional analysis verification of the two-dimensional analysis. Note the negative values are compression.

Table A-6.6 Three Dimensional Analysis Verification of Plaxis 2D Wall Friction Analysis

Pipe	D <sup>1</sup>	C <sup>2</sup>	R <sup>3</sup>	EPS <sup>5</sup>	EMS <sup>6</sup>	Disp <sub>1</sub>	IEWS <sup>7</sup>	IEPS <sup>8</sup>	Disp <sub>2</sub>	PM <sup>9</sup>	Disp <sub>3</sub>
<b>FRCP</b>	18"	Dense	1	-23650	-13830	0.236	-7340	-24630	-0.060	-6170	0.057
<b>SRCP</b>	18"	Dense	1	-21600	-12690	0.237	-7280	-22440	-0.065	-5230	0.064
<b>FRCP</b>	18"	Dense	0.05	-24430	-15400	0.331	-4840	-4590	-0.143	-961	0.090
<b>SRCP</b>	18"	Dense	0.05	-24440	-15400	0.331	-4840	-4550	-0.143	-877	0.090
<b>FRCP</b>	24"	Dense	1	-24520	-14690	0.230	-7410	-24960	-0.696	-11090	0.067
<b>SRCP</b>	24"	Dense	1	-22180	-13380	0.234	-7380	-22610	-0.077	-9600	0.076
<b>FRCP</b>	24"	Dense	0.05	-26430	-14760	0.333	-4790	-5800	-0.194	-2220	-0.113
<b>SRCP</b>	24"	Dense	0.05	-26450	-14750	0.333	-4790	-5740	-0.195	-2070	0.113

\*All values reported are extreme values (i.e. the maximum values).

1. D is the pipe diameter in inches.
  2. C is the compaction of the backfill.
  3. R is the interface value of strength. A value of 1 represents a friction angle the same as the backfill soil. A value of 0.05 represents a friction angle less than five degrees.
  4. DM is the deformed finite element mesh after loading 16,000 lbs/ft<sup>2</sup>
  5. EPS is the effective principal stress for the entire model box in lbs/ft<sup>2</sup>
  6. EMS is the effective mean stress for the entire model box in lbs/ft<sup>2</sup>
  7. IEWS is the interface effective normal wall stress in lbs/ft<sup>2</sup>
  8. IEPS is the interface effective normal pipe stress in lbs/ft<sup>2</sup>
  9. PM is the pipe bending moment in lbs-ft/ft
- Disp<sub>1</sub> is the total displacements for the entire box in feet.  
 Disp<sub>2</sub> is the total displacements for interface around the perimeter of the pipe in feet.  
 Disp<sub>3</sub> is the total displacement of the concrete pipe in feet.

### Three-Dimensional Wall Friction Analysis

A three dimensional analysis examined the friction on all four walls of the soil box. Friction on the walls parallel to the pipe is assigned a friction value through the interface on the sidewall. The two sidewalls are assigned interfaces, but Plaxis is limited by not featuring interfaces for the front and rear walls. The test pipe will lie perpendicular to the front and rear wall and parallel to the sidewalls. The concern is whether shear stress will be induced on the ends of the pipe due to the test pipe sliding against the front and rear wall during loading. Plaxis

3D was used to induce shear stress on the ends of the pipe and examine the effects of the stress along the length of the pipe and the total displacement along the length of the pipe. The friction on the front and rear wall was created using a beam element activated over a thin slice, 0.01', in the z direction, i.e., the third dimension.

Shear stress induced on the ends of the pipe became a concern for the test pipe when attempting to simulate in situ conditions. In situ will experience no shear stress on the ends of the pipe, where as, in a test facility, the boundary conditions pose a concern for the ends of the pipe. A three-dimensional analysis examined the stress and displacement along the length of the pipe when the shear stress was induced on the ends of the pipe as shown in Figure A-6.10.

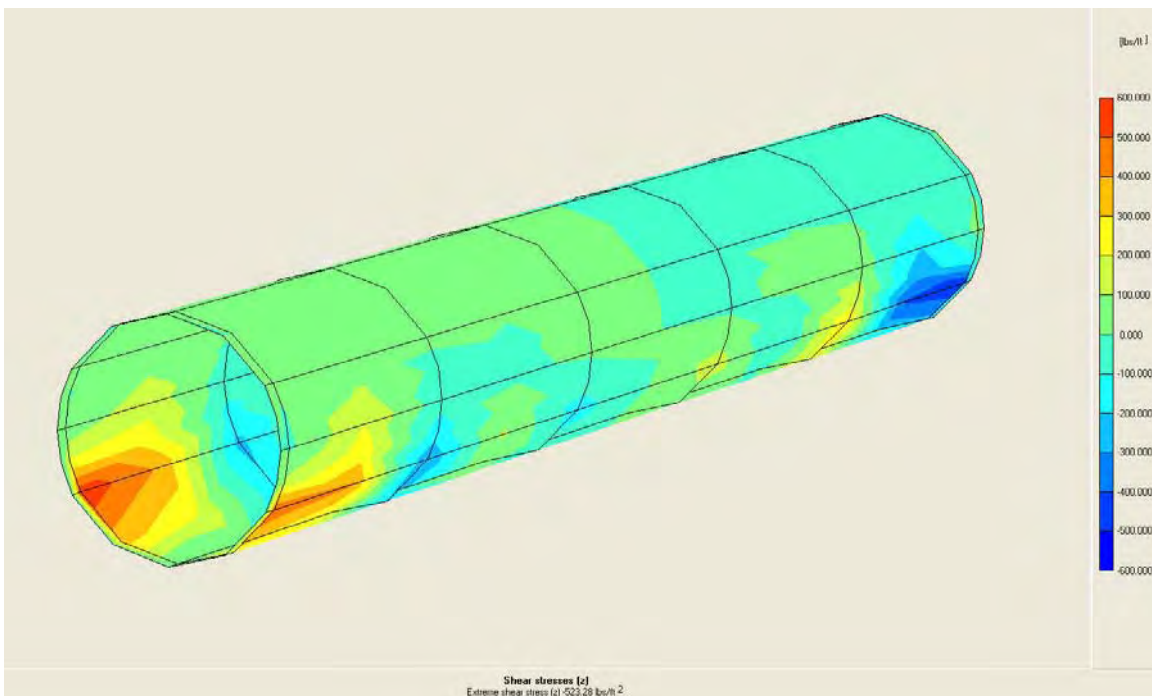


Figure A-6.10 Plaxis 3D test pipe with shear stress induced on ends of pipe.

Eight different analyses were done using 18" and 24" diameter FRCP and SRCP compacted in dense soil backfill. Each diameter pipe was modeled using sidewall friction angles of 35 degrees, the same as that of the soil, and less than 5 degrees simulating near zero friction.

Displacements along the span length of the test pipe are shown in Table A-6.7 with displacements at the front, middle, and rear of the pipe with reference to the front being the front plate of the analysis. As shown in Table A-6.7, the displacement along the length of the pipe does not differ from the front to the rear. Shear stress induced at the ends of the pipe does not affect the displacement along the length of the pipe. The stress at the middle of the pipe due to the shear stresses encountered at the ends of the pipe was also a concern. An interface was assigned around the perimeter of the test pipe modeled to examine the effective mean stress along the full length of the pipe. The eight analyses done show very little stress increases at the middle span of the pipe. Concerns of a stress increase at the middle span of the pipe were analyzed using Plaxis 3D.

Table A-6.7 Displacement of Pipe Length with Shear Stress Induced on the Ends

Pipe	Dia.	R*	Disp F	Disp M	Disp R
FRCP	18"	1	0.050	0.050	0.050
SRCP	18"	1	0.050	0.050	0.050
FRCP	18"	0.05	0.019	0.019	0.019
SRCP	18"	0.05	0.019	0.019	0.019
FRCP	24"	1	0.067	0.067	0.067
SRCP	24"	1	0.067	0.067	0.067
FRCP	24"	0.05	0.035	0.035	0.035
SRCP	24"	0.05	0.029	0.029	0.029

\* R is the Interface strength value representing the friction angle where R=1 is a friction angle equal to the soil and R=0.05 is near zero friction. Disp F, M, R represents the pipe displacement at the front (F), Midspan (M) and Rear (R) of the pipe in feet.

Table A-6.8 presents the extreme effective mean stress values around the middle span of the test pipe for each of the eight runs modeled. Of the eight simulations modeled, the stress values along the length of the pipe differ very little. To guarantee no shear stress induced at the

ends of the pipe, the test pipe shall be 1-2 inches short of the depth of the box allowing free settlement through the soil and no friction with the front and rear wall.

Table A-6.8 Extreme Effective Normal Stress Along the Length of Pipe with Shear Stress Induced on the Ends

<b>Pipe</b>	<b>Dia.</b>	<b>R*</b>	<b>EMS<sub>1</sub></b>	<b>EMS<sub>2</sub></b>
FRCP	18"	1	-25750	-25620
SRCP	18"	1	-25760	-25625
FRCP	18"	0.05	-3860	-3860
SRCP	18"	0.05	-3860	-3860
FRCP	24"	1	-23220	-23540
SRCP	24"	1	-23510	-23490
FRCP	24"	0.05	-5050	-5050
SRCP	24"	0.05	-5100	-5110

\* R is the Interface strength value representing the friction angle where R=1 is a friction angle equal to the soil and R=0.05 is near zero friction.

1. EMS is the extreme effective mean stress on the ends of the pipe in lbs/ft<sup>2</sup>
2. EMS is the extreme effective mean stress at the middle span of the pipe in lbs/ft<sup>2</sup>



## CHAPTER A-7 RECOMMENDATIONS

Two and three-dimensional analysis was performed using Plaxis Finite Element Analysis for Soil and Rock modeling soil structure interaction on buried pipes. A large soil test box was designed using the stress analysis from the finite element software. Plaxis 3D provides for a good examination of stress and displacement analysis on buried pipes. In this research a two-dimensional analysis was used which limited the analysis in the z direction. Plaxis 3D is a tunneling software program providing analysis in the z direction. Plaxis 3D was used to analyze stress and displacements along the full length of the test pipe while buried and under loads from the cover soil and distributed load. A three-dimensional analysis is recommended for further analysis of any buried pipe research.

Another concept of interest for future research is the level of compaction around the haunch of the buried pipe. Plaxis 3D will allow the user to define the compaction throughout a defined distance in the z direction running parallel to the buried test pipe. Properties for analysis would be the normal stresses, shear stresses, displacements, axial forces and bending moments along the full length of the pipe. A finite element analysis is possible for the area surrounding a defined loose compacted area around the haunch of the pipe at a specified distance along the test pipe. Plaxis 3D allows the user to input the stiffness of the soil in a desired geometry formation around the pipe. Benefits would include analysis of the trench width for installation of different size pipe diameters and also analysis of the cover soil whether compacted loose or dense.

Other analysis for Plaxis 3D are the effects of soil/ structure interaction between the test pipe and surrounding soil. Again the user can specify the stiffness of the soil surrounding the test pipe for analysis of the structural performance of the test pipe. Any geometry formation can be specified in the input program for Plaxis 3D. Beam elements are used for the lining of the

bored tunnel opening. The material specified is analyzed using a defined load for performance. The structural performance of a test pipe can be analyzed looking at the effective normal stresses acting on the test pipe. Plaxis 3D does an excellent job of providing shading images for the output of a finite element analysis. Stress distribution along the length of the pipe or any other material for analysis is displayed through the shading allowing the user to see visually where the stress intensity occurs in the analysis. Another great feature is the three-dimensional views in the output program. Having a three-dimensional view of a three-dimensional research project allows for a better understanding of the results.

Appendix A-A  
PLAXIS 2D ANALYSIS AND RESULTS

**Dimension Analysis**

A two-dimensional finite element analysis was conducted with and without the pipe inside the soil box to analyze the box dimensions. In the two-dimensional analysis, an approximate height of ten feet was used, based on the proper bedding needs of the 24" diameter pipe. Three different widths of soil box were analyzed, ten, fifteen and twenty feet. Each analysis was first run with no pipe inside the box and then with each of the 18" and 24" diameter concrete pipes. Symmetry was used in the size analysis of the box so that only the right half of the box need be included, as shown in Figure A-6.1 from Chapter A-6.

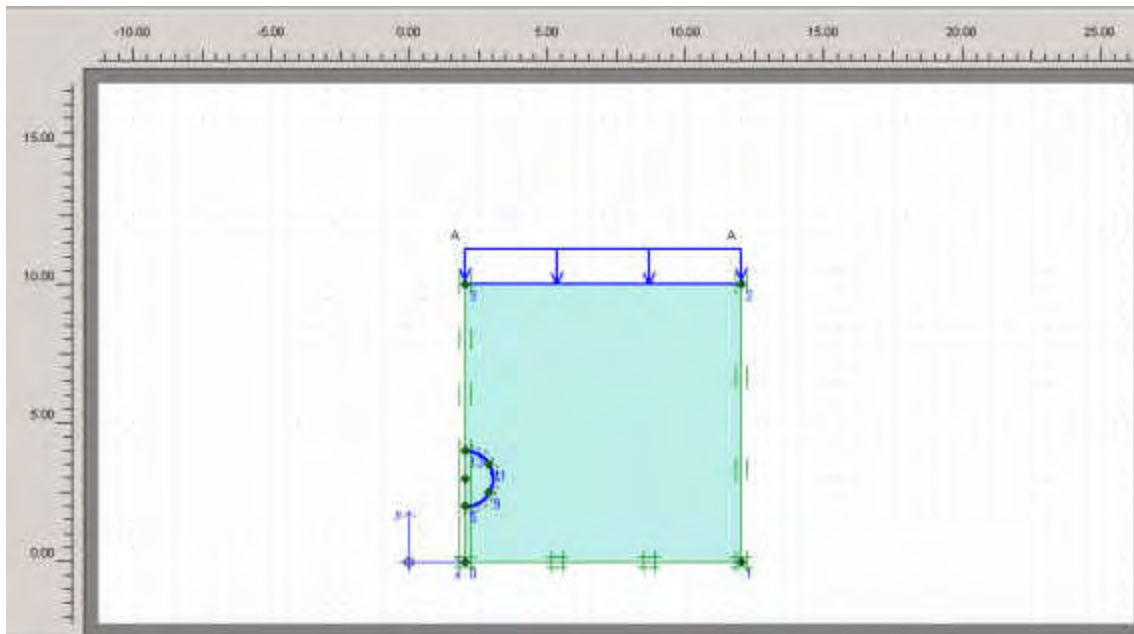


Figure A-6.1 Plaxis 2D symmetry model of 24" diameter FRCP.

Plaxis 2D modeling was used to determine the configuration that would minimize the sidewall stresses using the maximum load of 16,000 lbs/ft<sup>2</sup>. The first analysis involved three different widths with no pipe in the box, just the backfill soil. Figure A-6.2 shows the schematic of all three box analyses, for each length, executed in Plaxis 2D.

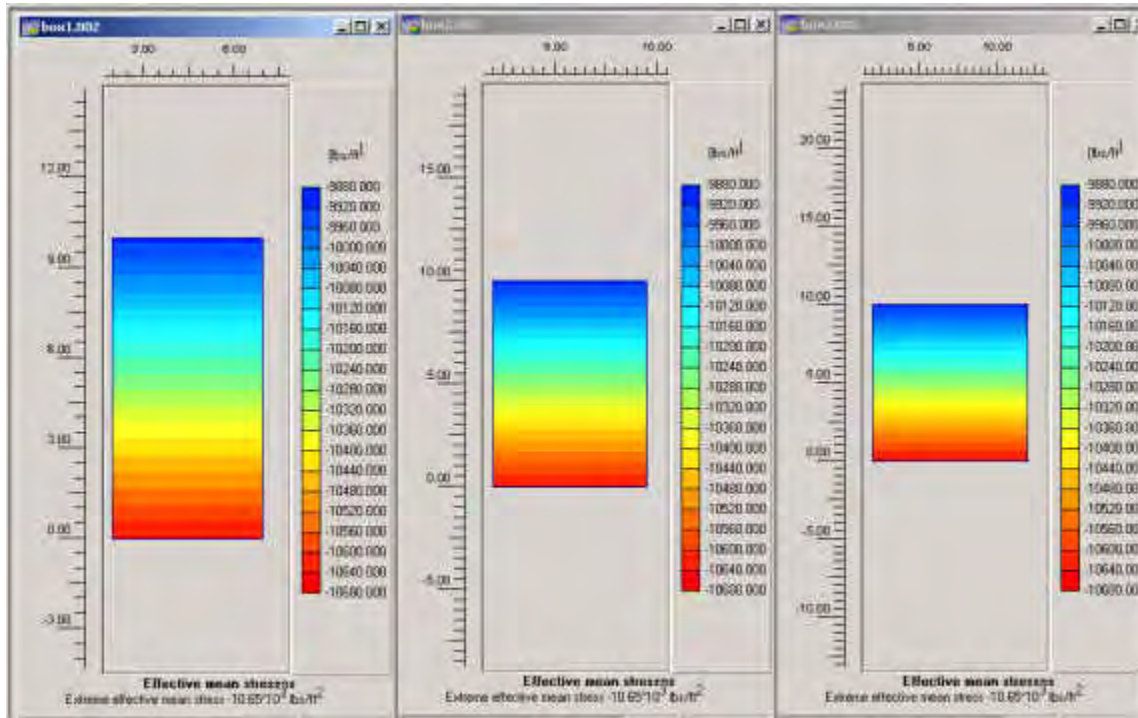


Figure A-6.2 Three different widths modeled in Plaxis 2D: 10, 15, 20 feet wide.

Results showed the same extreme value for the sidewall stresses for each length as 7,270 lbs/ft<sup>2</sup>. Modeling in only two dimensions, stresses are a direct result of the load applied and the unit weight of the soil. Plaxis 2D modeled with uniform compaction resulted in a uniform stress distribution along the sidewall. In order to obtain the sidewall stresses, a cross section was taken along the sidewall displaying the extreme effective normal stress. An example is shown in Figure A-6.3.

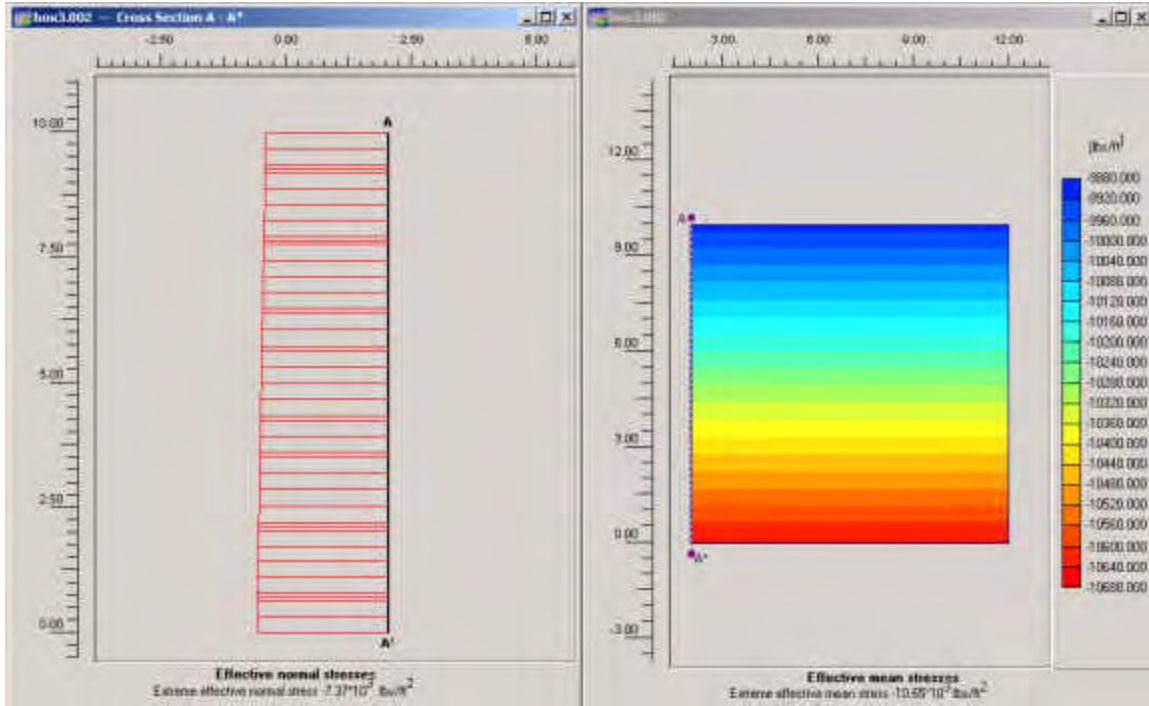


Figure A-6.3 Example of cross section used to examine the sidewall stresses (20' width).

A two-dimensional analysis was performed with a concrete pipe inserted in the soil box. Twenty four inch diameter versions of both SRCP and FRCP were used to examine the stress on the sidewalls. The 24" diameter pipes were used because the stress on the sidewalls increases as the diameter of the pipe increases. Again, three different soil box lengths were examined, with the right half of each of the FRCP and SRCP inserted into the soil model.

Stresses along the sidewalls for the ten, fifteen and twenty foot models with the FRCP are displayed in Figure A-6.4. FRCP is displayed in the figure for illustration purposes only, both FRCP and SRCP were analyzed and resulted in similar stresses along the sidewalls. Results show that the stress decreases as box length increases, creating a maximum stress on the sidewall of 7,300 lbs/ft<sup>2</sup> for the twenty-foot length. For verification, a full-scale finite element analysis was done for the twenty-foot length soil box model. The full-scale model reported the same stress on the sidewalls as the model using symmetry with only the right half of the SRCP and

FRCP. From the 24" diameter pipe analysis, the results showed that the stresses and boundary conditions were lowest for the 20' length.

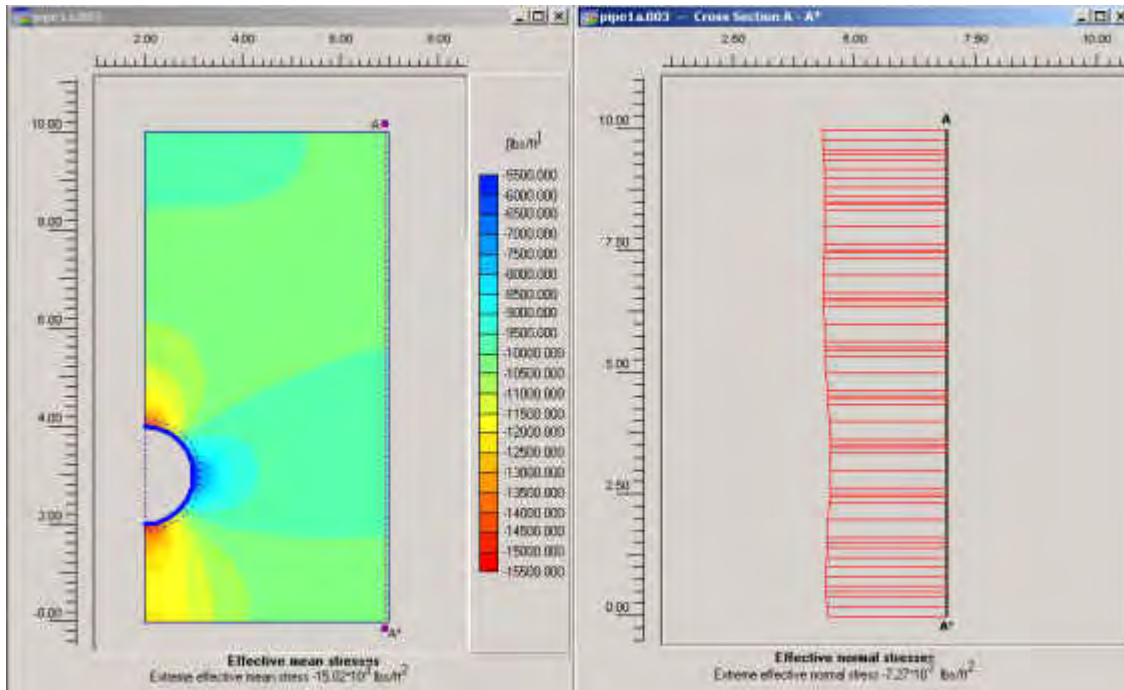


Figure A-6.4a Example FRCP cross section of sidewall stresses (10' wide box).

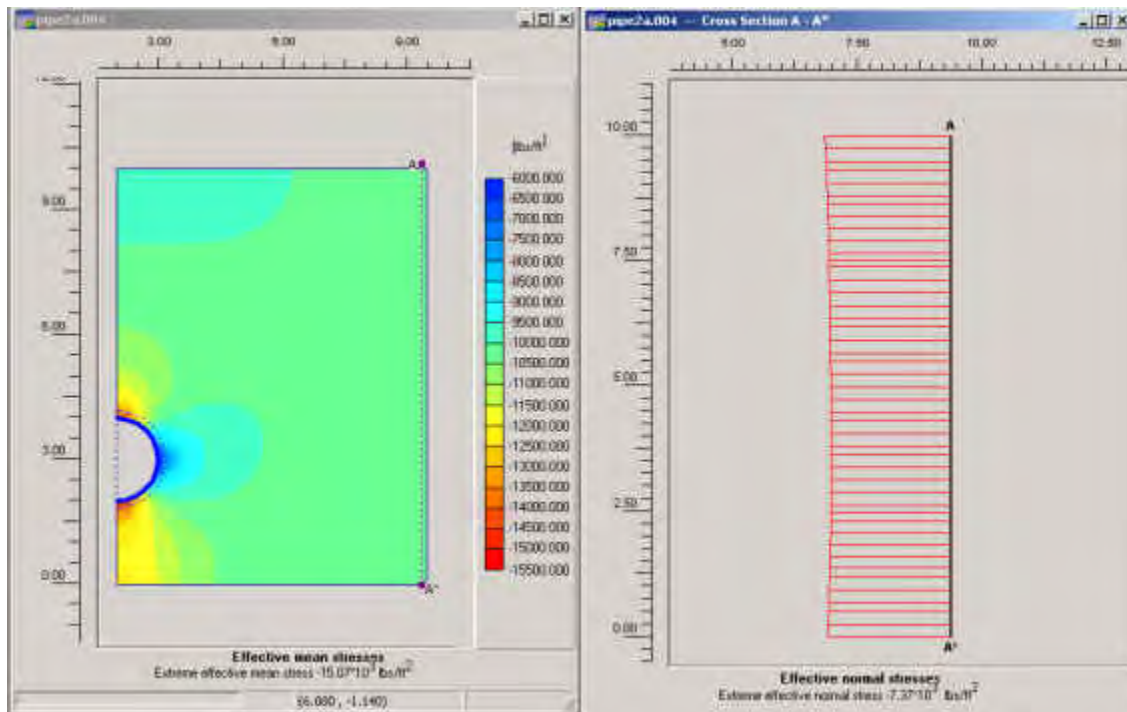


Figure A-6.4b. Example FRCP cross section of sidewall stresses (15' wide box).

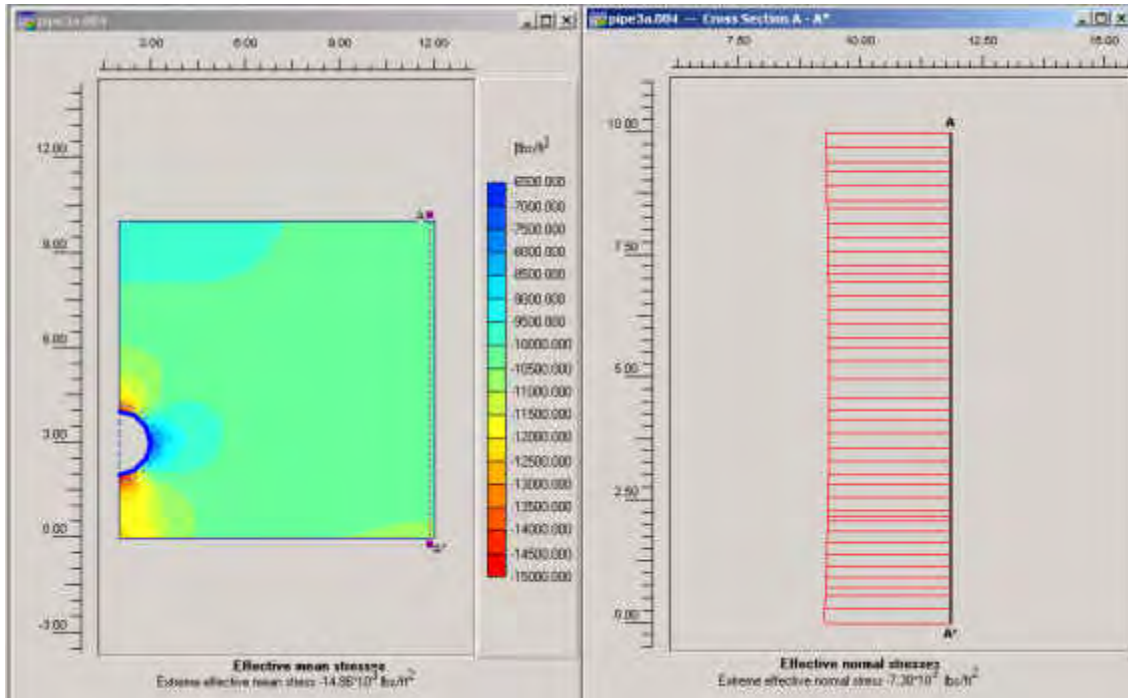


Figure A-6.4c. Example FRCP cross section of sidewall stresses (20' wide box).

### Wall Friction/ Soil Compaction Analysis

A two-dimensional analysis examined the sidewall friction of the selected box dimension length of twenty feet, altering the friction angle of the soil-structure interface with the sidewalls and the perimeter area of the pipe using two different compacted backfills.

Stresses and displacements were analyzed throughout the soil and along the specified areas of interest. Two different friction angles were assigned; a friction angle of 35 degrees and a friction angle of less than five degrees. I. D. Moore conducted research, as discussed in Chapter A-2, that indicated a minimization of the friction angle to less than five degrees helps to reduce boundary effects from inducing lateral stresses on the test pipe. The purpose is to simulate *in situ* conditions by minimizing the boundary condition effect on the structural response of the test pipe. A total of 24 different analyses were done to examine the wall friction and the effects of different compacted soils on the structural response of the test pipe. Three different pipe size

diameters were analyzed, 18", 24", and 48", with two types of concrete pipes, FRCP and SRCP, embedded in two different compacted backfills, loose and dense. Full-scale analyses were done to eliminate any doubt within the results. The extreme value results are presented in Table A-6.5 (see following page).

It is apparent from the finite element modeling results that the dense compaction is more stable than the loose compaction. Referring to the total displacement in Table A-6.5, the displacement is twice as large for the loose compacted soil. Dense compacted soil will provide better bedding conditions for allowing the pipe to sustain a load. The dense compacted soil was modeled using a soil modulus value compacted to 90% proctor.

In comparing both the FRCP and SRCP, the overall difference in results was minimal. The properties examined around the pipe, such as stress and displacements in the surrounding soil, showed minimal changes between the FRCP and SRCP. When comparing the variation in friction angle, the friction angle equal to the soil friction angle resulted in an effective normal stress along the sidewall that was twice the effective normal stress of the model with a friction angle less than five degrees. It should be noted that the negative stress values represent compression.



Table A-6.5. Wall Friction Analysis-Plaxis 2D Finite Element Analysis

Pipe	D <sup>1</sup>	C <sup>2</sup>	R <sup>3</sup>	EPS <sup>4</sup>	EMS <sup>5</sup>	Disp <sub>1</sub>	IEWS <sup>6</sup>	IEPS <sup>7</sup>	Disp <sub>2</sub>	PM <sup>8</sup>	Disp <sub>3</sub>
<b>SRCP</b>	24"	Loose	1	-24560	-14720	0.523	-7360	-24990	-0.157	-10550	0.151
<b>FRCF</b>	24"	Loose	1	-24550	-14710	0.523	-7450	-24990	-0.157	-11100	0.152
<b>SRCP</b>	24"	Dense	1	-24550	-14710	0.231	-7380	-24980	-0.069	-10550	0.067
<b>FRCF</b>	24"	Dense	1	-24530	-14700	0.230	-7260	-24970	-0.070	-10950	0.067
<b>SRCP</b>	24"	Loose	0.05	-26430	-14760	0.755	-4790	-5800	-0.442	-2090	0.257
<b>FRCF</b>	24"	Loose	0.05	-26430	-14760	0.755	-4790	-5800	-0.442	-2190	0.257
<b>SRCP</b>	24"	Dense	0.05	-26430	-14760	0.333	-4790	-5800	-0.195	-2090	0.113
<b>FRCF</b>	24"	Dense	0.05	-26430	-14760	0.333	-4790	-5800	-0.194	-2190	0.113
<b>SRCP</b>	18"	Loose	1	-23690	-13850	0.535	-7340	-24660	-0.135	-5780	0.129
<b>FRCF</b>	18"	Loose	1	-23680	-13840	0.535	-7340	-24660	-0.135	-6070	0.129
<b>SRCP</b>	18"	Dense	1	-23680	-13840	0.236	-7340	-24650	-0.059	-5770	0.057
<b>FRCF</b>	18"	Dense	1	-23660	-13840	0.236	-7340	-24640	-0.059	-6070	0.057
<b>SRCP</b>	18"	Loose	0.05	-24430	-15400	0.750	-4840	-4590	-0.325	-884	0.204
<b>FRCF</b>	18"	Loose	0.05	-24430	-15400	0.750	-4840	-4590	-0.324	-961	0.204
<b>SRCP</b>	18"	Dense	0.05	-24430	-15400	0.331	-4840	-4590	-0.143	-884	0.090
<b>FRCF</b>	18"	Dense	0.05	-24430	-15400	0.331	-4840	-4590	-0.143	-941	0.090
<b>SRCP</b>	48"	Loose	1	-23300	-13840	0.483	-7120	-22920	-0.289	-40150	0.283
<b>FRCF</b>	48"	Loose	1	-23290	-13840	0.482	-7120	-22920	-0.289	-41560	0.282
<b>SRCP</b>	48"	Dense	1	-23290	-13840	0.213	-7120	-22910	-0.127	-40140	0.125
<b>FRCF</b>	48"	Dense	1	-23280	-13840	0.213	-7120	-22910	-0.127	-41550	0.125
<b>SRCP</b>	48"	Loose	0.05	-30550	-17710	1.230	-5130	-11990	-1.130	-18600	0.624
<b>FRCF</b>	48"	Loose	0.05	-30550	-17710	1.230	-5130	-11990	-1.130	-19370	0.624
<b>SRCP</b>	48"	Dense	0.05	-30550	-17710	0.541	-5130	-11990	-0.499	-18600	0.275
<b>FRCF</b>	48"	Dense	0.05	-30550	-17710	0.540	-5130	-11990	-0.499	-19240	0.275

\*\*All values reported are extreme values (i.e. the maximum values).

1. D is the pipe diameter in inches.
2. C is the compaction of the backfill.
3. R is the interface value of strength. A value of 1 represents a friction angle the same as the backfill soil. A value of 0.05 represents a friction angle less than five degrees.
4. EPS is the effective principal stress for the entire model box in lbs/ft<sup>2</sup>
5. EMS is the effective mean stress for the entire model box in lbs/ft<sup>2</sup>
6. IEWS is the interface effective normal wall stress in lbs/ft<sup>2</sup>
7. IEPS is the interface effective normal pipe stress in lbs/ft<sup>2</sup>
8. PM is the pipe bending moment in lbs-ft/ft

Disp<sub>1</sub> is the total displacements for the entire box in feet.

Disp<sub>2</sub> is the total displacements for interface around the perimeter of the pipe in feet.

Disp<sub>3</sub> is the total displacement of the concrete pipe in feet.

**APPENDIX B.**

**PRELIMINARY ACOUSTIC EMISSION TESTING**

## B.1 Literature Review on Acoustic Emission

### B.1.1 AE Attenuation

In order to verify that AE will be useful in identifying minor progressive damage in both FRCP and SRCP, careful attention must be paid to wave attenuation and dispersion. Strong acoustic emissions originating far away from the transducer may not be detected or may reach the detector with very low amplitudes.

It has been reported that the attenuation was related to frequencies. Due to dispersion, higher frequencies attenuate quicker than lower frequencies (Bray and Stanley 1997, Rizzo and Lanza, 2001). The measured values of attenuation at 25 kHz, 265 kHz, 585 kHz and 1.2 MHz are shown in Table B-1. In the table, the coefficient of linear attenuation is determined by  $\alpha(f) = 20 \times \log[A_1(f)/A_2(f)]/2d$ . It is obvious that the attenuation increased with frequency.

Table B-1 Coefficient of Linear Attenuation (Rizzo and Lanza, 2001)

Mode	Frequency (kHz)	Linear-attenuation Coefficient $\alpha(f)$ (dB/m)
1	25	1.2
2	265	3.1
3	585	3.4
4	1200	10.2

AE signals are also attenuated by cracks. To study this aspect, peak amplitudes were recorded with respect to stress level during flexure and compression tests (Uomoto 1987). It was found that flexure cracks caused considerate attenuation, while compressive cracks had only a minor effect. The author suggested that the flexural cracks are orientated perpendicular to the direction of wave travel, while cracks formed in compression are orientated parallel to the direction of travel. Also, if flexural cracks lie between the acoustic emission source and the sensor, the signal could be greatly attenuated or even blocked.

A few methods have been proposed to minimize the effects of attenuation (Uomoto 1987). One remedy utilizes transducers at low frequencies, while another involves reinforcing bars embedded in concrete for AE monitoring.

### B.1.2 Noise Elimination

It has been reported by several researchers (Tinkey et al. 2000, Surgeon and Wevers 1999) that external noise was heard and detected by AE sensors. The noise source was possibly caused by movement of samples or by actual damage formation in the external equipment. The associated emission was determined to be low amplitude, long duration, all characteristics of mechanical rubbing. An example of noise is shown in the plot of amplitude vs. log duration in Figure B-1. This external emission was eliminated with a Swanson II filter.

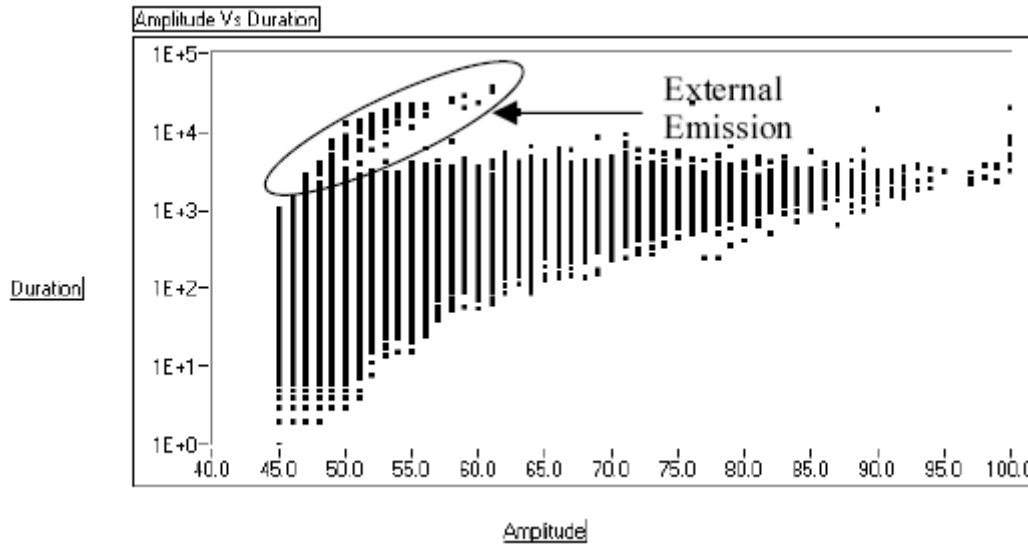


Figure B-1 Amplitude vs. log duration.

The Swanson II filter is a standard technique for identifying and eliminating extraneous emission from a data set. It is incorporated into a procedure for testing tank cars (AAR IM 101) and the MONPAC procedure (Fowler et al. 1989), and is normally used to filter external emission from sources such as leaks or mechanical rubbing. The filter works by identifying “telltale” hits and eliminating all data within a second before or after a telltale hit. Telltale hits are defined by their amplitude and duration and are listed in Table B-2.

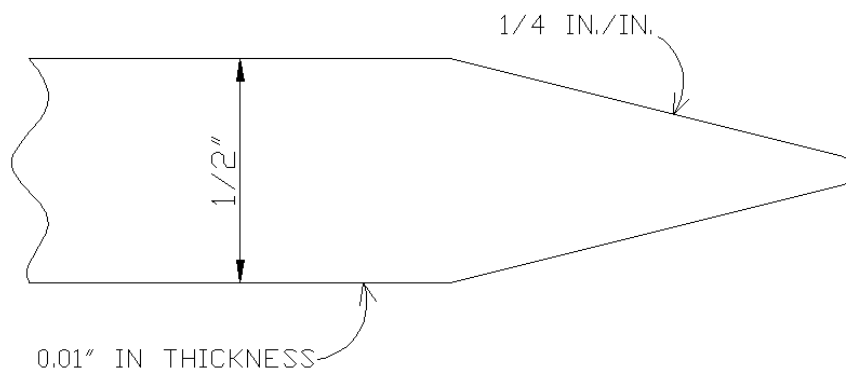
Table B-2 Definition of a “Telltale” Hit for the Swansong II Filter

Amplitude		Duration
< 5 dB plus the Threshold	And	> 2 milliseconds
	- Or -	
< 10 dB plus the Threshold	And	> 3.5 milliseconds
	- Or -	
< 15 dB plus the Threshold	And	> 4.5 milliseconds

### B.1.3 Damage Mechanisms in FRCP

Three-Edge-Bearing Test Requirements and Design Strength for SRCP:

- i). The strength test requirements in pounds-force per linear foot of pipe for reinforced concrete pipe subjected to the three-edge-bearing method shall be either the D-load (test load expressed in pounds-force per linear foot per foot of diameter) to produce a 0.01-in. crack, or the D-loads to produce the 0.01-in. crack and the ultimate loads as specified, multiplied by the internal diameter of the pipe in feet. (ASTM C 76-05)
- ii). The design strength is the maximum load expressed as a D-load, supported by the pipe before a crack having a width of 0.01 in. occurs through a continuous length of 1 ft or more measured parallel to the longitudinal axis of pipe barrel. The crack is 0.01 in. in width when the point of the measuring gage will, without forcing, penetrate 1/16 in. at close intervals throughout the specified distance of 1 ft.
- iii). The gage is made from a leaf spring, 0.01 in. in thickness (as in a set of standard machinist gages), ground to a point of 1/16 in. in width with corners rounded and with a taper of 1/4 in./in.



iv). The tested results depend highly on the inspector's testing skills, experience and visual capability.

There is no specific strength test requirements or design strength for FRCP.

As mentioned in the previous Progress Report, an ancillary objective of this project is to:

1. Attempt to discover a correlation (deformation) between the Three-Edge-Bearing test and large-scale soil box tests.
2. Develop an effective, practical, and reliable laboratory testing procedure for the Three-Edge-Bearing Test based on Acoustic Emission. This is a very unique aspect that will no doubt interest the various pipe manufacturers.
3. Using Acoustic Emission, a better understanding of the cracking/failure mechanism for different loading conditions.
4. Establish tentative strength requirements for FRCP.
5. Compare the mechanical properties of SRCP and FRCP under cyclic loading.

The above objectives have been formulated during the preliminary 3EBTs. One of the primary reasons for conducting the AE attenuation study is that:

AE signals attenuate with increasing of distance between a crack(s) and the transducers. At the same time, if a crack propagates across the surface of a sensor, the friction between sensor and pipe surface will transfer the kinematic stress to the surface of the sensor, and likely cause damage. Therefore, the sensors should be mounted as close to crack generation while remaining clear of it. The purpose of this attenuation study is to determine the most propitious distance.

The process developed so far involves breaking a 0.5 mm pencil lead at various locations along the pipe surface and checking the amplitudes received by the sensors. The compromised (amplitude versus location) distance should guarantee good signal sensitivity.

Failure of composite materials often involves more than one damage mode, such as matrix cracking, fiber breaking, fracture of the fiber-matrix interface, delamination and fiber pull-out (Barlow et al.). This is similar to FRCP with its fiber matrix.

Splitting of a thin ply unidirectional reinforced material along its fiber direction is the most simple damage mode in a composite. The composite will fail by a single damage mode, i.e. matrix cracking. Slight deviation of the crack path or of the fiber alignment will cause the crack front to intercept the fiber-matrix interface. If the interface is weak, fracture of the fiber-matrix interface will occur as a second damage mode in the failure process. The crack front will then continue to propagate within the fiber-matrix interface or kink out back into the matrix.

The crack front may also kink out from the fiber-matrix interface into the adjacent fiber, causing the fibers to break. In this case the failure process will be governed by a combination of three damage modes, i.e., matrix cracking, fiber-matrix fracture and fiber breaking. If the fiber-matrix interface is strong enough, the crack front which intercepted the interface will continue to propagate into the fibers, breaking them. Thus, failure of the composite will be contributed to by combination modes of matrix cracking and fiber breaking. The thought here is that under cyclic loading (loads well below failure levels), FRCP will exhibit internal damage that is not visually observable, but is identified by a change in the AE signal response.

#### **B.1.4 Damage Mode and AE signals**

It is a common aim among researchers and engineers to establish a correlation between damage modes and characteristics of their acoustic emission signals. Peak amplitude is the most frequent acoustic emission parameter which has been manipulated. It has been commonly accepted by several studies of AE testing on FRP that the larger amplitude acoustic events are generally associated with fiber breakage, whereas matrix cracking is more likely to produce medium-to-low amplitude signals. Quantitative results differ among individual studies due to variation in particular load tests, acquisition equipment and type or size of the test materials. Barre and Beneggagh (1994) provided a range of AE amplitude values measured for glass-fiber-reinforced Polypropylene composites: 40-55 dB for matrix cracks, 60-65 dB for interfacial fracture, 65-85 dB for fiber pullout and 85-95 dB for fiber fracture. For carbon / epoxy composites, Komai et al (1991) suggested less than 60 dB for interfacial debonding, less than 70 dB for matrix failure and less than 75 dB for fiber fracture. Ji and Ong (1994) reported less than 30 dB for delaminations, 30-40 dB for matrix cracks, and 40-80 dB for fiber fracture. Similar trends were observed by Rizzo and Lanza (2001).

The frequency content of AE signals can similarly be associated with a particular type of damage. Specifically, fiber and matrix failures in carbon-reinforced composites are generally associated with higher and lower acoustic frequencies. De Groot et al. (1995) proposed four ranges corresponding to acoustic frequency released by different types of damage: 90-180 kHz for matrix cracking, 180-310 kHz for fiber pullout or debonding, and more than 300 kHz for fiber failure. Surgeon and Wevers (1999) measured the acoustic frequency of matrix cracks below 530 kHz and that of fiber failure in the 1000-2000 kHz range. Bohse (2000) proposed the two ranges of 100-350 kHz and 350-700 kHz for matrix and fiber failure. For fiber-reinforced concrete, Kumar and Gupta (1996) reported low frequencies corresponded to failure in mortar, while frequency around 800 kHz accompanies bond failure in fiber.

### **B.1.5 Cracking and AE signals**

Based on its importance as a construction material, the fracture and failure of concrete has been the subject of extensive research. Concrete is understood to be a quasi-brittle material. Several of the mechanisms responsible for the quasi-brittle behavior have been identified and include crack bridging, friction, and microcracking.

The parameter of cumulative AE event counts has been a major interest for researchers working on cracking and fracture in concrete. Landis (1999) plotted the cumulative AE event counts and loads during three-point load testing on concrete beams. The rate of AE activity appears to increase just prior to the ultimate load, approximately 86% of the peak. Li and Shah (1994) attributed this jump to the localization of microcracking in a single critical crack. In their specimens of mortar and concrete, the jump occurred roughly at 80% of the peak load. Ohtsu (1989) attributed the AE event rate increase to the formation of the fracture process zone.

### **B.1.6 Kaiser and Felicity Effect**

The relationship between the cracking process of concrete and the Kaiser effect has been studied by several researchers. Yumaya et al (1994) concluded that the Kaiser effect actually is related to crack modes. The Kaiser effect exists during the growth of pure tensile cracks under cyclic loading, while the effect does not exist in the case of shear cracking. Kaiser effect exists while



the tensile crack width is smaller than 0.15-0.20 mm. It fails when the crack width exceeds this value or transverse shear cracks are generated. This effect is defined by ASTM as the Felicity Effect; the presence of acoustic emission, detectable at a fixed predetermined sensitivity level [threshold] at stress levels below those previously applied. The Kaiser and Felicity effect can be very useful to estimate the level of the deterioration in concrete structures. Based on the hypothesis, Tinkey et al (2000) suggested evaluation criteria for distributed damage in concrete as Table B-3:

Table B-3 Suggested Evaluation Criteria for Distributed Damage

Damage Level	Felicity Ratio		Total Number of Hits above 85 dB
Minor	> 0.9	And	< 15
Intermediate	> 0.9	And	< 25 but > 15
		-Or-	
	> 0.6 but < 0.9	And	< 25
Severe	> 0.6	And	> 25
		-Or-	
	< 0.6		

### B.2 Three-Edge-Bearing Test No. 3 on FRCP :

The 3<sup>rd</sup> three-edge-bearing test on FRCP was conducted on Oct. 27<sup>th</sup>, 2007. The Acoustic Emission sensors were mounted closer to presumed cracking locations to obtain more accurate signals. Strain gauges were applied for the first time in this test. The AE sensors and strain gauges are shown in Figures B-2 and B-3.

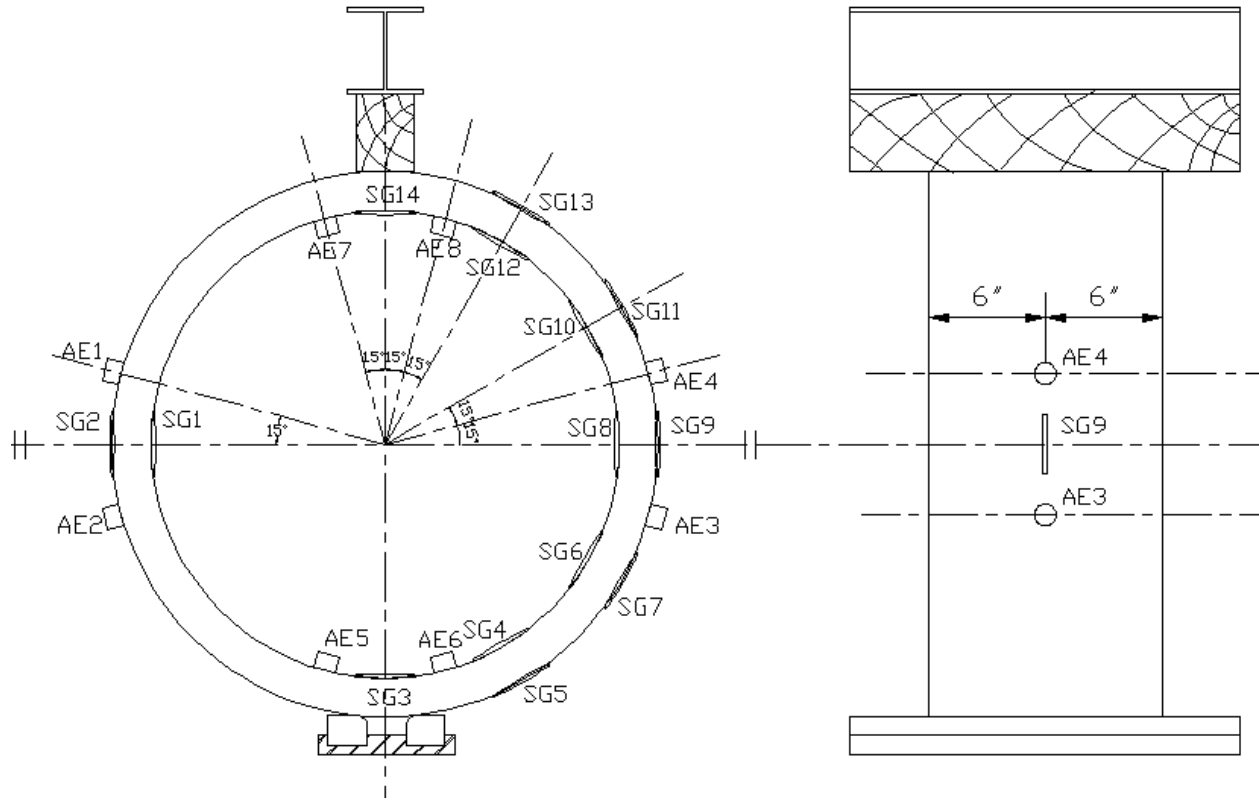


Figure B-2 The three-edge-bearing test setup on FRCP.



Figure B-3 The three-edge-bearing test on FRCP.

### B.2.1 Recording of strains

The strains are recorded by strain gages, and are shown versus time in Figure B-4.

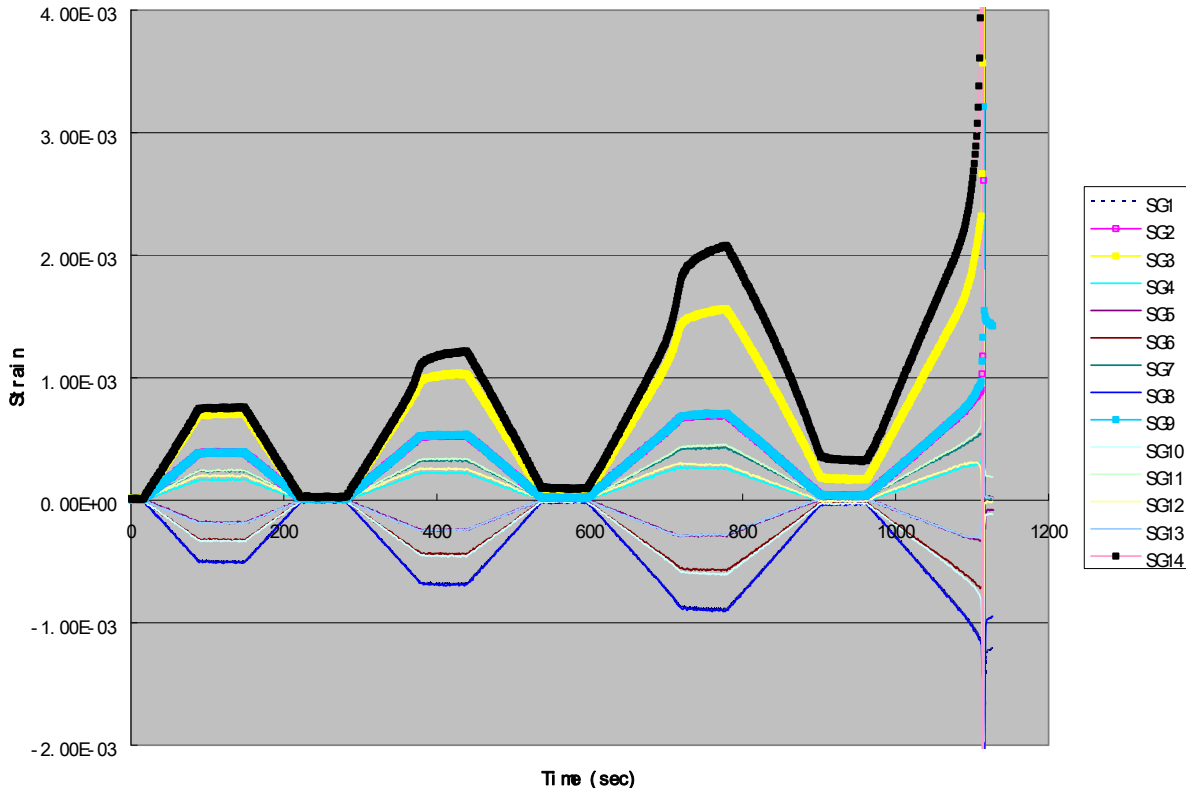


Figure B-4 Strains

By linking all the strain data at a particular time and surface locations one can observe the overall strain distribution shown in Figure B-5. On the inside surface, the strains around the top and bottom are positive, which means tensile stresses, while the strains around the springline are negative, which indicates compression. On the outside surface, the strains at the top and bottom are negative, (compression), while the strains around the springline are positive, which indicates tensile stresses.

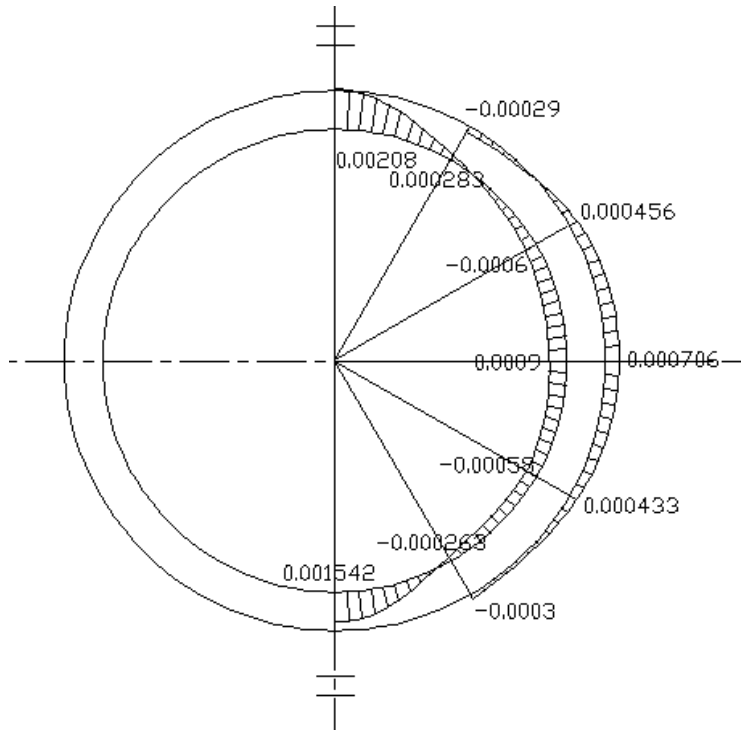


Figure B-5 Strains around pipe surface at the end of 3<sup>rd</sup> cycle, positive for tensile stress, negative for compressive stress.

### B.2.2 Acoustic Emission Results

A Swansong II filter was used to eliminate false emissions. The unfiltered and filtered data are listed for each channel are shown in Figure B-6a to Figure B-6h.

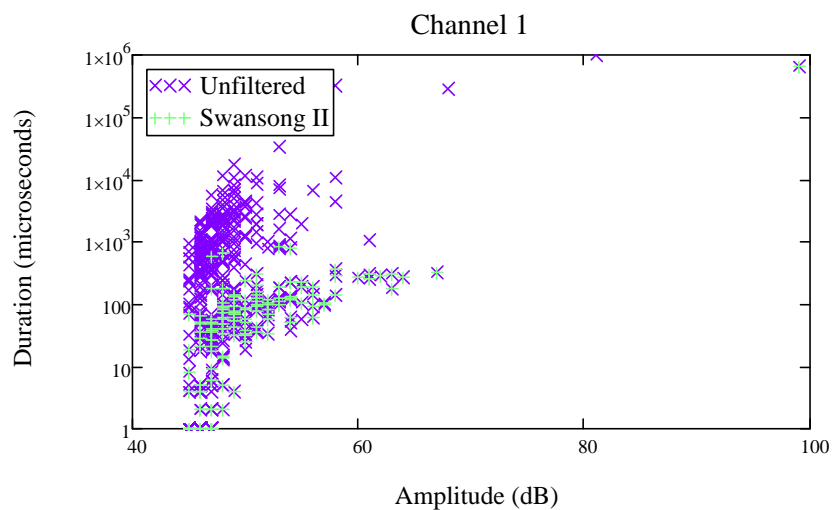


Figure B-6a Filtered and unfiltered data, duration vs. amplitude for Channel 1.

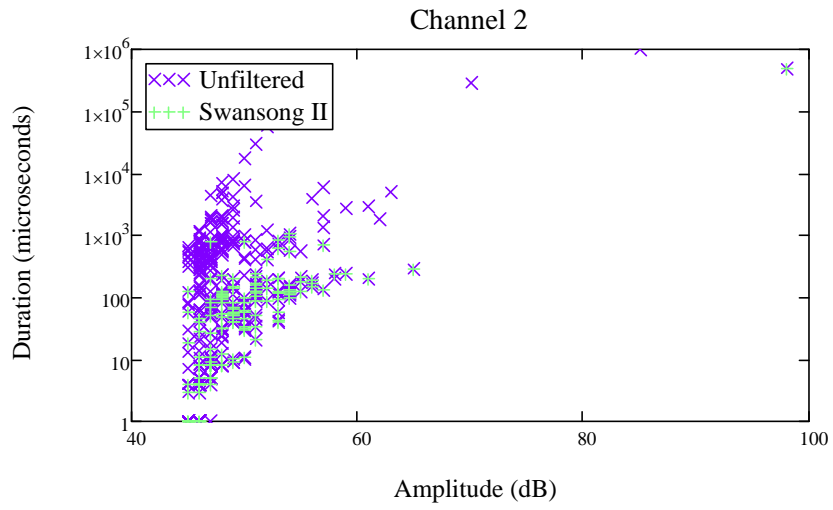


Figure B-6b Filtered and unfiltered data, duration vs. amplitude for Channel 2.

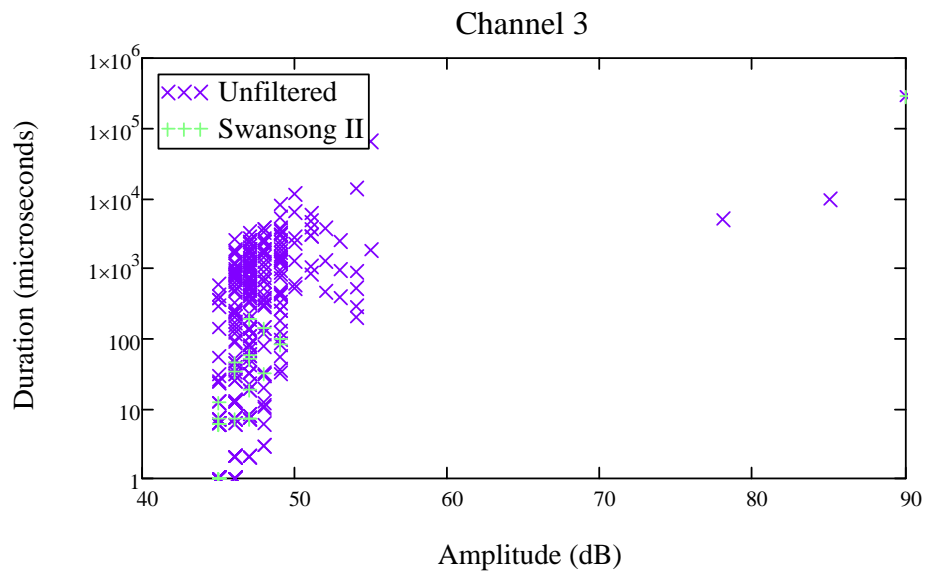


Figure B-6c Filtered and unfiltered data, duration vs. amplitude for Channel 3.

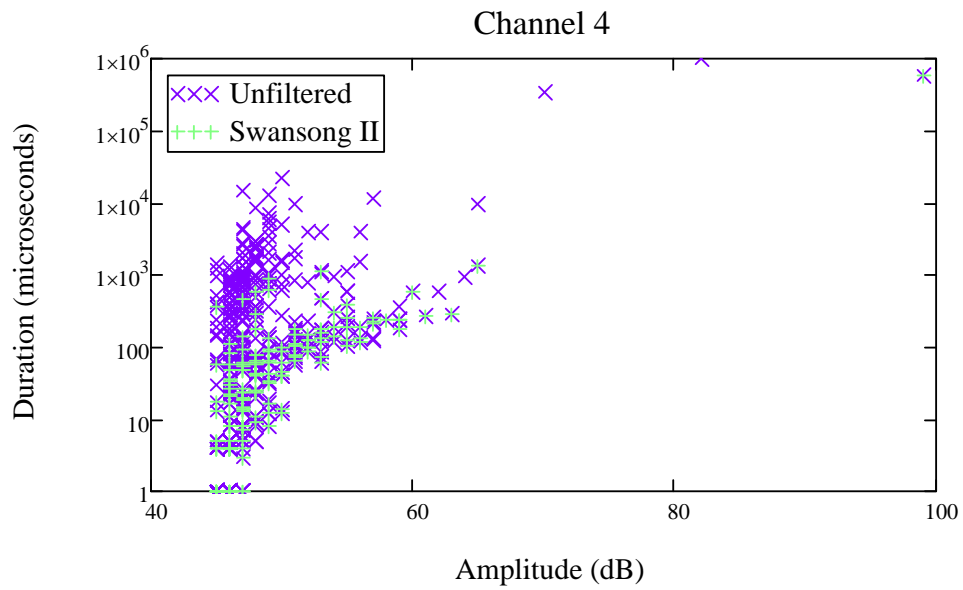


Figure B-6d Filtered and unfiltered data, duration vs. amplitude for Channel 4.

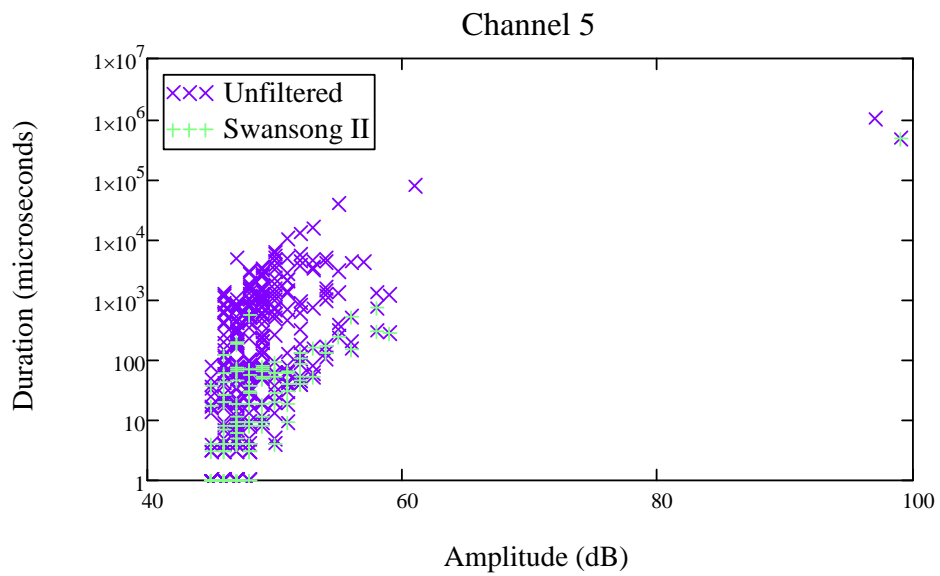


Figure B-6e Filtered and unfiltered data, duration vs. amplitude for Channel 5.

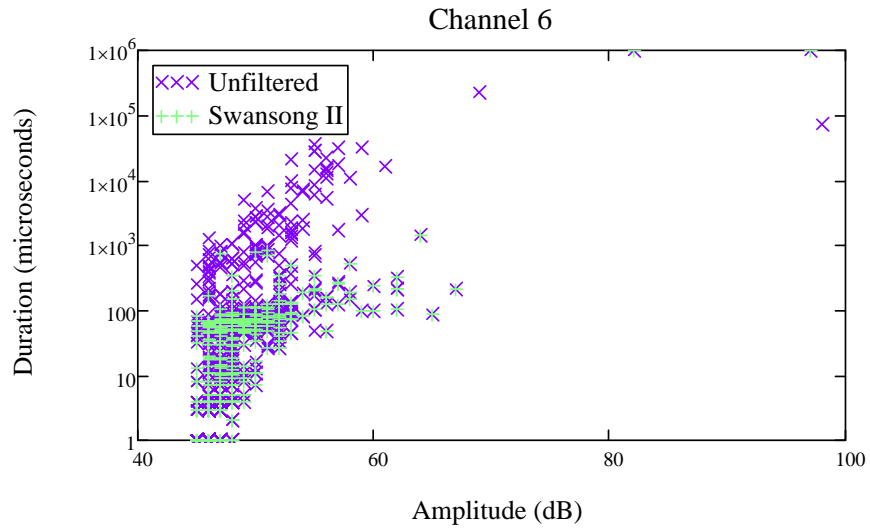


Figure B-6f Filtered and unfiltered data, duration vs. amplitude for Channel 6.

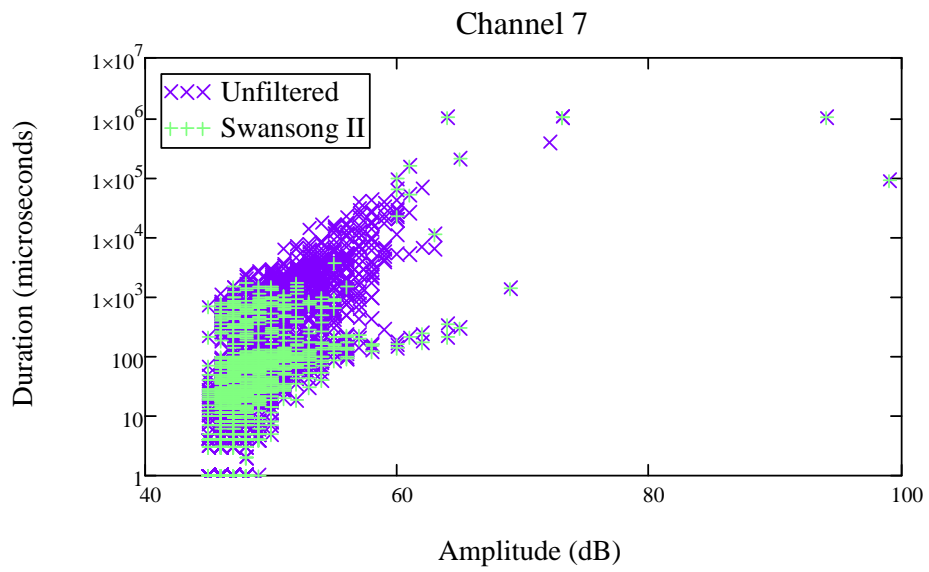


Figure B-6g Filtered and unfiltered data, duration vs. amplitude for Channel 7.

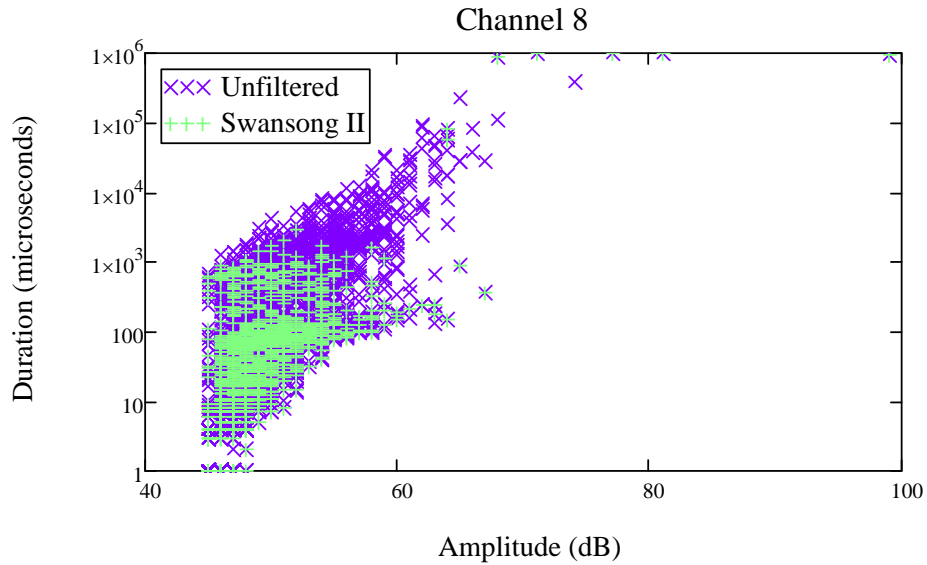


Figure B-6h Filtered and unfiltered data, duration vs. amplitude for channel 8.

From Figure B-6 we can see that the Swansong II filters large amount of the original data. Channels 7 and 8 received the most valid data as shown in Table B-4, while the data from Channel 3 filtered most of the valid data (larger values indicate more data).

Table B-4 Data Filtering Results

Channel	1	2	3	4	5	6	7	8
Unfiltered Data	482	427	339	493	429	671	2498	3008
Filtered Data	153	151	24	169	140	467	1473	1690

Preliminary data analysis compared the relation between amplitude and load history in Figure B-7. The AE picked up excellent signals immediately after load was applied. Afterwards, the emission decreased, until second loading started. However, the valid AE signals became more scattered and fewer relative to other cycles. In the third cycle, the AE signals are more concentrated around 45 to 55 dB, while for the last cycle, especially at the ultimate load level, the AE signals dramatically increased with the amplitude increasing to 90 dB. More analysis of these results will be included in the next report.



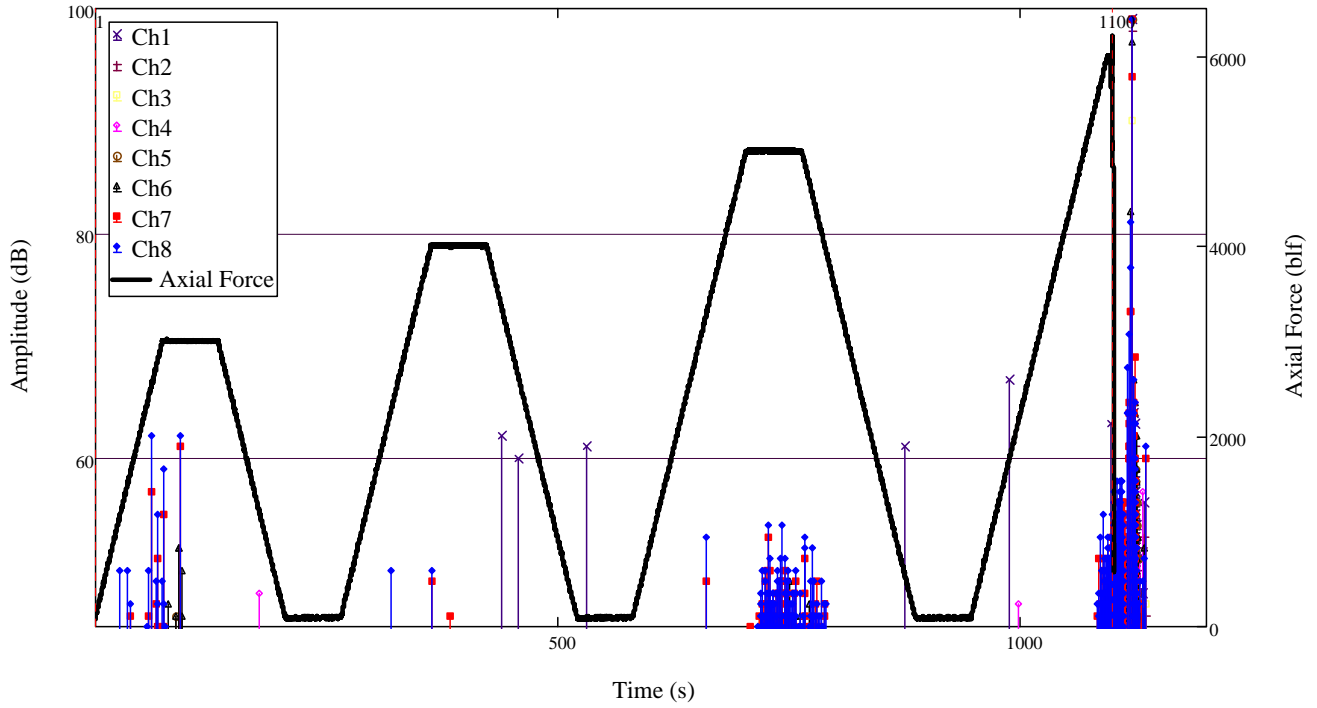


Figure B-7 Amplitude and load history vs. time.

### B.3 Attenuation Study

The attenuation study along the circumference is shown in Figure B-8.

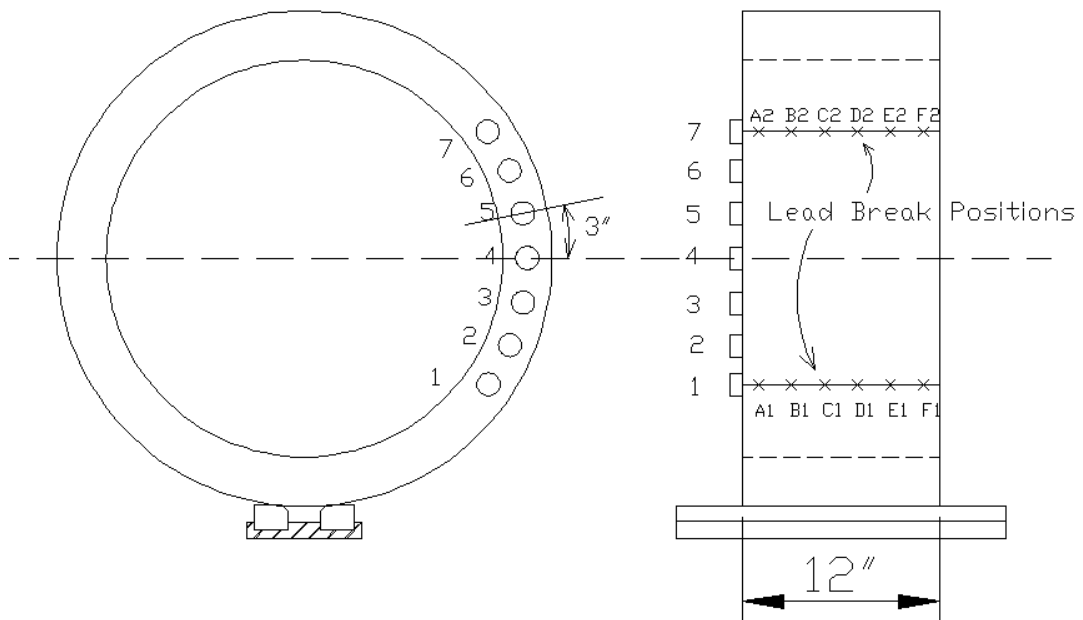
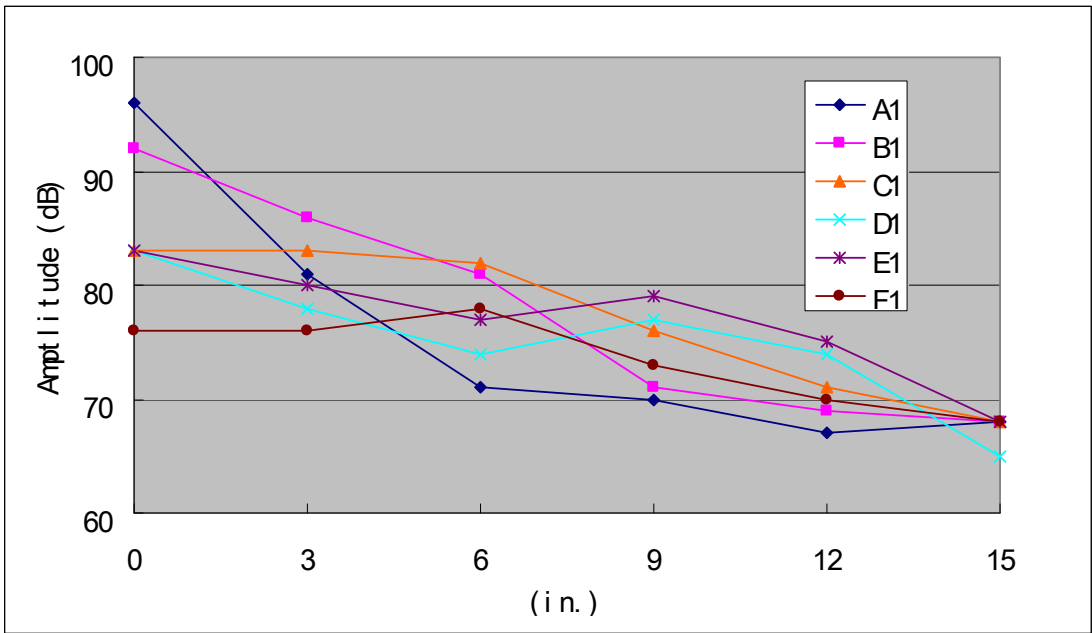
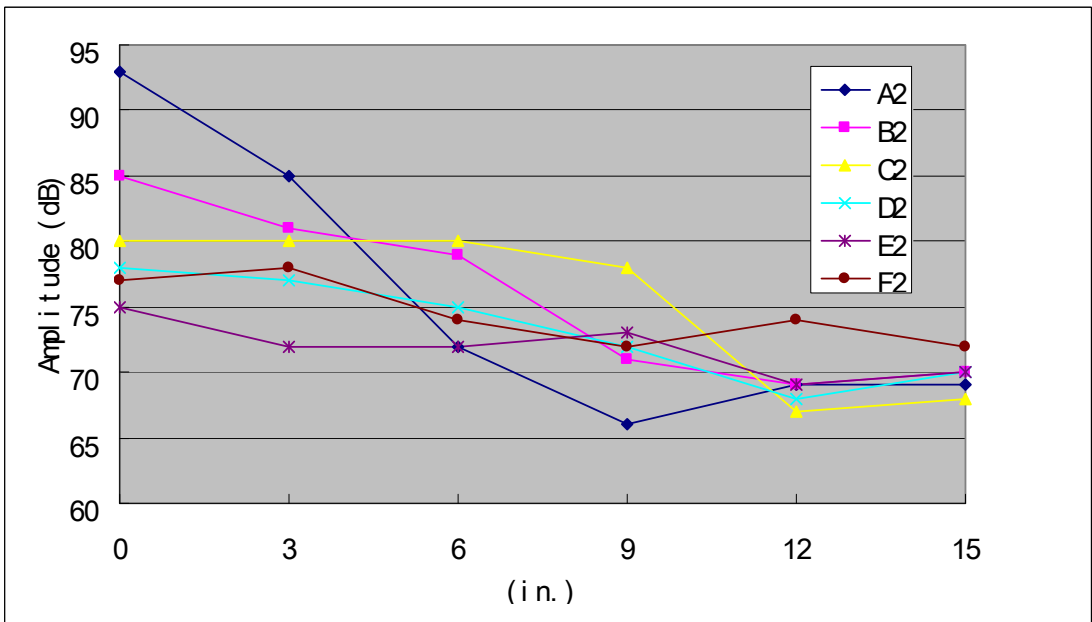


Figure B-8 Attenuation study setup.



(a)



(b)

Figure B-9 The attenuation of pencil lead breakage signals.

The attenuation study was conducted by breaking 0.5 mm lead along at the designated points. The fiber reinforced concrete is heterogeneous material so tests in two directions were taken as A1 to F1 and A2 to F2 in Figure B-8. Six sensors were mounted to receive and record signals from the same source of lead breaking from different distances. Figure B-9 shows that signal amplitudes decrease with an increase in distance. The main purpose of the attenuation study is to identify the mounting location for the AE sensors to guarantee signal quality. At the same time, the sensors should be kept away from possible crack locations to avoid breakage when the pipes reach their ultimate yield stage. To fulfill the above requirements, 3 in. was chosen as the distance from the sensors' mounting location to the possible cracking location which for the three-bearing-test will be the spring and top/bottom lines. The entire setup is illustrated in Figure B-10.

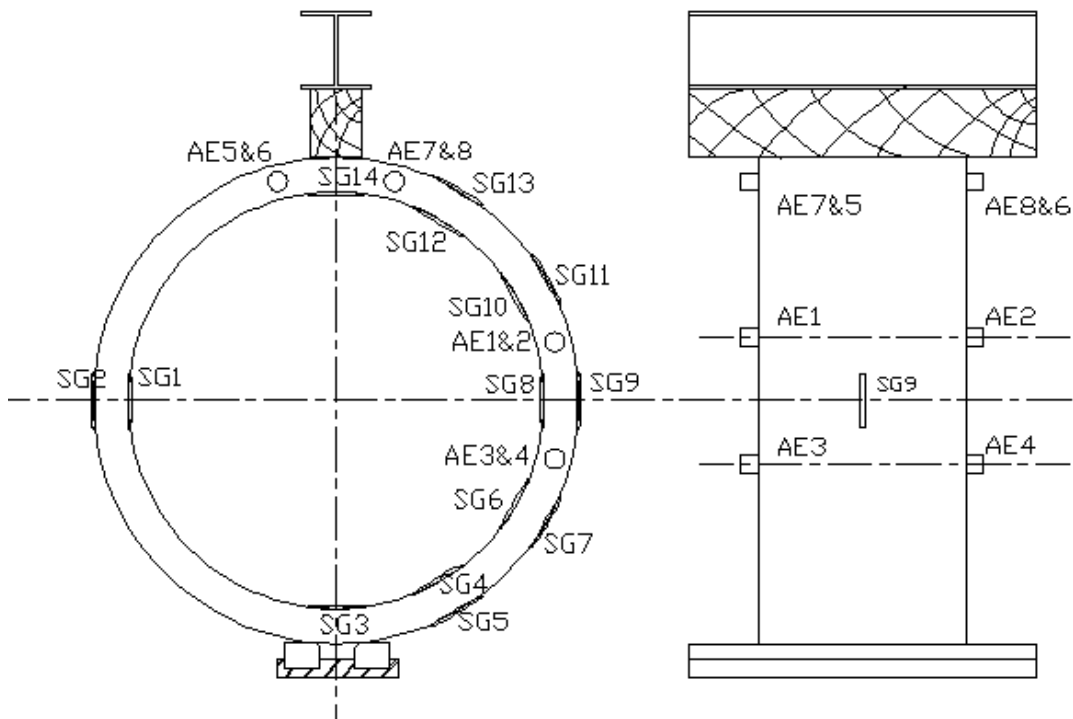


Figure B-10 The revised three-edge-bearing test setup.